TR2954S

Stellingen

(Propositions)

Low-Cost Smart Capacitive Sensors for Position and Speed Measurement

Xiujun Li

1. The definition of the smart sensor is upgraded with the accumulation of knowledge and the development of technology.

2. A smart sensor should be studied as a system that has to do with both hardware and software.

3. The capacitive sensor with a multiple-electrode structure is strongly competitive because of its simplicity, low power consumption and high sensitivity, and because many nonidealities can be eliminated in such a sensor.

4. Combining modern electronic technique with classic mathematics can result in a novel technique. The three-signal technique is a typical example.

5. Memory is a basic element of the smart sensor.

6. A good researcher can not only solve complicated problems in a simple way but can also create and discover new questions.

7. If three of us are together, at least one of the other two has something to teach me.

8. Self-confidence is based on your work being accepted. If you have self-confidence your work is more readily accepted.

9. You cannot judge a tree by its bark.

10. The best devices do not necessarily make an optimum system. An excellent group is not necessarily formed by excellent people.

11. An electronic system with a good negative feedback loop is a stable one. This also applies to the behaviors of societal, economic and political systems.

12. It is too late to improve the human living environment when it has been destroyed.

Low-Cost Smart Capacitive Sensors for Position and Speed Measurement

Low-Cost Smart Capacitive Sensors for Position and Speed Measurement

PROEFSCHRIFT

ter verkrijging van de graad van doctor
aan de Technische Universiteit Delft,
op gezag van de Rector Magnificus Prof. dr. ir. J. Blaauwendraad,
in het openbaar te verdedigen ten overstaan van een commissie,
door het College van Dekanen aangewezen,
op dinsdag 27 mei 1997 te 10:30 uur

door

Xiujun LI
Master of Science in Electronics, Nankai University
geboren te Tianjin, China

Dit proefschrift is goedgekeurd door de promotor:

Prof. dr. ir. A.H.M. van Roermund

Samenstelling promotiecommissie:

Rector Magnificus,	voorzitter
Prof. dr. ir. A.H.M. van Roermund,	Technische Universiteit Delft, promotor
Dr. ir. G.C.M. Meijer,	Technische Universiteit Delft, toegevoegd promotor
Prof. dr. ir. P.P.L. Regtien,	Technische Universiteit Twente
Prof. dr. ir. S. Middelhoek,	Technische Universiteit Delft
Prof. dr. ir. J.H. Huijsing,	Technische Universiteit Delft
Prof. dr. B. Puers,	Katholieke Universiteit Leuven
Dr. R. Utz	Novotechn. Stiftung & Co. Ostfildern, Duitsland

Published and distributed by:

Delft University Press
Mekelweg 4
2628 CD Delft
The Netherlands
Telephone+31 15 2783254
Fax +31 15 2781661

CIP-DATA KONINKLIJKE BIBLIOTHEEK, DEN HAAG

Li, Xiujun

Low-cost smart capacitive sensors for position and speed measurement / Xiujun Li. - Delft : Delft University Press. - Ill.
Thesis Delft University of Technology. - With ref. - With summary in Dutch.
ISBN 90-407-1454-1
NUGI 832
Subject headings: capacitive sensors / smart sensor systems / position and speed measurement

Printed in The Netherlands

To my wife Guijie,
my mother, and
my daughter Xinyu

Contents

1. Introduction 1

1.1 Capacitive position and speed sensors 1
1.2 What are smart sensors 1
1.3 Why smart capacitive sensors? 2
1.4 Statement of the problems 2
1.5 The purpose of this work 3
1.6 Organization of this thesis 3
References 4

2. Position and speed sensors 5

2.1 The sensors for mechanical quantities 5
2.2 Principle of capacitive position sensors 6
2.3 Principle of capacitive speed sensors 6
2.4 Current systems and their literature 7
2.5 New approaches 8
    2.5.1 A concept of smart capacitive sensors 8
    2.5.2 Capacitive/resistive-capacitive sensors 9
References 10

3. System architecture for smart capacitive sensors 13

3.1 Introduction 13
3.2 The capacitive sensing elements 14
    3.2.1 Three-electrode capacitive sensing elements 15
    3.2.2 Multiple-electrode capacitive sensing elements 16
3.3 The signal processor for capacitive sensors 18
3.4 Microcontroller 19
3.5 Nonidealities 21
    3.5.1 Physical nonidealities 21
    3.5.2 Mechanical nonidealities 21
    3.5.3 Electronic nonidealities 22
    3.5.4 Environmental influence 22
3.6 Systematic overall design 23
    3.6.1 System approach 23
    3.6.2 Mechatronic approach 25
    3.6.3 Systematic design 26
3.7 Conclusions 27
References 27

4. Signal-processing for capacitive sensors 29
4.1 Introduction 29
4.2 Parasitic-immune measurement methods of capacitance 30
4.2.1 A practical electrical model of a capacitive sensing element 30
4.2.2 The two-port measurement technique 30
4.2.3 The active guard technique 31
4.3 Oscillation method for capacitance measurement 31
4.3.1 Conventional oscillation methods 32
4.3.2 Charge-balancing oscillation method 33
4.3.3 Relaxation oscillation method 34
4.4 An integrated smart signal processor for capacitance measurement 34
4.4.1 An overview of the measurement system 35
4.4.2 Design of the capacitance-controlled oscillator 40
4.4.3 The selector 44
4.4.4 Implementation and measurement results 45
4.4.5 Conclusion 47
4.5 Measurement of time-variable capacitance 48
References 49

5. Capacitive angular-position sensor 51
5.1 Introduction 51
5.2 Basic principle of smart capacitive linear and angular position sensors 51
5.2.1 Systematic structure of a smart capacitive sensor 51
5.2.2 Capacitive sensing element 52
5.2.3 Measurement procedure 53
5.3 Electrode structure of an angular-position sensing element 54
5.3.1 Structure of the sensing element 54
5.3.2 Electric model of the sensing element 55
5.4 Nonidealities 56
5.5 The measurement algorithm 57
5.5.1 The direct 9-measurement algorithm 58
5.5.2 The indirect 7-measurement algorithm 58
5.6 The influence of various geometrical parameters that occurs due to the electric-field-bending effect 59
5.6.1 Introduction 59
5.6.2 Physical model of the sensing element 60
5.6.3 The solution of the two-dimensional electrostatic-field problem 61
5.6.4 The influence of the electric-field-bending effect on the accuracy 63
5.6.5 Numerical solution of the problem 64
5.6.6 The influence of the geometrical parameters on the nonlinearity of the sensor 65
5.6.7 Conclusions 69
5.7 The influence of the mechanical errors 70
5.7.1 Introduction 70

5.7.2 The influence of the eccentricity of the electrodes 70
5.7.3 The influence of the obliqueness of the electrodes 72
5.7.4 The influence of deformation of the screen electrode 73
5.7.5 The influence of the nonflatness 74
5.8 The influence of other geometrical errors 81
5.8.1 The influence of the pattern errors of the electrodes 81
5.8.2 The influence of the gaps and vias on the electrodes 82
5.8.3 The influence of the frayed edges 83
5.9 Piecewise self-calibration technique 85
5.9.1 Introduction 85
5.9.2 Basic concepts of the calibration technique 86
5.9.3 Application in the capacitive angular-position sensor 88
5.9.4 Calibration procedures 89
5.10 Experimental results 90
5.10.1 Realization of the sensor system 90
5.10.2 Measurement set-up 91
5.10.3 Measurement results 92
5.10.4 Discussion 96
5.10.5 Conclusions 98
5.11 Conclusions 99
References 99

6. Contactless potentiometric position sensor 101

6.1 Introduction 101
6.2 Basic principle 101
6.3 Electrode structure 102
6.4 Signal processing 103
6.5 Nonidealities 104
6.5.1 The effect of two NAND gates which have different ON resistances R_{ON} 104
6.5.2 The effect of the parasitic capacitances 105
6.6 Experimental results 106
6.7 Conclusions 108
References 108

7. Capacitive sensor for low-speed measurement 109

7.1 Introduction 109
7.2 Measurement principles 110
7.3 Capacitance in the sensing element 113
7.4 The measurement algorithm 114
7.5 The influence of nonidealities 115
7.5.1 The influence of some nonidealities of the signal processor 115
7.5.2 The influence of the slew rate of the OPAMP 116

7.5.3 The influence of the bandwidth of the OPAMP 116
7.6 Limitation of the measurement range 117
7.6.1 The minimum measurable speed 117
7.6.2 The maximum measurable speed 117
7.7 Experimental results 118
7.8 Conclusions 119
References 119

8. Contactless potentiometric sensor for low-speed measurement 121
8.1 Introduction 121
8.2 Measurement principle and algorithm 121
8.3 The influence of the parasitic capacitances 123
8.4 Experimental results 123
8.5 Conclusions 125
References 125

9. A comparison between capacitive and contactless potentiometric sensors 127

10. Conclusions and recommendations 129
10.1 Conclusions 129
10.2 Recommendations 131

Summary 133

Samenvatting (summary in Dutch) 137

Acknowledgments 141

List of publications 143

Biography 145

Chapter 1
Introduction

1.1 Capacitive position and speed sensors

Position and speed measurement techniques have been developed in many different fields. Because of the capacitor's low energy consumption and simple structure, capacitors are increasingly being used as sensing elements to measure some physical quantities, such as position, displacement, speed, liquid level, humidity, force, acceleration, gas concentration, etc.. In this thesis we limit ourselves to the measurements of (angular) position and (angular) speed by capacitive sensors and contactless resistive potentiometers.

Capacitive sensors are tandem transducers in which physical measurands are converted to an electrical (digital) output and where capacitance forms a characteristic intermediate signal. Two often-used capacitors in the capacitive sensors are parallel-planar plate and concentric cylindrical capacitors. The capacitances are varied by changing the effective electrode area, the electrode distance or the dielectric permittivity of the material between the electrodes. This thesis is limited to the capacitive sensors based on the parallel-planar plate capacitors whose value is modified by changing the effective electrode area.

A special type of capacitive sensor system is that in which the capacitor's excitation signal is modified by the measurand via other devices, such as resistors. However, the measurand is obtained by measuring the current through the capacitance. A new contactless resistive-potentiometric sensor is described in this thesis as a practical example of this kind of sensor.

1.2 What are smart sensors

There are many different definitions of smart sensors [1 – 5]. Four of them are dominant. The first definition is that any sensor with integrated electronics is smart. The second definition is that only those sensors with integrated microprocessors (microcontrollers) are smart. The third definition is that those sensors that include some logic functions and/or make some type of decisions are smart. The fourth definition is that a sensor with an off-chip microprocessor (microcontroller) used to communicate with the user and modify its response is considered to be smart.

Understanding these definitions of the smart sensor, we define a smart sensor as a sensor whose functions include at least one of the following:

- a logic function,
- the bi-directional communication,

- making a decision.

In addition to those functions, smart sensors enhance the following applications as well:

- self-calibration,
- computation,
- communication,
- multiple-sensing.

For the purposes of this thesis, the smart sensor is composed of a sensing element, a signal processor, and a microcontroller, performing all of the above-mentioned functions. However, to be smart, a sensor does not have to be integrated.

1.3 Why smart capacitive sensors?

Although sensors are employed in many different applications, the more complex the system becomes, the more powerful, comprehensive or intelligent are the sensors required. The major imperfections of the traditional (nonsmart) sensors are:

- time (or frequency) response,
- nonlinearity,
- noise,
- parameter drift,
- cross sensitivity,
- reliability and accuracy,
- dynamic range.

Smart sensors are a solution to improving these imperfections of the traditional sensors. For capacitive sensors, it is more attractive to smart them because of their natural characteristics of considerable sensitivity to pollution and condensation, EMI problems and the parasitic capacitances. The increase of the electronic signal-processing power per dollar and the development of new algorithms to obtain the measurand from measured capacitances enable the implementation of low-cost, high-performance smart capacitive sensors through the system approach and mechatronic approach. For instance, the capacitive sensing elements and the electronic signal-processing can be integrated on the same printed circuit board [6]. Here, the printed circuit board is used as the carrier of the capacitive sensing elements as well as the electronic signal-processing.

1.4 Statement of the problems

In general, the problem to be solved depends on the application of the capacitive sensors. Then the main problem can be stated:

- Is it possible to realize a capacitive sensor with a high performance/price ratio?
- What is the optimum architecture of this sensor system?
- What is the optimum structure of the capacitive sensing element and what is the optimum signal processor?

1.5 The purpose of this work

The main objective of the described work is to realize low-cost, high-performance *smart capacitive position* and *speed sensors*, by using the following means:

- concept of the systematic design for smart capacitive sensors using the system approach and the mechatronic approach,
- optimization of the structure of the capacitive sensing elements,
- the use of improved algorithms to obtain the measurand from the capacitive sensing elements,
- the measurement of small multiple capacitances,
- optimization of the interface between the capacitive sensors and the computer.

Four types of smart sensors have been thus designed and they are described in this thesis:

- a low-cost, high-performance capacitive angular-position sensor,
- a low-cost, contactless potentiometric angular-position sensor,
- a low-speed sensor using a capacitive sensing element,
- a low-speed sensor using a contactless potentiometer.

1.6 Organization of this thesis

Chapter 2 contains a brief overview of position and speed sensors and some general physical aspects of capacitive sensors.

In Chapter 3, the system architecture of the smart capacitive sensors is given. A concept of the systematic design is described, taking the main nonidealities into account.

Chapter 4 describes an accurate measurement method for small capacitances using low-cost signal processors.

The design of a low-cost, high-performance capacitive absolute angular-position sensor is described in Chapter 5. The design aspects of the capacitive sensing element, improved algorithms, the influence of the nonidealities in the capacitive sensing element and self-calibration technique are discussed in detail.

In Chapter 6, a novel low-cost contactless resistive-potentiometric position sensor is presented. The sensing element is a modified resistive potentiometer with a sliding contact which is not directly in contact with the resistive layer of the potentiometer.

How, by improving the algorithms and using the sensing elements described in Chapters 5 and 6, low speed can be measured as well, is discussed in Chapters 7 and 8, respectively.

In Chapter 9, a comparison of the specifications between capacitive and contactless resistive-potentiometric sensors is presented.

Finally, in the last chapter, conclusions are given and recommendations are made for further research.

References

[1] E.T. Powner and F. Yalcinkaya, "Intelligent sensors: structure and system," Sensor Review, vol. 15, no. 3, 1995, pp. 31-35.
[2] E.T. Powner and F. Yalcinkaya, "From basic sensors to intelligent sensors: definations and examples," Sensor Review, vol. 15, no. 4, 1995, pp. 19-22.
[3] J.M. Giachino, "Smart sensors," Sensors and Actuators, vol. 10, 1986, pp. 239-248.
[4] S. Middelhoek and S.A. Audet, "Silicon sensors," Academic Press, London, 1989.
[5] J.M. Riviere, M. Robert, F. Hermann and C. Aubrun, "Modelling of smart sensors: application to a smart temperature transmitter," International Symposium on Intelligent Instrumentation for Remote and On-Site Measurements, IMEKO TC-4, Technical Committee on Measurement of Electrical Quantities, Antwerp, Belgium, 1993, pp.173-179.
[6] X. Li and G.C.M. Meijer, "A high-performance capacitive absolute angular encoder," in Proc. Dutch conference on Sensor Technology, Delft, The Netherlands, March 1996, pp. 151-154.

Chapter 2
Position and Speed Sensors

2.1 The sensors for mechanical quantities

Measurement technology embraces a wide vocabulary with poorly defined meanings. A device which can perform a measurement conversion is variously called one of the following: sensor, sensing element, transducer, transmitter, converter, detector, cell, gauge, pick-up, probe, transponder, X-meter where X is any measurand. The word "sensor" in this thesis is defined simply as "a device which provides a usable *electronic* output in response to a specific *nonelectronic* measurand". The word "sensing element" in this thesis is defined as "a device which converts the specific measurand to a usable output based on a basic physical principle and without use of electronic signal processing". In this thesis we also use the word "smart sensor" which has been defined in Section 1.2.

Based on the physical or chemical principle used for the measurement in the sensor, it is concluded that sensors are used for the primary measurement of six classes of variables, namely electrical, magnetic, thermal, radiation, chemical and mechanical quantities [1].

Table 2.1 provides a list of measurands which will be regarded as having a 'mechanical' classification.

Table 2.1 List of mechanical measurands

1. Displacement and dimensional
   Linear, angular position, size, level, area, thickness, shape, strain, volume, surface finish
2. Speed
   Linear, angular speed, flow rate
3. Acceleration
   Vibration
4. Mass
   Weight, load, density
5. Force
   Load, weight, pressure, differential pressure, absolute pressure, dynamic pressure, torque, stress, power
6. Other physicomechanical qualities
   Viscosity, hardness, phase concentration

In this thesis, we limit ourselves to the sensors for two mechanical quantities, position and speed (especially, angular), as the title suggests.

Sensors also can be characterized by the nature of their electrical output impedance, that is, by the form of the electrical impedance seen on looking back into their output terminals. In most cases, this output impedance takes one of four simple forms, namely resistive, capacitive, inductive, or resonant. Capacitive sensors are preferred in many applications because of their high resolution, which permits a high accuracy in the micrometer range.

Using the capacitor as the sensing element (capacitive sensor), it is possible to accurately measure many mechanical quantities, directly or indirectly, for instance, linear or angular position [2 – 5], linear or angular displacement [6, 7, 8], liquid or solid level [9], force [10], pressure, torque [11], weight, etc. It can also be used for vibration, speed, acceleration and displacement measurement in dynamic deformation testing [2, 12, 20]. This thesis is concerned with the capacitive sensors for the measurement of position and low speed.

2.2 Principle of capacitive position sensors

Capacitive (angular) position sensors use (at least) a capacitive sensing element, which senses the position, to convert the position to an electrical (digital) output. Two often-used capacitive sensing elements are the parallel-planar plate and the concentric cylindrical capacitors. The capacitances are varied by changing the effective electrode area, the electrode distance or the dielectric permittivity of the material between the electrodes. Figure 2.1 shows three simple capacitive sensors in which displacement affects a change in capacitor value by *(a)* separation of the plates, *(b)* displacement of the dielectric and *(c)* axial displacement of one electrode of a coaxial capacitor. This thesis is limited to the capacitive (angular) position sensors based on the parallel-planar plate capacitors which value is modified by changing the effective electrode area.

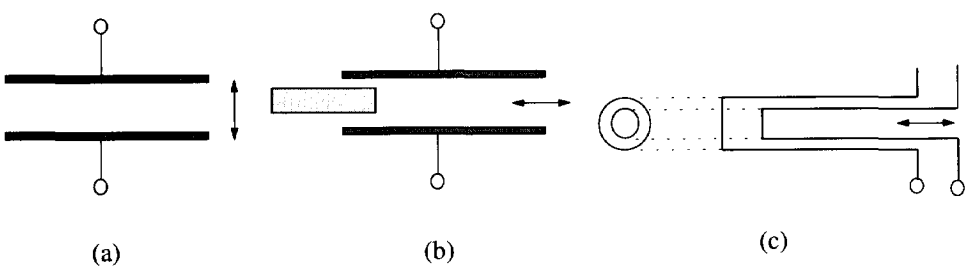

Figure 2.1 Some simple capacitive position sensors.

2.3 Principle of capacitive speed sensors

By utilizing capacitance change with the time (or position), the mechanical quantity, speed, can be measured. Such a sensor is called a capacitive speed

sensor. A direct way to measure speed using linear capacitance change is: one terminal of the capacitor, which value senses the speed, is supplied by a DC voltage source. The change of the capacitance with the time (or position) will create a current through the capacitor $i_C = V_{DC}dC/dt$. Then the speed can be measured by measuring this speed-variable current. Other direct way is that: using the capacitor with spatial-periodic multiple-electrode structure, similar to the optical encoder, creates a periodic electronic signal whose period is affected by the speed. By measuring this period the speed can be measured. Both these two direct methods are especially suited to the measurement of moderate and high speed [2].

An indirect method is based on two adjacent position (or two adjacent capacitance) measurements and time interval measurement. Then the speed can be obtained by using $\vartheta = (x_2-x_1)/t_{12}$. This method is especially suited to the measurement of low speed [12, 20].

2.4 Current systems and their literature

Although the capacitor is one of earliest discovered electronic devices, its wide application in sensors has only happened in recent decades. This is because that it is difficult to accurately measure small capacitances in a simple way. The statistical results on the number of publications about capacitive sensors in recent years, found by Toth [13], clearly shows that there is a rapid development in the fields of capacitance measurement and capacitive sensors.

The rapid development of the capacitive sensors can be attributed to the fact that some main problems have been solved, recently, in a progress of technology push and market pull.

The main aspects of the market pull are:

- the fast-growing need for small, accurate, low-cost sensors,
- the need for noncontact measurement of some mechanical quantities.

The main aspects of the technology push are:

- the development of low-cost signal processors with memory (Smart Signal Processor) resulted in the concept of smart sensors,
- the development of accurate and low-cost planar multiple-electrode structures,
- small capacitance can accurately be measured in a simple way.

Recent research shows that capacitive sensors can often replace expensive and complicated conventional sensors in industrial applications. The concept of the smart sensor system enables the realization of low-cost, practical smart capacitive sensors. The application of the smart-sensor concept offers a number of important advantages, such as:

- the improvement of the accuracy by, for instance, combining many sensor signals to reduce the effects of mechanical nonidealities,
- the improvement of the reliability by, for instance, using the memory to compare and combine present results with former ones,
- the wide measurement range made possible by using a multiple-electrode structure in the sensing element.

The main ideas of the smart-sensor concept are discussed below.

2.5 New approaches

2.5.1 A concept of smart capacitive sensors

According to the definitions given in Chapter 1, a smart sensor must do one of the following: perform a logic function, perform two-way communication, or make a decision. Thanks to the rapid development in micro-electronic technology, it is now possible to realize smart capacitive sensors in a practical way.

The most popular concept of a smart sensor is a microcontroller-based smart sensor combining a sensing element, a signal-processing circuit, and a microcontroller as shown in Figure 2.2. This concept is employed in our work.

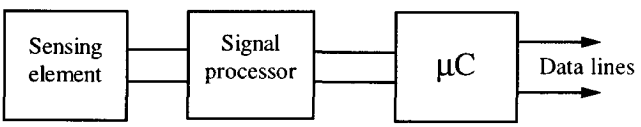

Figure 2.2 Schematic diagram of a smart sensor with microcontroller.

Such a smart sensor is probably provided with the following abilities:

- calibration and compensation in real time,
- computational ability,
- communicating ability with its environment,
- the ability to measure more than one physical or chemical quantity,
- logic decision.

Offset and gain are the two sensor parameters most often adjusted during fabrication. These adjustments usually change in time for various reasons, requiring the device to be recalibrated. Smart sensors are a solution to such cases where the servicing of sensors is too expensive. The key to this problem is the use of a built-in microcontroller that has the correction functions in its memory to compensate for the changes that have occurred over time. These sensors also include the capability to take factory calibration data stored in memory and to do the appropriate compensation, calibration and linearization. The use of the three-signal technique presented by Meijer, *etc.* [15], in the smart sensor results in an auto-calibration for the gain error and offset in real time. The three-signal technique is simply described in Section 3.3.

Computational ability is another very important characteristic of smart sensors. For instance, in order to eliminate the effect of some nonidealities, the measurand is calculated from several measured sensing element signals using an appropriate algorithm [2, 3, 14]. Further, computational statistics can be applied to find the average value and standard deviation for a set of measurements.

The communication ability of the smart sensor enables communication between the sensor and higher system levels. Generally, a smart sensor should be able to accept commands from and send data to higher system levels.

A smart sensor is expected, depending on the application, of course, to have the ability to measure simultaneously more than one physical or chemical quantity. An example of such a smart sensor is a chip which contains a resistive bridge for pressure measurement as well as a temperature sensor for temperature compensation.

The logic-decision ability of a smart sensor can, for instance, include logic selections and decisions based on the acquired information.

The logic-decision ability enables, for example,

- the extension of the measurement range by using multiple sensing elements,
- the decrease of the power consumption,
- improvement of the signal-to-noise ratio,
- the measurement of more than one measurand.

For a smart capacitive sensor, the multiple-electrode capacitive sensing element is an often-used structure [2 – 5, 8]. Combining such an element with a smart signal processor results in a high-performance and low-cost smart capacitive sensor with a wide measurement range, multiple quantities measurement and elimination of many nonidealities.

2.5.2 Capacitive/resistive-capacitive sensors

The simple capacitive sensors shown in Figure 2.1 have some disadvantages, such as a small measurement range, a large electric-field-bending effect and a large mechanical tolerances effect.

Multiple-electrode capacitive sensors are an attractive means to overcome these disadvantages. In the last few years, many multiple-electrode capacitive sensors have been developed for position measurement [2 – 5, 7, 8, 13, 16, 17]. A relatively high accuracy has been achieved in a wide measurement range, especially, in combination with the multiple-electrode capacitive sensing element and the use of smart signal processing results in high-performance low-cost smart sensors. In the work described in this thesis, the multiple-electrode structure for capacitive position and speed measurement has been adopted. This structure and the applied smart signal processing will be extensively discussed in the following chapters.

The most simple sensor for position measurement is that using a potentiometer. However, its long-term stability is bad, because the sliding contact is directly in contact with the resistive layer. A solution to this problem, which results in a contactless potentiometer or "resistive-capacitive sensor", has been presented by Li and Meijer [18] and NovoTechnik [19]. Figure 2.3 shows a schematic structure of the contactless potentiometer. In this structure, the sliding contact of the conventional potentiometer is replaced by a capacitive electrode, which capacitively picks up a displacement current whose level depends on the position of the electrode in the direction of the displacement. The working principle and applications of this contactless potentiometer in the measurements of position and speed are discussed in detail in Chapters 6 and 7.

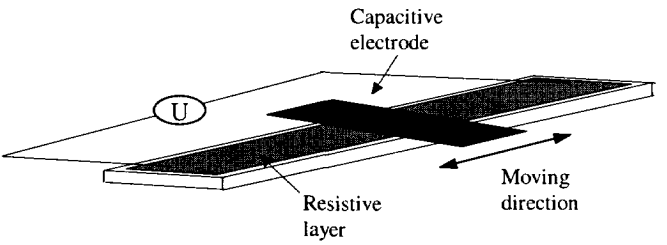

Figure 2.3 Schematic structure of the contactless potentiometer.

References

[1] S. Middelhoek and S.A. Audet, "Silicon sensors," Academic Press, London, 1989.
[2] G.W. de Jong, "Smart capacitive sensor (physical, geometrical and electronic aspects)," Ph.D. Thesis, Delft University of Technology, April, 1994.
[3] X. Li, G.C.M. Meijer, G.W. de Jong and J.W. Spronck, "An accurate low-cost capacitive absolute angular-position sensor with a full-circle range," IEEE Trans. Instrum. Meas., vol.45, no.2, April 1996, pp. 516-520.
[4] F. Zhu, "Development of capacitive position transducers through a mechatronic approach," Ph.D. Thesis, Delft University of Technology, April 1992.
[5] H.U. Meyer, "An integrated capacitive position sensor," IEEE Trans. Instrum. Meas., vol. 45, no.2, April 1996, pp. 521-525.
[6] P.B. Kosel, G.S. Munro and R. Vaughan, "Capacitive transducer for accurate displacement control," IEEE Trans. Instrum. Meas., vol. 30, no. 3, June 1981, pp. 114-123.
[7] R.F. Wolffenbuttel and R.P. van Kampen, "An integrable capacitive angular displacement sensor with improved linearity," Sensors and Actuators, A25-27(1991), pp. 835-843.
[8] M.H.W. Bonse, F. Zhu and H.F. Beek, "A long-range capacitive displacement sensor having micrometre resolution," Meas. Sci. Technol. vol. 4, 1993, pp. 801-807.
[9] F.N. Toth, G.C.M. Meijer and , "A new capacitive precision liquid-level sensor," in Conference Digist, IEEE CPEM/96, Braunschweig, Germany. June 1996, pp. 356-357.
[10] F.N. Toth and G.C.M. Meijer, "A smart, capacitive force sensor" in Proc. 1994 National Sensor Conference, The Netherlands, Feb. 1994, pp. 123-128.
[11] A. Falkner, "A capacitor-based device for the measurement of shaft torque," IEEE Trans. Instrum. Meas., vol. 45, no.4, Aug. 1996, pp. 835-838.
[12] X. Li and G.C.M. Meijer, "A new method for the measurement of very low speeds using a multiple-electrode capacitive sensor," in Conference Digist, IEEE CPEM/96, Braunschweig, Germany. June 1996, pp. 349-350.
[13] F.N. Toth, "Intelligent sensor and sensor system," Ph.D. Thesis, Delft University of Technology, January 1997.

[14] X. Li and G.C.M. Meijer, "A low-cost high-performance capacitive absolute angular encoder," in Proc. 1996 National Sensor Conference, Delft, The Netherlands, March 1996, pp.151-154.
[15] G.C.M. Meijer, Jaap van Drecht, Paul C. de Jong and Harry Neuteboom, "New concepts for smart signal processors and their application to PSD displacement transducers," Sensors and Actuators, A35(1992), pp. 23-30.
[16] G.T. Jankauskas, J.R. LaCourse and D.E. limbert, "Optimization and analysis of a capacitive contactless angular transducer," IEEE Trans. Instrum. Meas., vol. 41, no. 2, April 1992, pp. 311-315.
[17] G.A. Bertone, Z.H. Meiksin and N.L. Carroll, "Investigation of a capacitive-based displacement transducer," IEEE Trans. Instrum. Meas., vol. 39, no. 2, April 1990, pp. 424-427.
[18] X. Li and G.C.M. Meijer, "A novel smart resistive-capacitive position sensor," IEEE Trans. Instrum. Meas., vol. 44, no. 3, June 1995, pp. 768-770.
[19] —, "Non-contacting potentiometer opens up new perspectives," NovoTechnik, 1996.
[20] X. Li and G.C.M. Meijer, "A new method for the measurement of low speed using a multiple-electrode capacitive sensor," IEEE Trans. Instrum. Meas., vol. 46, no. 2, April 1997.

Chapter 3

System Architecture for Smart Capacitive Sensors

3.1 Introduction

The development of micro-electronic circuits (stronger processing ability and lower cost) makes it possible to realize practical smart capacitive sensors with high performance at low cost. In a modern measurement and control system, a great number of sensors are needed to collect information about the processes available in the system being monitored. This can only be made technically feasible if these sensors or the sensor signal processors can be made smart and able to communicate over a shared bus channel in a distributed data-acquisition system. There are various ways in which the smart sensors and smart signal processors can communicate with a central manager, for instance, via a computer. Figure 3.1 shows some possible configurations to realize a smart sensor system.

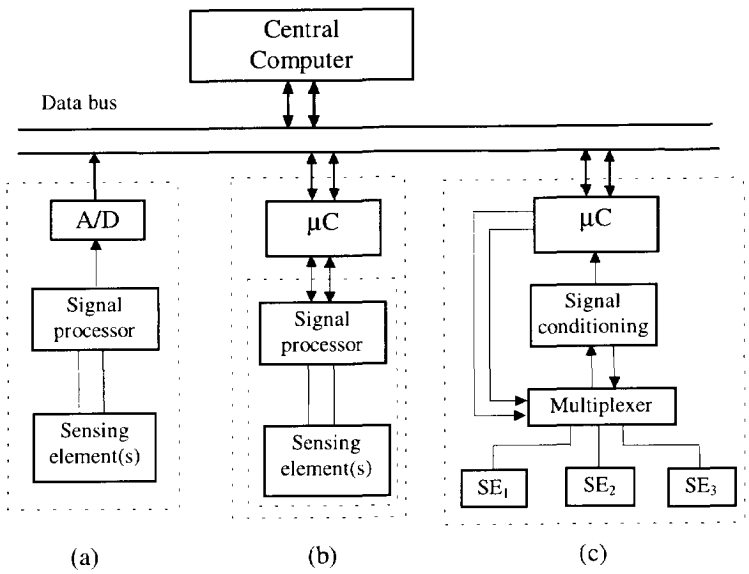

Figure 3.1 Some possible smart sensor systems.

In this configuration, the central computer picks up information from different sensor systems via the data bus, and either does some signal processing before sending the signals out or directly sends them to the actuator again after some basic conversion operations.

In Figure 3.1(a), the output signal of the sensing element is first processed, for instance, amplified and corrected for offset, nonlinearity and other types of sensing-element errors, before transferring it to the A/D converter. An A/D converter is employed to convert the analog signal to a digital computer-compatible signal.

In Figure 3.1(b), the signal processor can perform the same operation as that shown in Figure 3.1(a), or it only transfers the sensor signal to a microcontroller-compatible signal. The microcontroller performs the pre-processing for this signal, such as some calculations, logic decision, filtering, calibrations and compensations for the nonidealities of the sensing element and the signal processor, and transfers a corrected signal to the data bus. An interesting property of this smart sensor architecture is that the microcontroller also permits the central computer to send data back to the sensor, which can be used to change the measurement range, to effect a recalibration, or to adjust the offset.

Based on the architecture in Figure 3.1(b), a smart sensor system with a multiple sensing element is shown in Figure 3.1(c). Here, the multiplexer is controlled by the microcontroller to select the sensing element(s) to be measured.

In this thesis, we employ the configuration shown in Figure 3.1(c) and design a contactless potentiometric sensor and a capacitive sensor with multiple electrode. A schematic diagram of a smart capacitive sensor with a multiple electrode is shown in Figure 3.2.

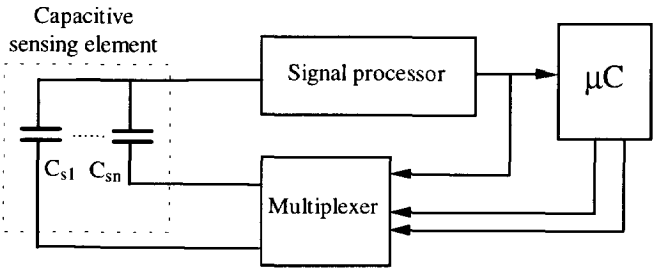

Figure 3.2 Schematic diagram of a smart capacitive sensor with multiple electrode.

In the following sections, the main elements, such as the capacitive sensing element, the signal processor and the microcontroller are described and their nonidealities are considered. Finally, a concept of a systematic design of smart capacitive-sensor systems is described, taking the main nonidealities into account.

3.2 The capacitive sensing elements

The capacitance of a capacitor with a homogeneous dielectric can be described with the basic expression:

$$C = \varepsilon_0 \varepsilon f(G), \tag{3.1}$$

where C is the capacitance in Farads, ε_0 the permittivity of the vacuum, being a physical constant of 8.854×10^{-12} F/m, ε the relative permittivity of the dielectric material, and $f(G)$ is a geometry-dependent factor.

For the simple ideal parallel-plate capacitor with a homogeneous electric field between electrodes, the geometry-dependent factor can be approximated by the equation

$$f(G) = \frac{S}{d}. \tag{3.2}$$

In this case, the capacitance is directly proportional to the overlapping area S and inversely proportional to the distance between electrodes d.

A common problem in capacitive sensor designs is the effect of parasitic capacitances, due to contributions of fringes, the backs of electrodes and connecting wires. This is modeled in Figure 3.3(b) for the simple two-terminal parallel-plate capacitor shown in Figure 3.3(a).

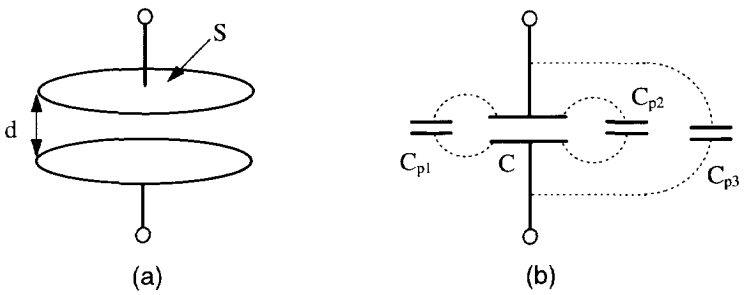

Figure 3.3 (a) Simple plate capacitor, (b) Parasitic capacitances.

The parasitic capacitances, C_{p1}, C_{p2} and C_{p3} are small, yet they result in inaccurate and unreliable gauge factors in capacitive sensors. These and other effects have been described by Jones and Richards [1].

3.2.1 Three-electrode capacitive sensing elements

Already in the nineteenth century, Maxwell [2] gave a solution to the elimination of the parasitic capacitances for the capacitor shown in Figure 3.3, which is based on the use of a guard-ring as a third electrode (Figure 3.4). If the width of the gap between the island electrode and the guard-ring is extremely small, compared with the electrode distance d, the capacitance C_{12} between the island and the opposite electrode can be calculated with a high degree of accuracy, using the ideal parallel-plate capacitor formula:

$$C_{12} = \varepsilon_0 \varepsilon \frac{S}{d}, \tag{3.3}$$

where the area S is defined as the average radius of the gap between the island electrode and the guard-ring.

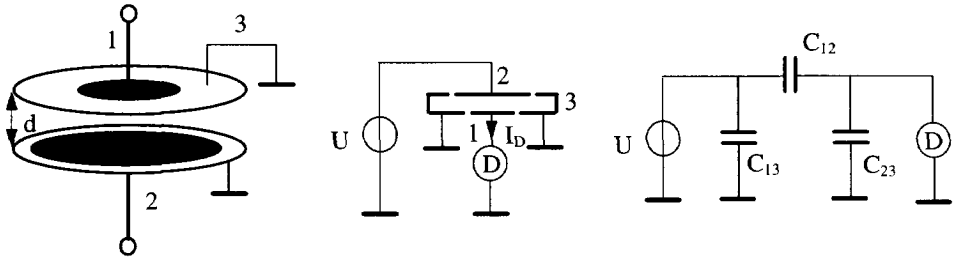

Figure 3.4 Parallel-plate capacitor with guarding electrode.

In metrology, this type of capacitor is called a three-terminal capacitor. Analytically calculated details about the width limitation of this Kelvin guard-ring capacitor are given in an article by Heerens and Vermeulen [3].

The basic capacitance of the sensor is represented by capacitance C_{12} in this case. The parasitic capacitance C_{13} creates an additional load on generator U and does not affect the measurement if the generator output impedance is sufficiently low (voltage source). Similarly, parasitic capacitance C_{23} forms a condenser shunt of the current detector D and can be neglected, assuming that input impedance of the detector is sufficiently low.

In the arrangement shown in Figure 3.4, under the conditions mentioned above, the parasitic capacitances C_{13} and C_{23} will have no affect even when their values are considerably higher than the capacitance C_{12}.

Structure restrictions of the guard-ring capacitor, which must be fulfilled for the validity of the analytical calculations, are given by Heerens [4].

3.2.2 Multiple-electrode capacitive sensing elements

In the accurate capacitive sensor systems with a large measurement range, the capacitive sensing elements are implemented as multiple-electrode elements [5 – 9, 26]. The advantages of multiple-electrode elements are:

- the large measurement range,
- the high accuracy,
- the reduction of the electric-field-bending effect,
- the reduction of the mechanical errors,
- the very small nonlinearity.

Two often-used structures of the capacitive sensing element with multiple electrodes are bi-layered and three-layered electrode structures.

3.2.2.1 Bi-layered electrode structure

Figure 3.5 shows a simplified bi-layered electrode structure. The (multiple) segmented electrode is fixed. Multiple capacitors which are formed between the moving common electrode and the segments carry the position information of the moving common electrode.

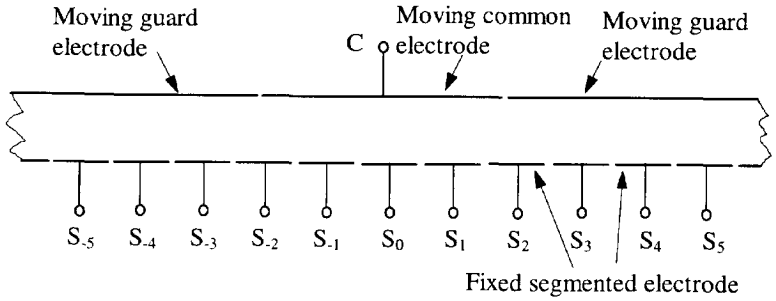

Figure 3.5 A bi-layered electrode structure.

3.2.2.2 Three-layered electrode structure

Figure 3.6 shows a three-layered electrode structure. The segmented (multiple) electrode and the common electrode are fixed. The moving screen electrode shields the segmented electrode from the common electrode and so decreases the capacitance between two fixed electrodes. The multiple capacitors, which are formed between the common electrode and the segments, carry the position information of the moving screen electrode.

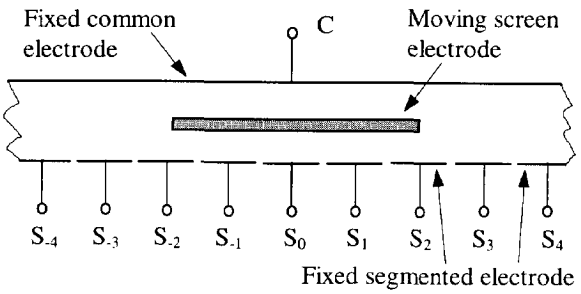

Figure 3.6 A three-layered electrode structure.

As an example of this type of electrode structure, an angular-position sensor is discussed in detail in Chapter 5.

3.3 The signal processor for capacitive sensors

For our low-cost application, the signal processor requires a high degree of accuracy and a medium conversion speed. The specification requirements of the signal processor for capacitance measurement are:

- low cost,
- suited for multiple-electrode capacitive sensors,
- microcontroller-compatible output,
- insensitive to the parasitics of the sensing element,
- no expensive calibration,
- good long-term stability.

In order to achieve these specifications, some advanced techniques are adapted in the design of the signal processor, such as:

- two-port measurement,
- three-signal technique.

Figure 3.7 shows the principle of a smart signal processor for multiple capacitance measurement.

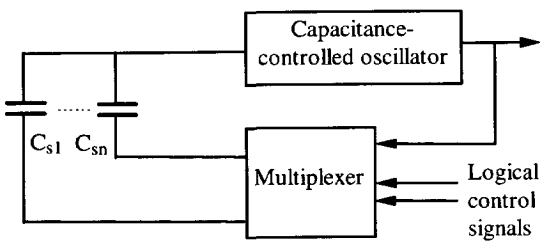

Figure 3.7 The principle diagram of the smart processor.

The smart processor has multiple-capacitance inputs and one microcontroller-compatible output. As, for example, there are three capacitances C_{s1}, C_{s2} and C_{s3} ($C_{s1} < C_{s2} < C_{s3}$) to be measured, the waveform of the output signal of the signal processor is as shown in Figure 3.8. The capacitances C_{s1}, C_{s2} and C_{s3} are linearly converted to the time intervals T_1, T_2 and T_3 of the output signal, respectively.

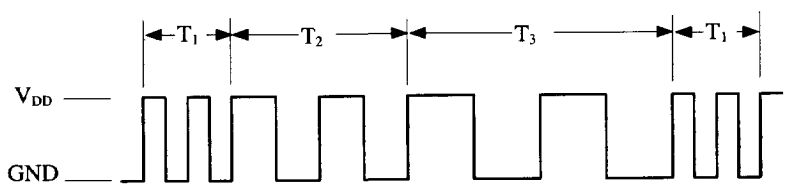

Figure 3.8 The output signal of the processor.

In order to implement two-port measurement for multiple capacitances, the signal processor has to be meet the following requirements:

- small input impedance of the capacitive-controlled oscillator,
- small output impedance of the multiplexer as possible.

The three-signal technique is a technique to eliminate the effects of unknown offset and unknown gain in a linear system [10, 11]. In order to apply this technique, in addition to the measurement of the sensor signal (in our case capacitance), two reference signals are required to be measured in an identical way. Suppose a system has a linear transfer function of

$$M_i = kE_i + M_{off}. \tag{3.4}$$

The measured three signals are

$$\begin{aligned} M_{off} &= M_{off} \\ M_{ref} &= kE_{ref} + M_{off}. \\ M_x &= kE_x + M_{off} \end{aligned} \tag{3.5}$$

Then the measuring result is the ratio

$$M = \frac{M_x - M_{off}}{M_{ref} - M_{off}} = \frac{E_x}{E_{ref}}. \tag{3.6}$$

When the system is linear, then in this ratio the influence of the unknown offset M_{off} and the unknown gain k of the measurement system is eliminated.

According to the working principle of the three-signal technique, a memory is required to implement this technique. A better solution for this is to use a microcontroller which can perform the data storage and some calculations, such as formula (3.6).

In Chapter 4, we discuss in detail such a signal processor for capacitance measurement.

3.4 Microcontroller

The rapid decrease in unit cost and the increase of on-chip capabilities have enabled the widespread use of the single-chip microcontroller in instrumentation and measurement technology. The application of microcontrollers in the sensor systems results in advanced smart sensors [7, 8, 11, 12, 13]. Moreover, the development of the single-chip microcontroller has enabled the use of new compensation, calibration and linearization techniques [14 – 17, 25].

In the microcontroller-based smart sensor system as described by Figure 3.2, the microcontroller can perform the control of the output situation of the multiplexer, the measurement of the output signals of the signal processor, the processing of the data and the communication with the digital world, such as a personal computer. Figure 3.9 shows a block diagram of a microcontroller with the input/output mechanisms [18] which are used in our smart sensor system.

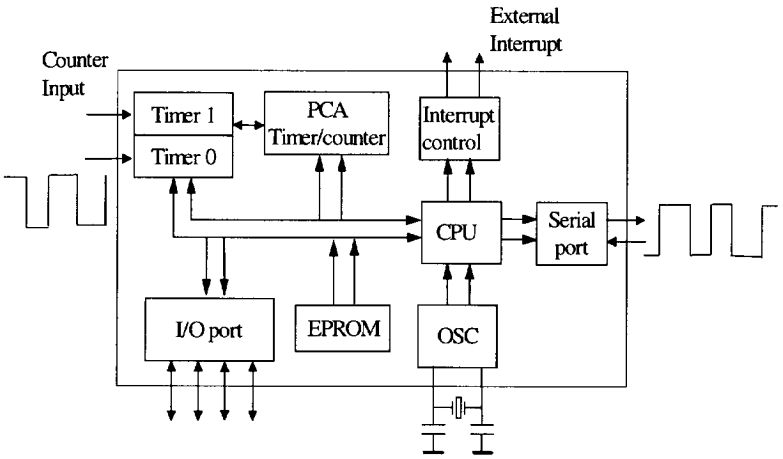

Figure 3.10 Block diagram of a microcontroller showing the input/output mechanisms which are used in our smart sensor system.

As a counter, the microcontroller can measure the period, frequency and duty cycle of the input signal by counting the number of internal clock cycles fitting in each period to be measured. The counter can be triggered at a positive edge or a negative edge for period and frequency measurement, and at both a positive and a negative edge for duty cycle measurement. The frequency of the internal clock can be set in 1/4 or 1/12 of the oscillator frequency. In our case, the output signal of the signal processor will be a period modulated one. The counter of the microcontroller is used to measure the period length over a certain time interval T. It can be shown that for the quantization noise it holds that [19]

$$\varepsilon_q = \frac{1}{\sqrt{6}} \frac{t_s}{T}, \tag{3.7}$$

where ε_q represents the standard deviation of the quantization noise, t_s is the period of the internal clock of microcontroller, T is the measured time interval.

The interrupt structure of the microcontroller is also important for the smart sensor system. The measurement can be started and stopped using external interrupt.

The microcontroller is equipped with addressable bidirectional parallel and serial I/O ports to communicate with outside circuits. The bidirectional parallel I/O ports, commonly with 8 bits, can be used as input or output. As input they receive the signals from outside circuits. As output they can control the working situations of outside circuit and, for instance, control the situation of the multiplexer. The serial port, at its simplest, comprises two pins connected to an internal UART (Universal Asynchronous receiver/transmitter) which enable the contents of an internal register to be transmitted or received in conventional eight-bit serial format with parity, start and stop bits added.

The memory in the microcontroller can contain a small software program to manage the microcontroller and to perform simple data processing for compensation and calibration, and algorithm processing.

The principal defects of the microcontroller as a real-time signal processor are that it is sequential in operation and therefore slow, and that its internal signals are discrete in amplitude and time.

3.5 Nonidealities

The nonidealities in the smart sensor system depicted in Figure 3.2 can originate from four main categories: physical, mechanical and electronic ones, and environmental influence.

3.5.1 Physical nonidealities

The physical nonidealities are mainly embodied in the electric-field-bending effect in the capacitive sensing element. Due to this effect, the capacitor value between two electrodes (see Figure 3.3) is not strictly described by $C = \varepsilon_0 \varepsilon S / d$. The influence of the electric-field-bending effect on the sensor accuracy depends on the shape and dimensions of the electrodes.

By applying guarding technique, and appropriate electrode structures and algorithms, the influence of the electric-field-bending effect can effectively be reduced [4, 7, 8].

3.5.2 Mechanical nonidealities

The mechanical nonidealities mainly originate from the nonflatness of the surface of the electrodes, the eccentricity, the obliqueness, the deformation, the pattern errors and the frayed edges of the electrodes, and the gaps and vias on the electrodes in the capacitive sensing element.

The nonflatness is an important error source in the parallel-capacitive sensors. Its influence can be significant when electrodes are made of low-cost material, for instance, the print-circuit board [7, 8]. By modeling the nonflatness of the electrode surface and using the principle of Fourier analysis, the influence of the nonflatness can be found. Generally, the influence of the nonflatness on the sensor accuracy also depends on the shape and dimensions of the capacitor electrodes [9].

The eccentricity only exists in the angular sensors, and is due to the eccentric positioning of the capacitor electrodes.

The influence of these systematic and stochastic mechanical nonidealities can be significantly reduced by using a redundant and symmetrical electrode configuration in the sensing element [7, 8]. Also a microcontroller-based calibration and compensation technique can considerably reduce the influences of those systematic mechanical nonidealities [14, 25].

3.5.3 Electronic nonidealities

The electronic nonidealities mainly originate from the signal processor. These nonidealities include nonlinearity, inaccuracy, finite response time, temperature drift, thermal noise, quantization noise, and the influence of the parasitic capacitances.

By using advanced measurement techniques, for instance two-port measurement, three-signal approach, dynamic element matching, synchronous detection and calibration/compensation, some main systematic nonidealities can be eliminated or significantly reduced [19, 20].

High-frequency interference from the microcontroller can affect the signal processing. This interference can, for instance, cause undesired locking effects in the signal processor [19]. The oscillator frequency does not perfectly represent the signal from the sensing element. The use of the appropriate low-pass filter and the low bandwidth for all parts on the processor reduce this locking effect.

3.5.4 Environmental influence

The humidity, temperature and EMI are three important environmental influence sources. They affect every practical measurement system. Sometimes their influence can be quite serious and difficult to control.

In the capacitive sensing element, temperature will affect the measured capacitor value by changing the size and distance of the electrodes. The use of low-expansion-coefficient materials for the electrode structures can reduce these influences. Optimizing the electrode structure can reduce the sensitivity of measured quantities, for instance, position, to the electrode structure parameters [9], and therefore to variations in ambient temperature. The capacitor value is also affected by variation of the dielectric permittivity with ambient temperature. This influence can be eliminated by measuring the ratio of two capacitances if both capacitors are filled with dielectrics having the same permittivity. Distortions of the electrodes due to temperature gradients are difficult to predict. This is another reason to use low-expansion-coefficient materials for the electrode structures. A symmetrical structure of the capacitive sensing element is very helpful to reduce the influence of thermal expansion.

The relative humidity will affect the measured capacitance by changing the dielectric permittivity. Figure 3.11 shows an electrical model of capacitance considering the influence of the humidity.

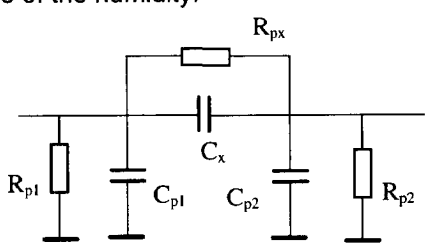

Figure 3.12 An electrical model of capacitance.

The influence of moisture (light humidity) can be eliminated by measuring the ratio of two capacitances if both capacitors are filled with dielectrics having the same permittivity. However, the condensation, which can cause a conductive layer, can short-circuit the electrodes with the guardings and make measurement impossible. This influence on the cross-capacitance and trans-capacitance has been studied by Toth *et. al.* [21]. An impedance break-down was observed at 90% and about 60% humidity at 20°C and 80°C, respectively.

The use of appropriate shielding and guarding in the capacitive sensing element and processing circuit can reduce the EMI effect. Although the use of guarding electrodes causes a relatively large parasitic capacitance, the two-port measurement technique can reduce their influence sufficiently.

3.6 Systematic overall design

The system architecture, main elements and some main nonidealities of the smart capacitive sensor have been described in the above sections. Now, the next problem proposed to be solved is the characterization and design of an optimum smart sensor as a system. Here, this characterization will be based on both a specific system approach and a mechatronic approach. The system approach and a mechatronic approach are described in the following sections.

3.6.1 System approach

Actually a smart sensor system as described in Figure 3.1 has a hierarchical multiple-layered structure, as shown in Figure 3.13 [22].

The processing in each layer can be characterized as follows:

- signal processing in the lower layer,
- information processing in the middle layer,
- knowledge processing in the upper layer.

The top layer acts like the brain of the smart system where high-level information processing is being conducted. In the top layer, processing is more centralized than in the other layers. Processed knowledge is not dependent on the operating principle and physical structure of the sensors. In contrast, information processing in the lower layer is strongly dependent on the sensor's underlying principles and structures. A group of smart sensors, or ordinary sensors, on the lower layer collects information from the external objects. Signal processing of these smart sensors is done both in a distributed and in a parallel manner.

The role of sensor intelligence in the lower layer is limited to selective processing of the sensor signals and adoption to the characteristics of the individual sensors. This includes simple operations of the outputs from multiple sensing elements for feature extraction. However, this does not include the optimization of device parameters or signal integration, because these require knowledge of the sensing elements and the objects.

In the middle layer, there are intermediate signal-processing functions. One possible function of intermediate signal processing is the integration of signals from multiple sensing elements. When the signals come from different types of sensors,

the function is referred to as sensor-signal fusion. Another role of the middle layer is the parameter tuning of the sensors to optimize the total system performance. Optimization is done based on the extracted feature and knowledge about the target signal. The knowledge is given by the upper layer as a form of an optimization algorithm.

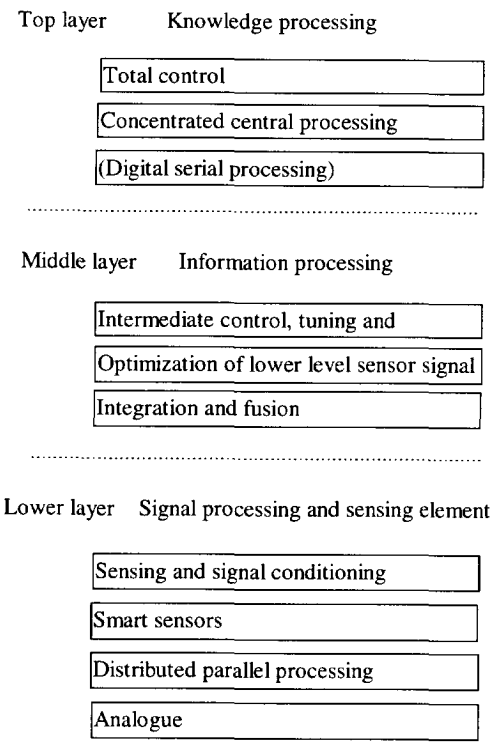

Figure 3.13 Structure of a smart sensor system.

In general, the property of information processing done in the lower layer is more directly related to hardware, and it is less hardware-related in the higher layer. The algorithm of information processing is more flexible and more knowledge-oriented in the higher layer and less flexible and less knowledge-related in the lower layer.

A typical example to help on understanding the system approach is the microcontroller-based smart sensor as described in Figure 3.1(b), which combines the sensing element, the signal-processing circuit, and a microcontroller. The sensing element and the signal processor perform the signal processing, for instance, transfer from measurand to electronic quantities, amplification and analog-to-digital conversion. In the microcontroller, the information and a part of the knowledge are processed, such as the performance of the algorithm, calibration, digital filtering and communication. Of course, the knowledge processing is often performed by a central computer.

3.6.2 Mechatronic approach

Mechatronics is defined as an integration of the following [23, 24]:

- mechanics,
- electronics,
- information technology.

The tasks within a mechatronic system are performed both on the mechanical and on the electronic side. Here, interrelations during the design play an important role. Whereas the design and the local arrangement of the mechanical and electronic components in a conventional system are made separately, in a mechatronic system they must be considered as parts of an integrated overall system from the beginning (see Figure 3.14).

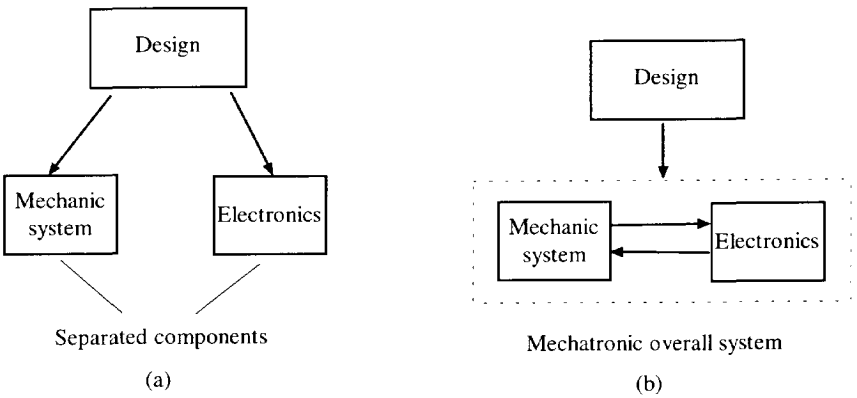

Figure 3.14 Relations during the design of a mechatronic system. (a) Conventional procedure. (b) Mechatronic procedure.

Of special importance for mechatronic systems are the interaction with the mechanical manufacturing process, the dynamics, the resolution, mechanical and thermal robustness, wear resistancy, touchless transfer, miniaturization, and easy transfer to electronic signal processors.

The integration of the sensing elements and the electronic signal processing on a common carrier, for instance, a printed-circuit board or a single chip, becomes more important. This integration has the following advantages:

- low cost,
- small space,
- high accuracy,
- small influence of parasitics and EMC.

Meanwhile, the digital processing of the signal processor allows the programming of noise filtering, linearization of nonlinear characteristics, correction of cross-sensitivities or hysteresis, self-calibration, and compensation of dynamic lags and of drift.

The integration of the information processing for high-performance mechatronic systems requires that the static and dynamic behavior of all components be well

designed. This means that systematic development is started with a model and simulation, and a good design can be achieved by taking the main nonidealities into account.

3.6.3 Systematic design

For a systematic design, firstly, the required specifications of the overall sensor system, such as the type of measurand and the output signal, the accuracy, the resolution, the repeatability, the linearity, the speed, the dimensions, cost, etc., have to be defined in accordance with the practical application. Based on these requirements, a sensor system architecture is found. In this section, as an example, the systematic overall design of the microcontroller-based smart capacitive sensor for the measurement of mechanical quantities is described. As described in Section 3.1, the microcontroller-based smart capacitive sensor is mainly composed of a sensing element, a signal-processing circuit and a microcontroller. The different signals and information are processed in these three elements, described in Section 3.6.1.

After designing the sensor system architecture, the design of the sensing element structure should be based on the requirements of the measurand, the accuracy, the resolution, the dimensions and cost. Then, the relationship between the output(s) and the measurand of the sensing element is characterized. Similarly, the structure and the transfer function of the signal processor are found. This is based on the output signal(s) of the sensing element, the input of the microcontroller and the requirements for the signal processor.

The microcontroller mainly performs the data acquisition and processing, and communication as well as calibration, compensation and linearization.

To obtain a well-designed sensor, it is not enough to design the structures and transfer functions of the elements. Many main nonidealities must be taken into account and their effects should be minimized. During the design process, the mechanical and electronic components must be considered as parts of an integrated overall system from the beginning.

The use of models is very useful to optimize each element and the overall sensor system. For example, for a capacitive sensing element, several physical models can be used to simulate the physical and mechanical nonidealities, such as the electric-field-bending effect, nonflatness, eccentricity, obliqueness and deformation, and to optimize the geometrical parameters of the sensing element. Practical examples of the use of these models are described in Chapter 5, and it is shown that these models are very useful in finding the optimum geometrical parameters. The guarding electrodes, which are used to reduce the electric-field-bending effect and EMI, should be considered as a part of the sensing element. Electronic models for the sensing element are used to simulate its sensing mechanism and the parasitics, such as parasitic capacitances. The results are used to determine or select the input stage of the signal processor. For example, the two-port measurement is used to eliminate the influence of large parasitic capacitance in the measurement of small capacitance (see Section 4.2.2).

For the signal processor, it is necessary to create some models to simulate the nonidealities, for instance offset, gain error, noise, parasitics, nonlinearity, unstability, etc.

Finally, a model of the systematic error of the total system is very useful for the calibration or compensation by the microcontroller. This can further reduce the systematic errors in an effective way. Some practical designs of smart capacitive sensors are described in detail in later chapters.

3.7 Conclusions

A microcontroller-based smart capacitive sensor system can yield a high performance/price ratio in practical applications. The three-layered multiple-electrode structures of capacitive sensing elements are very suited for the measurement of some physical quantities. The use of the two-port measurement and the three-signal technique will effectively improve the sensor system's performance and decrease its cost. The design methods, system approach and mechatronic approach, enable the design of smart capacitive sensors to be easy, standard and flexible. To obtain a high-performance sensor, many main nonidealities must be taken account and their effects should be minimized. During the design process, the mechanical and electronic components must be considered as parts of an integrated overall system from the beginning. The use of models is very useful to optimize each element and the overall sensor system.

References

[1] R.V. Jones and J.C.S. Richards, "The design and some applications of sensitive capacitance micrometers," J. Phys. E: Sci. Instrum., vol.6, 1973, pp. 589-600.

[2] J.C. Maxwell, "A treatise on electricity and magnetism," vol. I, Clarendon Press, Oxford, 1873.

[3] W.Chr. Heerens and F.C. Vermeulen, "Capacitance of Kelvin guard-ring capacitors with modified edge geometry," J. Appl. Phys., vol. 46, 1975, pp. 2486-2490.

[4] W.Chr. Heerens, "Application of capacitance techniques in sensor design," J. Phys. E: Sci. Instrum., vol. 19, 1986, pp. 897-906.

[5] M.H.W. Bonse, F. Zhu and H.F. van Beek, "A long-range capacitive displacement sensor having micrometre resolution," Meas. Sci. Technol. vol. 4, 1993, pp. 801-807.

[6] H.U. Meyer, "An integrated capacitive position sensor," IEEE Trans. Instrum. Meas., vol. 45, no. 2, Apr. 1996, pp. 521-525.

[7] X. Li, G.C.M. Meijer, G.W. de Jong and J.W. Spronck, "An accurate low-cost capacitive absolute angular-position sensor with a full-circle range," IEEE Trans. Instrum. Meas., vol. 45, no. 2, Apr. 1996, pp. 516-520.

[8] G.W. de Jong, G.C.M. Meijer, K. van der Lingen, J.W. Spronck, A.M.M. Aalsma and Th.D.A.J.M. Bertels, "A smart capacitive absolute angular-position sensor," Sensors and Actuators, vol. A41-A42, 1994, pp. 212-216.

[9] X. Li, "Design of smart capacitive sensor with full-circle measurement range," Internal report, Faculty of Electrical Engineering, TU Delft, Aug. 1994.
[10] G.C.M. Meijer, Jaap van Drecht, Paul C. de Jong and Harry Neuteboom, "New concepts for smart signal processors and their application to PSD displacement transducers," Sensors and Actuators, vol. A35, 1992, pp. 23-30.
[11] F.N. Toth and G.C.M. Meijer, "A low-cost, smart capacitive position sensor," IEEE Trans. Instrum. Meas., vol. 41, no. 6, Dec. 1992, pp. 1041-1044.
[12] T. Ohmae, T. Matsuda, K. Kamiyama and M. Tachikawa, "A microprocessor-controlled high-accuracy wide-range speed regulator for motor drives," IEEE Trans. Ind. Elec., vol. IE-29, no. 3, Aug. 1982, pp. 207-211.
[13] J.E. Brignell and A.P. Doreg, "Sensors for microprocessor-based applications," J. Phys. Sci. Instrum., vol.16, 1983, pp. 952-958.
[14] X. Li and G.C.M. Meijer, "A self-calibration technique for a smart capacitive angular-position sensor," in Proc. IEEE IMTC/96, Brussels, Belgium, June 1996, pp. 774-777.
[15] Paul T. Kolen, "Self-calibration/compensation technique for microcontroller-based on sensor arrays," IEEE Trans. Instrum. Meas., vol. 43, no. 4, pp. 620-623, August 1994.
[16] P. Hille, R. Hohler and H. Strack, "A linearisation and compensation method for integrated sensors," Sensors and Actuators, vol. A44, 1994, pp. 95-102.
[17] J. Brignell, "Software techniques for sensor compensation," Sensors and Actuators, vol. A25-A27, 1991, pp. 29-35.
[18] —, "Embedded microcontrollers and processors," INTEL Corporation, 1992.
[19] F. van der Goes, "Low-cost smart sensor Interfacing," Ph.D. Thesis, Delft University of Technology, Apr. 1996.
[20] X. Li, G.W. de Jong, F.N. Toth, F.M.L. van der Goes and G.C.M. Meijer, "Low-cost CMOS interface for capacitive sensors and its application in a capacitive angular encoder," to be published in Analog Integrated Circuits and Signal Processing, Special issue on smart sensor interfaces, 1997.
[21] F.N. Toth, D. Bertels and G.C.M. Meijer, "A low-cost, stable reference capacitor for capacitive sensor systems," IEEE Trans. Instrum. Meas., vol. 45, no. 2, Apr. 1996, pp. 526-530.
[22] E.T. Powner and F. Yalcinkaya, "Intelligent sensors: structure and system," Sensor Review, vol. 15, no. 3, 1995, pp. 31-35.
[23] R. Isermann, "Modeling and design methodology for mechatronic system," IEEE Trans. Mechatronics, vol.1, no.1, March 1996, pp. 16-28.
[24] D.M. Auslander, "What is mechatronics?," IEEE Trans. Mechatronics, vol.1, no.1, March 1996, pp. 5-9.
[25] X. Li, G.C.M. Meijer and G.W. de Jong, "A microcontroller-based self-calibration technique for a smart capacitive angular-position sensor," IEEE Trans. Instrum. Meas., vol. 46, no. 3, June 1997.
[26] G. Brasseur, "A robust capacitive angular position sensor," in Proc. IEEE IMTC/96, Brussels, Belgium, June 1996, pp. 1081-1086.

Chapter 4

Signal-Processing for Capacitive Sensors

4.1 Introduction

The measured value of most capacitors in capacitive sensors is often in the range of 0.1–100 pF, depending on the type of sensor, while the required resolution of these sensors is often better than 10^{-5}. Therefore, the capacitance measurement circuits should have high sensitivity and a low drift as well as a high degree of accuracy, a good linearity and high stability.

Many kinds of capacitance measurement circuits have been developed and most of them belong to the following categories [1]:

- AC bridges
- impedance comparison
- charge/discharge circuits
- resonance circuits
- oscillator circuits

As have been discussed in Chapter 3, a microcontroller-based smart sensor system requires a signal processor with a microcontroller-compatible output. The signal processor based on the oscillator is very suitable to fulfill this requirement. In this chapter, we describe mainly the capacitance-dependent oscillator circuits. The chapter starts with a description of some parasitic-immune measurement techniques and of the oscillator measurement method. Then, the design of a simple, low-cost and high-performance integrated signal processor for the measurement of capacitive sensors, which is based on a relaxation oscillator, is presented. The signal processor, which has multiple inputs for the capacitive sensing elements and a microcontroller-compatible output, has been realized in a 0.7-μm CMOS process. The input stage has been optimized so that relatively large parasitic capacitances are allowable. This signal processor is used in the smart sensors described in Chapters 5 and 6.

4.2 Parasitic-immune measurement methods of capacitance

4.2.1 A practical electrical model of a capacitive sensing element

Usually, a practical capacitive sensor and its connecting wires require shielding and guarding. Shielding is used to reduce the influence of interfering sources by preventing the direct coupling of these sources with the sensor electrodes, or with the connecting wires. Guarding is used to eliminate or to reduce electric-field-bending effects [2 – 7]. Sometimes, a part of the capacitive sensing electrodes are also used as guarding electrodes as is shown, for instance, in the multiple-electrode capacitive sensor system [3, 4, 5]. As a consequence, rather large parasitic capacitances between the two terminals of the capacitor on the one hand and ground at the other hand can occur. Figure 4.1 shows an electrical model of a capacitive sensor. The capacitor C_s is the capacitance to be measured. The capacitors C_{p1} and C_{p2} are the parasitic capacitances. In most applications, the value of these parasitic capacitances are much larger than the capacitance C_s. The values of these parasitic capacitors are application dependent and these values are not very stable. For instance, due to movements of the connecting wires, the parasitic capacitances can easily change. Therefore, the influence of these parasitic capacitors should be eliminated or strongly reduced.

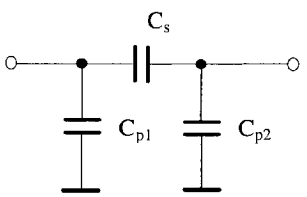

Figure 4.1 An electrical model of the capacitive sensing element.

4.2.2 The two-port measurement technique

The effect of the two parasitic capacitances C_{p1} and C_{p2} can be eliminated by applying a two-port measurement technique[1, 8, 9]. Figure 4.2 shows a typical configuration of this kind of circuit, in which one of the sensor electrodes is connected to a voltage source and the other to the input of a current detector, which has a very low input impedance to ground. The parasitic capacitances C_{p1} and C_{p2} are in parallel with the voltage source and the low input impedance of the current detector, respectively, and thus do not affect the detected current I.

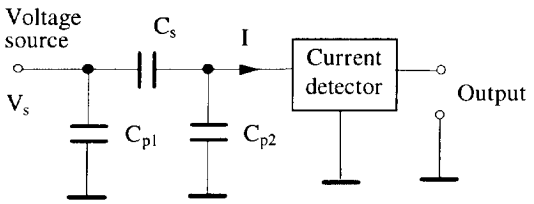

Figure 4.2 The two-port capacitance-measuring circuit.

4.2.3 The active guard technique

Sometimes, particular applications require the use of a capacitive sensor with one earthed electrode usually connected to a shield. In this case, the parasitic capacitance is in parallel to the sensor capacitance. By using a guard which is connected to the same potential as the sensing electrode, the capacitance between the sensing electrode and the shield is eliminated, while the capacitance between the guard and the sensing electrode does not affect the measurement, because there is no voltage over this capacitance [1]. Figure 4.3 shows the outlines of the active guarding technique.

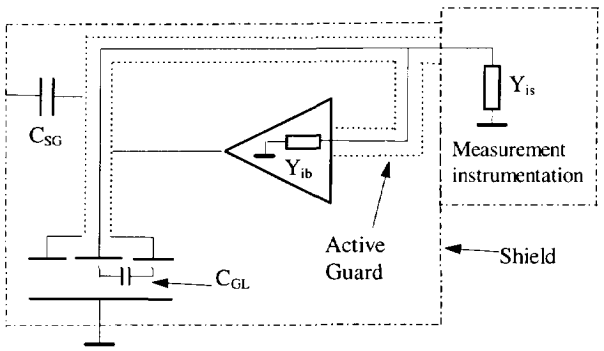

Figure 4.3 Outlines of the active guarding technique.

The main limitation of the active guarding technique, however, is that it cannot eliminate the effect of the input impedances of both the measurement instrument and the guard driving buffer connected to the sensing electrode, Y_{is} and Y_{ib}.

4.3 Oscillation method for capacitance measurement

Figure 4.4 shows a diagram of the oscillation method for the capacitance measurement. C_s is the capacitance to be measured. C_{p1} and C_{p2} are the parasitic capacitances between the terminals of capacitor C_s and ground.

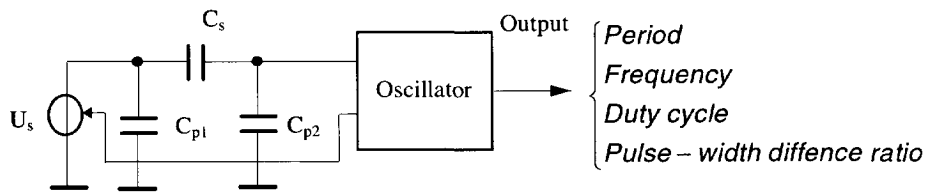

Figure 4.4 A diagram of the oscillation method for the capacitance measurement.

When the excitation signal U_s is grounded, the capacitance measurement is a one-port measurement. If U_s is a voltage source and the input circuit of the oscillator acts as a low-impedance current detector, the two-port measurement will be effective. The output signal of the oscillator is a period, a frequency, a duty cycle or a pulse-width difference ratio, which in all of these cases depends on the capacitance C_s to be measured. The output signal is measured, either by using a digital counter to obtain a digital output, or by using a converter, for instance an FVC, or a filter to obtain an analogue output. Generally, in most applications, the requirements for the capacitance measurement system are:

- low-cost,
- high accuracy,
- high resolution,
- high transfer linearity from the capacitor value to the output signal,
- small effect of parasitic capacitances,
- high stability (short- and long-term).

To date, many oscillating circuits have been developed for the capacitance measurement. Two kinds of often-used oscillating circuits in the capacitance measurement are the charge-balancing oscillator and the relaxation oscillator. This is because of their simplicity, their suitability to be integrated on the chip and their microcontroller-compatible output.

4.3.1 Conventional oscillation methods

4.3.1.1 The RC oscillation method

This is the most popular method used in conventional general-purpose capacitance meters. The circuit types include multivibrators, various timers and phase-locked loops. Generally, these circuits suffer from some common drawbacks: poor immunity to strays, oscillation frequency influenced by the shunting conductance of C_s, poor sensitivity to small capacitance changes, and poor frequency stability. Therefore, the RC oscillation method generally is not suitable for applications requiring a measurement resolution of better than 0.01pF.

4.3.1.2 The LC oscillation method

The LC oscillator can provide measurement frequency ranging from several hundred kHz to a few hundred MHz. Figure 4.5 shows the principle of a typical LC oscillator transducer. The change in the oscillation frequency can be expressed as:

$$\Delta f = -\frac{f_0}{2(C_s + C_p)}\Delta C_s \tag{4.1}$$

where C_p is the overall energy stray capacitance in parallel with C_s, and f_0 is the standing oscillation frequency. The baseline drift of this circuit is mainly due to the stray capacitance influence and drift in the FM demodulator.

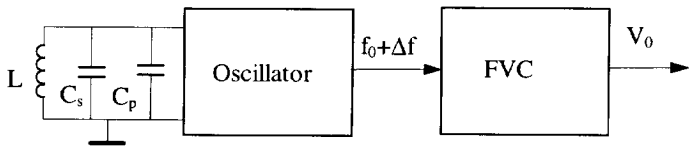

Figure 4.5 The LC oscillation method.

The oscillation frequency of the LC oscillator is not very sensitive to a loss component in parallel with C_s. This , and its capability to produce high oscillation frequencies, make this method useful for applications concerning the measurement of high-loss materials.

The main disadvantages of the above circuit are that the stray capacitance, C_p is included in the measurement, and it is not suitable for integration on the chip.

4.3.2 Charge-balancing oscillation method

Figure 4.6 shows a typical charge-balancing oscillator for the capacitance measurement. It is mainly consists of an SC integrator, a comparator, a controlled current source and a D-type flip-flop as timing circuit. The MOS switches are controlled by a two-phase clock, where φ_1 and φ_2 are two nonoverlapping clock phases.

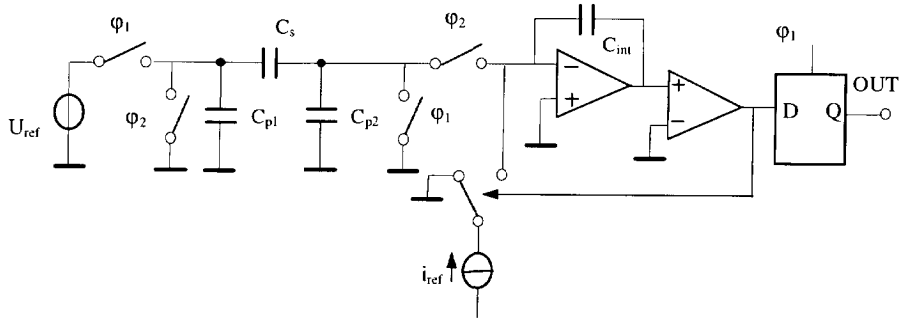

Figure 4.6 A typical charge-balancing oscillator for the capacitance measurement.

The output period equals:

$$T = C_s \frac{U_{ref}}{i_{ref}} \tag{4.2}$$

The advantages of the charge-balancing oscillation method are: high linearity, high resolution and accuracy, stray-immune, microcontroller-compatible output.

4.3.3 Relaxation oscillation method

Figure 4.7 shows a typical relaxation oscillator for the capacitance measurement [10]. In this circuit, C_s denotes the capacitance to be measured and C_{int} is a noncritical value integration capacitance. The circuit consists of a standard SC integrator and a voltage comparator. The switches are controlled by an external clock.

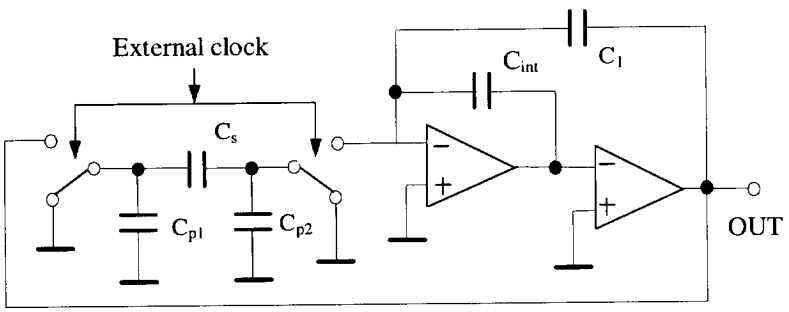

Figure 4.7 A relaxation oscillator for the capacitance measurement.

If one makes the assumption that $C_1 >> C_s$, then the period of the oscillator is given by:

$$T_0 = \frac{C_s}{C_1} \frac{4}{f_{CLK}} \tag{4.3}$$

Some modified versions of this oscillator have been developed and they show its advantages: simplicity, high linearity, high resolution and accuracy, stray-immune, microcontroller-compatible output.

4.4 An integrated smart signal processor for capacitance measurement

Special care has to be taken in processing the small capacitances of the capacitive sensors. In ref [2, 11], measurement systems for capacitive sensors based on a modified Martin oscillator [12] have been presented. These systems offer a relatively high resolution. Moreover, a very low baseline drift has been obtained by using an auto-calibration technique called the three-signal method [13]. However, the limited gain bandwidth product of the applied OPAMP in the input stage limits the

allowable parasitic capacitor value to a value of only a few tens of pF. Moreover, the systems use a large number of discrete components, which prevents their application in low-cost or small-sized equipment.

The use of very high frequencies would increase the values of the signals from the capacitance, but this has the disadvantage that the limited bandwidths of the amplifiers and comparators would impose a limitation on the accuracy of the processing. However, wide bandwidths usually require large current consumption. For these reasons, often, high-performance capacitive elements appear with frequencies below 100 kHz. To handle the small sensor signals in an accurate way, a number of precautions have to be taken. Amongst these precautions are shielding to reduce the effect of EMI, and guarding to limit the effect of the field bending. However, these techniques introduce rather large parasitic capacitances between the two terminals of the capacitor and ground (see Figure 4.2). The values of the two parasitic capacitors are application dependent and are not very stable. For instance, due to movement of the connecting wires, the two parasitic capacitances can easily change. Fortunately, as has been shown in previous papers [1, 2], the effects of these parasitic capacitances can be eliminated by applying the two-port measurement method.

In this method, the effect of the parasitic capacitances C_{p1} and C_{p2} (Figure 4.1) is reduced by applying a low impedance voltage source and a low impedance current detector, respectively. Synchronous detection can be used to limit the effect of both noise and EMI. For a user, the signal processing can be simplified by using a special transducer interface for capacitive sensors. Recently, a Universal Transducer Interface (UTI), based on an asynchronous modulator, has been presented by Van der Goes [14, 15]. The UTI can offer an interface for various types of sensing elements, such as capacitive and resistive types and resistive bridges. The use of some advanced techniques in the UTI, such as two-port measurement, three-signal technique, dynamic element matching technique and synchronous detection technique enables the achievement of a highly accurate measurement of the capacitance at medium and low speeds. Because of the complexity of the circuit, the chip size is relatively large (about 5.5 mm^2).

In this section, an alternative design of such a signal processor for the capacitive sensors, based on a modified Martin oscillator, is presented. The signal processor, which has multiple inputs for the capacitive sensing elements and a microcontroller-compatible output, is realized in a 0.7-μm CMOS process. The input stage has been optimized so that relatively large parasitic capacitances are allowable.

4.4.1 An overview of the measurement system

Figure 4.8(a) shows a diagram of the complete smart sensor system, which is mainly composed of three parts, the capacitive sensing element, the signal processor and a microcontroller as described in Chapter 3.

The capacitive sensing element is a multiple-electrode structure of which the capacitor's values are sensitive to the physical quantities, such as position, speed, force and humidity. The signal processor has a multiple-capacitance input and a single period-modulated output, and includes a nearly linear capacitance-controlled

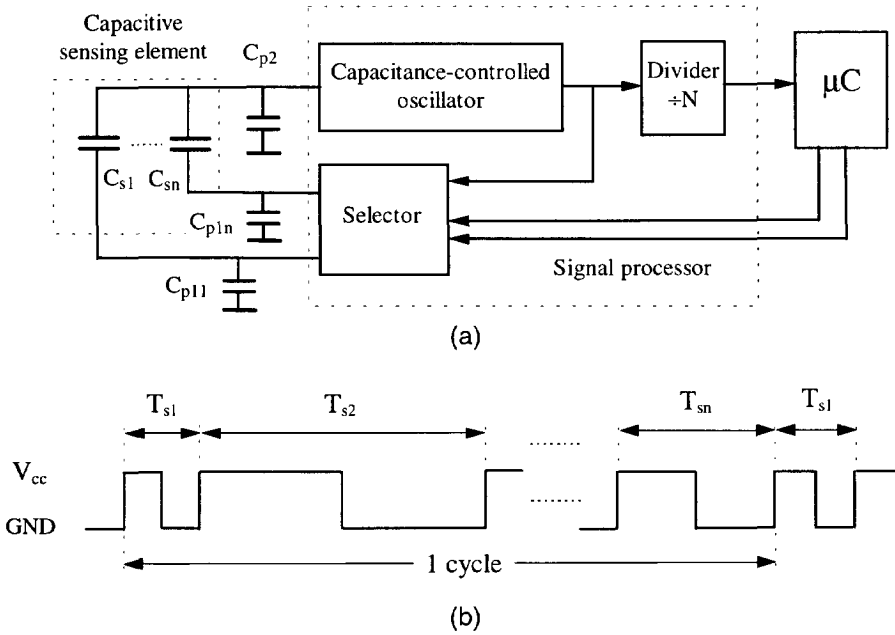

Figure 4.8 (a) A diagram of the smart capacitive sensor system. (b) The waveform at the output of the signal processor.

oscillator, a selector and a frequency divider [17]. In our realization, the capacitance-controlled oscillator and the frequency divider are integrated in a single chip, the selector is integrated in another single chip. The capacitance-controlled oscillator linearly converts the capacitor's values of the sensing element to period-modulated signals. The selector, which is controlled by a microcontroller, selects the capacitance to be measured. A frequency divider decreases the frequency of the output signal of the signal processor to obtain a lower interruption rate of the microcontroller. This increases the throughput and thus the efficiency of the microcontroller. Figure 4.8(b) shows the waveform at the output of the signal processor, where the periods $T_{s1} \cdots T_{sn}$ correspond to the measured capacitances $C_{s1} \cdots C_{sn}$, respectively. Their relationship is:

$$T_{si} = KC_{si} + T_{off} \quad (i = 1, 2, \cdots, n) \tag{4.4}$$

where K and T_{off} are the transfer coefficient and the offset of the signal processor, respectively.

The microcontroller performs the measurement and data processing. It also enables the communication with the outside digital world. In order to eliminate or reduce the effect of parasitic capacitances between the two terminals of capacitor and ground, according to the two-port measurement technique, the input terminal of the capacitance-controlled oscillator should have a very low input impedance to

ground (current detector), and the output terminal of the selector should have a very low output impedance to ground (voltage source).

4.4.1.1 Capacitance-controlled oscillator

In view of its simplicity and the linearity of the capacitor's value-to-period transfer, a relaxation oscillator has been used for the capacitance-controlled oscillator. Figure 4.9 shows the circuit diagram of this capacitance-controlled oscillator [16, 17], which is based on the modified Martin oscillator. It is mainly composed of five parts: an OTA-C integrator, a comparator, a switched current source, a switch-control logic block and a Schmitt trigger buffer. The capacitances $C_{s1} \cdots C_{sn}$ are to be measured. C_{p2} and C_{p3} are parasitic capacitances. The resistors R_{div1} and R_{div2}, and the operational amplifier (OA) supply a voltage bias level of $V_{CC}/2$.

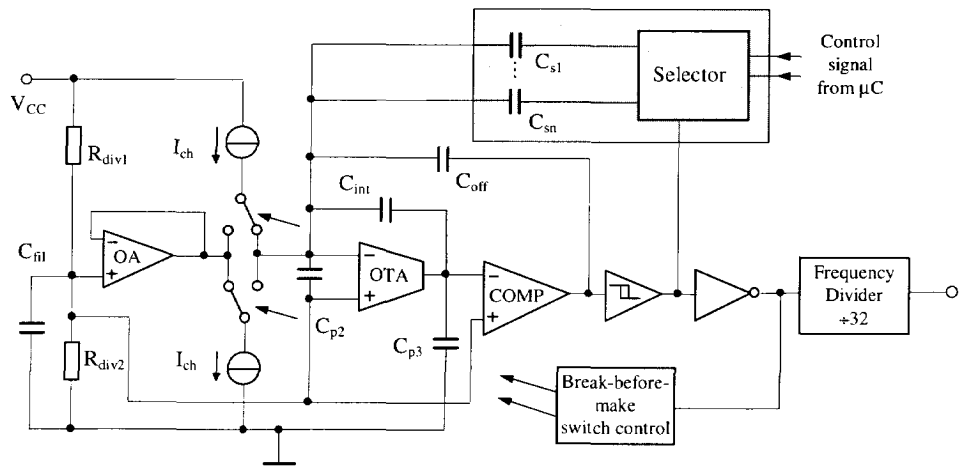

Figure 4.9 A capacitance-controlled oscillator.

The operational transconductance amplifier (OTA) and the capacitor C_{int} form an OTA-C integrator with a low input impedance for the switched current I_{ch}. The output state of the comparator changes as soon as the output voltage of the integrator crosses the value of the voltage bias ($V_{CC}/2$). The charge on the capacitors C_{off} and ΣC_{si} ($i = 1 \cdots n$) is periodically dumped into and undumped from C_{int}. The charge/discharge states of the switched current source are controlled by the switch-control logic which is synchronized with the output signal of the oscillator. In the ideal situation, the relationship between the period of the square-wave signal at the output of the oscillator and the capacitance C_{si} to be measured, can be described by:

$$T_p = 2\frac{(\Sigma C_{si} + C_{off})V_{cc}}{I_{ch}} + 4t_d, \tag{4.5}$$

where V_{CC} is the power supply voltage, I_{ch} is the amplitude of the charge/discharge current, t_d is the delay time in the oscillator loop, which is mainly determined by the delay time of the comparator.

4.4.1.2 Nonlinearities

By using the three-signal approach in the measurement of the capacitances, the effect of most of the nonidealities in the oscillator, which cause additive or multiplicative errors, are eliminated [13]. However, the measurement errors caused by the nonlinearity in the capacitance-controlled oscillator will not be eliminated. The main nonlinearity sources of the capacitance-controlled oscillator and their influence on the measurement result M (formula (3.6)) are discussed in the following.

A. The parasitic capacitance C_{p2} and limited OTA transconductance

One of the main aims of the present design is to allow a large parasitic capacitance at the input terminal. However, due to the finite HF bandwidth of the integrator, the effect of the parasitic capacitance C_{p2} cannot be eliminated completely.

To investigate the effect of the parasitic capacitance C_{p2} and limited OTA transconductance on the nonlinearity, consider the simplified oscillator in Figure 4.10. Suppose that the comparator, charge/discharge current source and voltage source V_{ex} are ideal. The voltage V_{ex} is a square-wave excitation signal which makes a step change at time t_0. The comparator detects when V_{iout} is equal to zero and corresponds to t_0+T_1 and $t_0+T_1+T_2$. The situations of the charge/discharge current source and voltage source V_{ex} are followed by the output of the comparator.

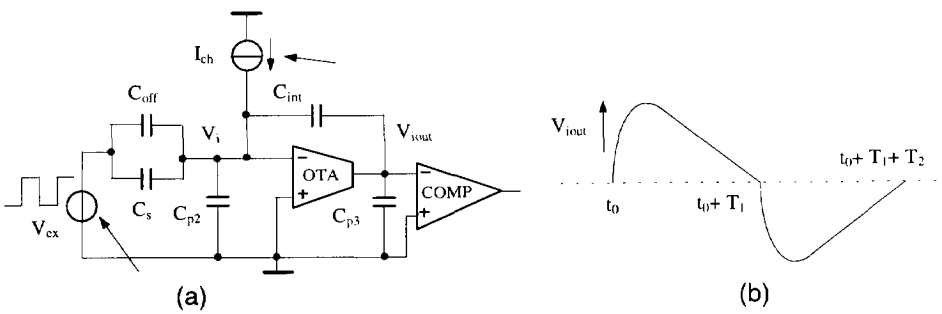

Figure 4.10 A simplified oscillator.

The limited OTA transconductance g_{m0} cause a finite HF bandwidth of the integrator which is expressed by,

$$B = \frac{g_{m0}}{2\pi} \frac{C_{\text{int}}}{C'_{p2}C_{\text{int}} + C'_{p2}C_{p3} + C_{p3}C_{\text{int}}}, \tag{4.6}$$

where T_p is the oscillator period and

$$C'_{p2} = C_{p2} + C_{off} + \Sigma C_{si}. \tag{4.7}$$

This finite HF bandwidth will cause a nonlinearity of the conversion of capacitance C_s to T_1+T_2. Substituting to the measurement result M (formula (3.6)), this will cause a relative nonlinearity ε_{NL} with a value of [17]:

$$\varepsilon_{NL} \cong \left(\frac{1}{2}+\frac{I_{ch}}{V_{cc}C_{off}}\frac{C'_{p2}C_{int}+C'_{p2}C_{p3}+C_{p3}C_{int}}{C_{int}g_{m0}}\right)\exp\left(-\frac{T_p}{2}\frac{C_{int}g_{m0}}{C'_{p2}C_{int}+C'_{p2}C_{p3}+C_{p3}C_{int}}\right). \quad (4.8)$$

To illustrate the effects of the various parameters in equation (4.8) on the nonlinearity, Figure 4.11 depicts, as an example, the ε_{NL} for C_{int} = 60 pF, C_{p3} = 40 pF and T_p = 10 µs, versus the value of the parasitic capacitance C_{p2} for three conditions of the remaining parameter g_{m0}.

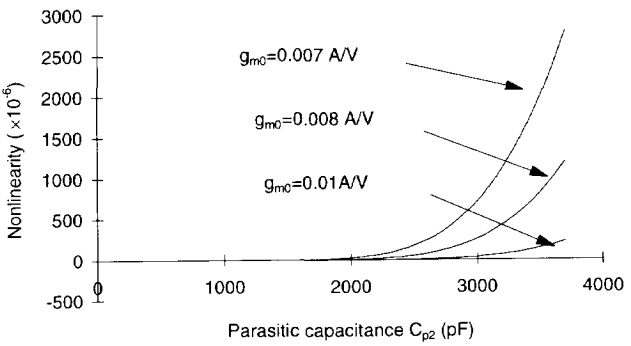

Figure 4.11 The effect of the parasitic capacitance C_{p2} on the nonlinearity according to equation (4.8).

It is shown that a large transconductance of the OTA decreases the effect of the parasitic capacitance C_{p2}, which is in agreement with general feedback theory, and large parasitic capacitance C_{p3} increases the effect of the parasitic capacitance C_{p2}.

The parasitic capacitance C_{p2} also results in an additive term on the period of the oscillator. It is:

$$T_{add} = \frac{2(C_{int}+C_{p3})C'_{p2}}{g_{m0}C_{int}}. \quad (4.9)$$

For constant parasitic capacitances, this additive term will be eliminated by using the three-signal method in the capacitance measurement.

B. Output impedance of switched current source

The output impedance R_{so} of the switched current source results, in combination with the input impedance of the integrator, in an LF pole. This pole, with a time constant $\tau_{LF} = g_{m0}R_{oo}R_{so}C_{int}$ results in a relative nonlinearity ε_{NL} [16]:

$$\varepsilon_{NL} = \frac{T_p}{2g_{m0}R_{oo}R_{so}C_{\text{int}}}, \tag{4.10}$$

where R_{oo} is the output resistance of the OTA. For instance, when substituting some values $g_{m0} = 0.01$ A/V, $C_{int} = 60$ pF, $T_p = 10$ µs, $R_{oo} = 100$ MΩ and $R_{so} = 100$ MΩ, we find that the nonlinearity amounts to only 8×10^{-10}. This shows that no very large output resistances of the OTA and the switched current source are required to obtain a small nonlinearity. It can also be calculated that the effect of the limited bandwidth of the OTA via the output resistance of the switched current source can be neglected.

C. Frequency-variable delay time of comparator

The frequency-variable delay time t_d ($= t_{d0} + aT + bT^2 + cT^3 + \cdots$) of the comparator will cause nonlinearity in the transfer from the capacitance to the period. A constant and linear-variable delay time of the comparator with the period will not cause nonlinearity. However, the second- and higher-order terms of the delay time of the comparator will cause a relative nonlinearity ε_{NL} [17],

$$\varepsilon_{NL} \cong 4T_p(b + \cdots + cT_p + \cdots), \tag{4.11}$$

where b and c are the second- and third-order term coefficients of the delay time of the comparator, respectively.

From the above discussion, it can be concluded that a small nonlinearity requires large values for transconductance g_{m0} and the integrator capacitance C_{int}. However, a large value of the integrator capacitance C_{int} will decrease the value of the output signal of the integrator, which negatively affects the SNR and thus the resolution for a certain measurement time. Meanwhile, formula (4.8) shows that the value of the parasitic capacitance C_{p3} should be as small as possible when a large parasitic capacitance C_{p2} is allowed and a small nonlinearity is required. Formula (4.8) also shows that a small HF nonlinearity component can be obtained by selecting a long oscillator period T_p.

4.4.2 Design of the capacitance-controlled oscillator

4.4.2.1 OTA-C integrator

Figure 4.12 shows the circuit diagram of an OTA-C integrator which is comprised of an operational transconductance amplifier (OTA) and the capacitor C_{int}. The OTA is a simple differential operational transconductance amplifier with two input MOS transistors, M_{11} and M_{13}, and some current mirrors. The current mirrors at the output stage are cascaded to obtain a large output impedance.

For the OTA with a single pole with a time constant τ_p, the transfer function of the integrator is:

$$\frac{V_{out}}{I_{ch}} = -\frac{g_{m0} - sC_{int}(1+s\tau_p)}{sg_{m0}C_{int}\left(1+s(C_{p2}C_{p3}+C_{p2}C_{int}+C_{int}C_{p3})(1+s\tau_p)/(g_{m0}C_{int})\right)}, \tag{4.12}$$

where the capacitances C_{p2} and C_{p3} are the parasitic capacitances at the input and output of the integrator, respectively.

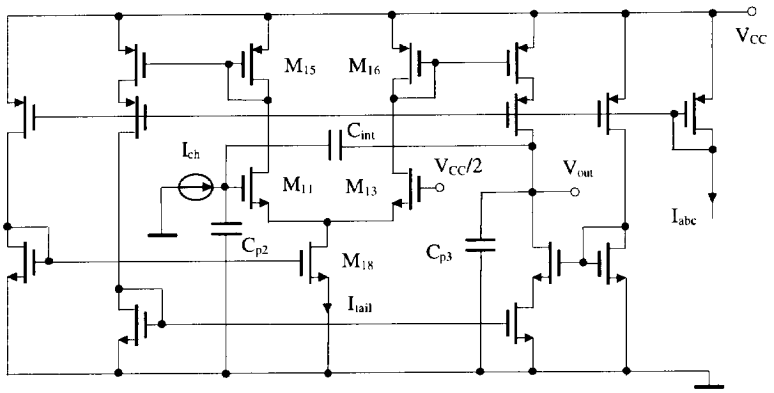

Figure 4.12 A circuit diagram of the OTA-C integrator.

If the transconductance and the bandwidth of the OTA are large enough, formula (4.12) can be simplified to:

$$\frac{V_{out}}{I_{ch}} \cong -\frac{1}{sC_{int}}. \tag{4.13}$$

The large transconductance and the limited bandwidth of the OTA will cause instability of the integrator. The phase margin is [17]

$$Phm \cong 90^0 - \tan^{-1}\left(\sqrt{\frac{\tau_p g_{m0}}{C_{p2}+C_{p3}+C_{p2}C_{p3}/C_{int}}}\right). \tag{4.14}$$

Formula (4.14) shows that to ensure a minimum phase margin of, for instance, 60°, the values of C_{p2} or C_{p3} should exceed a certain minimum value. However, a large value of C_{p3} would seriously affects the nonlinearity of the oscillator as shown by formula (4.8). Therefore, it is preferable to ensure that C_{p2} is not too small. This is realized by connecting a capacitor C_{p2}'' to the input terminal of the oscillator. For instance, consider a phase margin of 60°. When g_{mo} = 0.01 A/V, $f_p = 1/(2\pi\tau_p)$ = 40 MHz, C_{p3} = 40 pF and C_{int} = 40 pF, the value of the capacitance C_{p2} should be larger than 40 pF.

It has been shown that an OTA with large values of the transconductance g_{m0} is required to enable a large parasitic capacitance at the input of the oscillator. A straightforward way to obtain an OTA with a large transconductance value is to increase the width/length ratio *W/L* of the input transistors M_{11} and M_{13}, or the tail

current I_{tail} of these transistors. In our design with W/L = 4000/1.2 and I_{tail} = 500 µA, we obtain $g_{m0} \cong$ 0.01 A/V.

4.4.2.2 Switched current source

Figure 4.13 shows a switched current source which supplies the charge/discharge current I_{ch} for the OTA-C integrator. Simple current mirrors with source resistors are employed to obtain a current source with a sufficiently high output impedance.

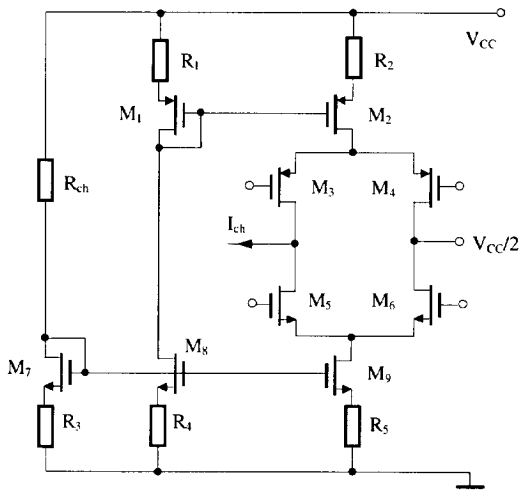

Figure 4.13 Switched current source.

The required amplitude of the charge/discharge current I_{ch} can be determined from the formula (4.5). It is:

$$I_{ch} = \frac{2C_{off}V_{cc}}{T_{off} - 4t_d}, \tag{4.15}$$

where T_{off} is the period of the oscillator when no capacitance to be measured is connected. For instance, when T_{off} = 10 µs, C_{off} = 1.3 pF, V_{CC} = 5 V and t_d = 0.5 µs, then a current I_{ch} of 1.6 µA is required. The sizes of the transistors M_2 and M_9, which supply the charge/discharge current, are chosen according to the following formula:

$$\begin{cases} \dfrac{W_{M2}}{L_{M2}} = \dfrac{K_{pn}}{K_{pp}} \cdot \dfrac{W_{M9}}{L_{M9}} \\ L_{M2} = \dfrac{\lambda_{0p}}{\lambda_{0n}} L_{M9} \end{cases}, \tag{4.16}$$

where K_{pn}, K_{pp}, λ_{0n} and λ_{0p} are the process parameters. The first formula ensures that the V_{gs}-to-I_{DS} transfers of the NMOS and PMOS transistors are equal in spite of

different values of K_p. The second one ensures that the output resistances of the charge and discharge current sources are equal in spite of different values of λ_0.

The cascading transistors M_3 and M_5, M_4 and M_6 are used to obtain the high output impedance R_{so}. Further, they act as switches, which are controlled by a break-before-make logic circuit. The break-before-make logic circuit ensures that at all times the switched current source has a high output impedance.

4.4.2.3 Comparator

A frequency-variable delay time of the comparator will cause nonlinearity in the transfer of the capacitance-controlled oscillator (see formula (4.11)). In our design, a standard cell for the comparator with a delay time of about 0.4μs is used.

4.4.2.4 Simulated results

The circuits shown in Figure 4.12 and Figure 4.13 have been simulated using PSPICE with level 2 models [18]. Table 4.1 shows some parameters and simulated results for the OTA and the switched current source for a 5 V power supply.

Table 4.1 Some parameters and results of the simulation for the OTA and switched current source.

Quantities	Symbol	Value
Transconductance	g_{m0}	12.4 mA/V
Tail current	I_{tail}	500 μA
Output resistance of OTA	R_{oo}	280 MΩ
Bandwidth (-3dB)	f_p	44 MHz
Charge/discharge current	I_{ch}	1.6 μA
Output resistance	R_{so}	1.2 GΩ

A complete oscillator has also been simulated. The comparator was modeled with a constant delay time of 0.4 μs. The oscillation frequency is about 100 kHz. Figure 4.14 shows some periods of some voltages in the oscillator, under the conditions, C_{p2} = 60 pF, C_{off} = 1.3 pF, C_{int} = 40 pF and V_{CC} = 5 V.

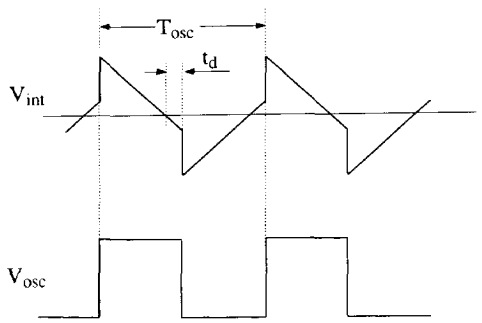

Figure 4.14 Some periods of some voltages in the oscillator.

4.4.3 The selector

In the multiple-capacitance measurement based on the above-mentioned measurement principle, a selector is required to select the capacitance to be measured. According to the two-port measurement method, the outputs of the selector should have a low impedance.

Figure 4.15 shows a diagram of the selector which was especially designed and fabricated for application in the angular-position sensor and which is based on a shift register [16, 17]. It has nine signal outputs, one control output (Shift out), one signal input, one shift input, one clock input and one clear input. The shift input and clock input are used to set up the output state. The shift output can be used as an input for a second selector chip, for instance, when more than nine capacitances are to be measured.

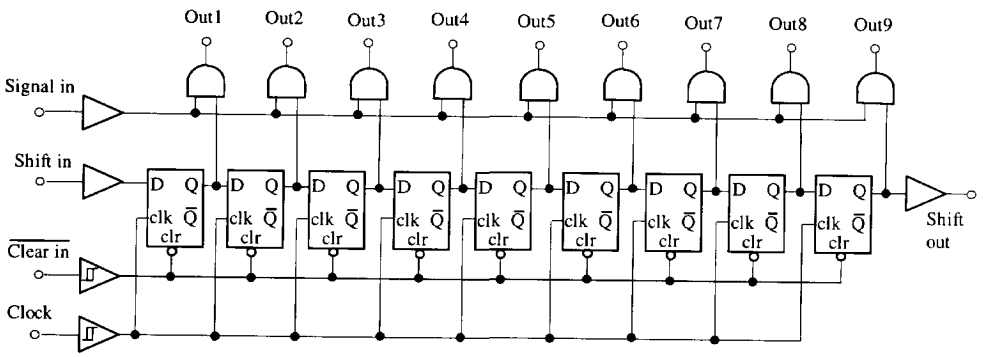

Figure 4.15 Logic diagram of the selector.

Table 4.2 and Figure 4.16 show the truth table and the timing diagram of the selector chip, respectively. Figure 4.16 shows that it is easy to set one capacitance or multiple capacitances to be measured by using the selector.

Table 4.2 Truth table of the selector.

INPUTS				OUTPUTS			
$\overline{CLEAR}$	CLOCK	SHIFT IN	SIGNAL IN	OUT1	OUT2	.....	OUT9
L	×*	×	×	L	L	.....	L
H	↓	×	×	NO CHANGE			
H	↑	L	×	L	OUT1n*	.....	OUT8n
H	↑	H	×	H	OUT1n	.....	OUT8n

* Note: 1. ×: Don't care,

2. *OUT1n ~ OUT8n*: The output of *OUT1 ~ OUT8*, respectively, before the most recent positive transition of the clock.

The selector outputs have a resistance of about 65 Ω, the maximum output

current amounts to about 8 mA. The capacitive load capability is about 10 nF.

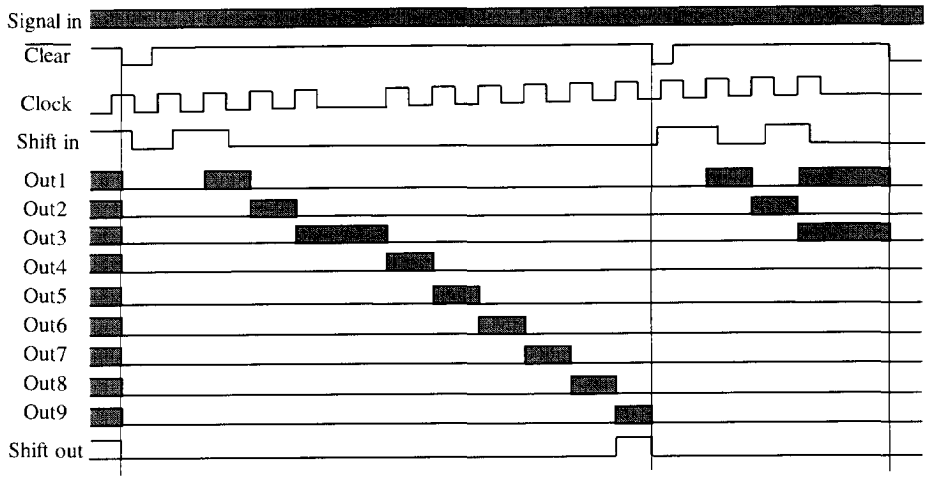

Figure 4.16 The timing diagram of the selector chip.

4.4.4 Implementation and measurement results

A prototype of the proposed signal processor has been fabricated in 0.7-μm technology . The capacitance-controlled oscillator and the selector are implemented on two separate chips to avoid cross-talk effects by the parasitic capacitances between the pins and the sensor electrodes. The internal capacitors values amount to C_{off} = 1.3 pF, C_{int} = 60 pF and C_{p2} = 40 pF, respectively. The signal processor is used to measure multiple capacitances in the range 0 - 2 pF. The standard output buffer with a output current of 8 mA was used as the digital output stage in the oscillator and the selector. The CMOS Schmitt trigger input buffer was used as the input stage of the $\overline{Clear\ in}$ and *Clock* to eliminate the effect of the interference at these inputs. All inputs and outputs are equipped with protection circuits against static discharge and transient excess voltage. Figure 4.17 shows the photomicrographs of the oscillator chip and the selector chip. Table 4.3 shows some important experimental results and parameters.

Table 4.3 Some important experimental results and parameters.

Parameters	Values
Supply voltage	5 V ± 10%
Power consumption	12 mW
Oscillator frequency	90 kHz
Frequency divider number	32
Nonlinearity over 2 pF range	300×10^{-6}
Resolution	11.3×10^{-6}
Allowed parasitic capacitance at input	See Figure 4.19
Allowed parasitic capacitance at output	10 nF

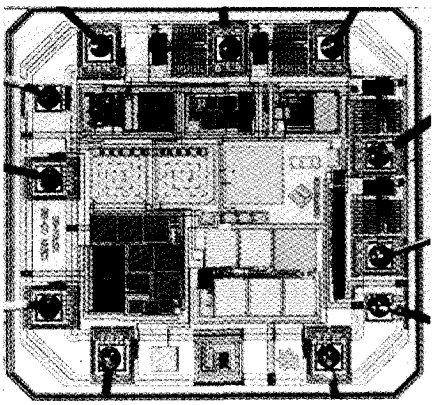

(a)

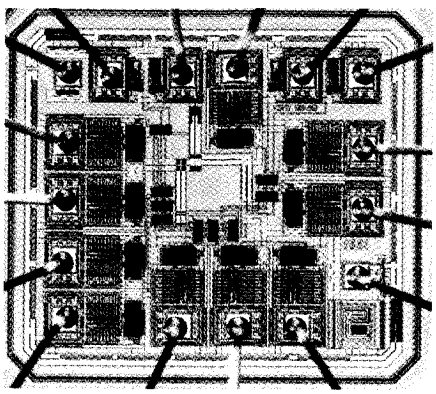

(b)

Figure 4.17 (a) A photomicrograph of the oscillator chip whose size is 1.45×1.5 mm^2, (b) A photomicrograph of the selector chip whose size is 1.25×1.25 mm^2.

The measurement resolution has also been determined as a function of the measurement time by using the three-signal approach (see Figure 4.18). Therefore, in the measurement of the resolution, three phases, T_{Cx1}, T_{Cx2} and T_{off} (C_x = 0) which respectively correspond to C_{x1} of 1 pF, C_{x2} of 1 pF and C_x of 0 pF, have been measured for the different measurement times. The ratio of two capacitance is calculated from $C_{x1} / C_{x2} = (T_{Cx1} - T_{off}) / (T_{Cx2} - T_{off})$. The parasitic capacitance C_{p2} amounts to 20 pF.

For short measurement times, the quantization noise which originates from the sampling by the microcontroller is dominant. For these short times, the resolution is inversely proportional to the measurement time.

The effects of the parasitic capacitance C_{p2} at the input of the oscillator on the nonlinearity is also measured (see Figure 4.19).

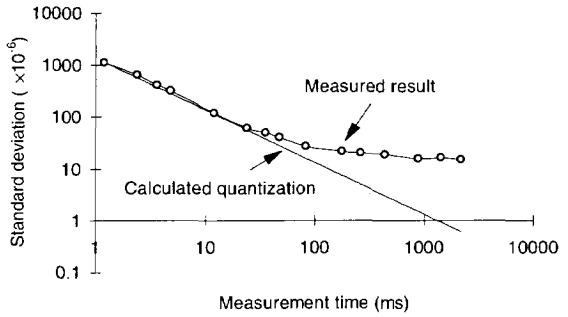

Figure 4.18 Resolution of the ratio of two capacitances versus the total measurement time.

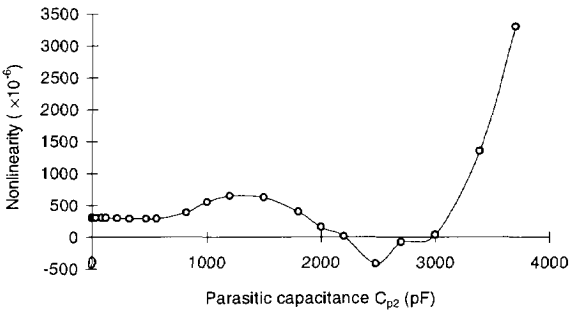

Figure 4.19 The effects of the parasitic capacitance C_{p2} on the nonlinearity.

In Figure 4.19, it is shown that for the large parasitic capacitances (larger than 3 nF) the measured nonlinearity is in agreement with the result calculated from formula (4.8) (see Figure 4.11).

4.4.5 Conclusion

A low-cost CMOS smart signal processor based on Martin relaxation oscillator has been presented for the capacitive sensor. Because the application of the two-port measurement and the optimization of the input stage, the parasitic capacitances of up to about 3 nF are allowed for the measurement of small capacitances. The structure of two separated chips of the signal processor is able to measure several capacitances accurately and to avoid cross-talk effects. The prototypes of the signal processor have been implemented in 0.7-μm CMOS technology. The measured resolution and nonlinearity over a measurement range of 2 pF are 11.3×10^{-6} and 300×10^{-6}, respectively. The remaining nonlinearity can be further reduced by improving the delay time of the comparator and reducing one of the internal parasitic

capacitances. The designed signal processor has been found to be very useful to implement an accurate measurement system.

4.5 Measurement of time-variable capacitance

We have discussed the measurement of nontime-variable capacitance using oscillator circuits in the above sections. However, the measurement of time-variable capacitance is required sometimes, for instance, in capacitive speed sensors [5, 19, 20]. For a time-variable capacitance C_s (see Figure 4.2), the current through this capacitance is

$$i = \frac{\mathrm{d}(C_s U_s)}{\mathrm{d}t} = C_s \frac{\mathrm{d}U_s}{\mathrm{d}t} + U_s \frac{\mathrm{d}C_s}{\mathrm{d}t}. \tag{4.17}$$

When C_s is linearly related to the position, $\mathrm{d}C_s/\mathrm{d}t$ is proportional to the speed. Based on this principle, a capacitive speed measurement with the modified Martin oscillator is possible. This is called the direct $\mathrm{d}C_s/\mathrm{d}t$ (speed) measurement. This method is especially suited for the measurement of moderate speeds.

In ref. [5], it is also reported that a direct $\mathrm{d}C_s/\mathrm{d}t$ (speed) measurement can be performed by using a damped integrator and a comparator (see Figure 4.20).

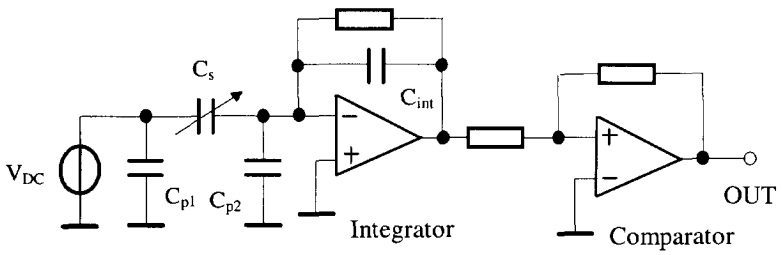

Figure 4.20 The diagram of a circuit especially suited to measuring the high speed of periodic electrode structure.

This method is especially suited to measuring the high speed of periodic electrode structures. The frequency of the output signal from the comparator is proportional to the speed ϑ to be measured:

$$f_0 = \frac{\vartheta}{x_{per}}, \tag{4.18}$$

where x_{per} is the spatial period of the periodic electrode structure. The speed can be obtained by measuring the output frequency f_0.

A measurement method especially suited to low speed has been presented in ref. [19, 20]. Its working principle is discussed in detail in Chapter 7 and two applications of this method are presented in Chapters 7 and 8.

References

[1] S.M. Huang, M.S. Beck, R.G. Green, A.L. Stott, "Electronic transducers for industrial measurement of low value capacitances," J. Phys. E: Sci. Instrum., vol. 21, Oct. 1988, pp. 242-250.
[2] F.N. Toth and G.C.M. Meijer, "A low-cost, smart capacitive position sensor," IEEE Trans. Instrum. Meas., vol. 41 no. 6, Dec. 1992, pp.1041-1044.
[3] X. Li, G.W. de Jong, G.C.M. Meijer, "An accurate smart capacitive angular-position sensor with a full circle range," in Proc. IEEE, IMTC/95, Boston, USA, Apr. 1995, pp.80-83.
[4] X. Li, G.C.M. Meijer, G.W. de Jong and J.W. Spronck, "An accurate low-cost capacitive absolute angular-position sensor with a full-circle range," IEEE Trans. Instrum. Meas., vol. 45, no. 2, April 1996, pp. 516-520.
[5] G.W. de Jong, "Smart capacitive sensor (physical, geometrical and electronic aspects)," Ph.D. Thesis, Delft University of Technology, April 1994.
[6] W. Ch. Heerens, "Application of capacitance technology in sensor design," J. Phys. E: Sci. Instrum., vol. 19, 1986, pp. 897-906.
[7] W. Ch. Heerens and F.C. Vermeulen, "Capacitance of Kelvin guard-ring capacitors with modified edge geometry," J. Appl. Phys. vol. 46, no. 46, American Institute of Physics, June, 1975, pp. 2486-2490.
[8] A.M. Thompson, "The precise measurement of small capacitances," IRE Trans. Instrum., 1-7(3-4), 1958, pp. 245-253.
[9] M.C. McGregor, J.F. Hersh, R.D. Cutkosky, F.K. Harris and F.R. Kotter, "New apparatus at the national bureau of standards for absolute capacitance measurement," IRE Trans. Instrum., 1-7(3-4), 1958, pp. 253-2261.
[10] K. Martin, "A voltage-controlled switched-capacitor relaxation oscillator", IEEE J. Solid-State Circuits, vol. 16, no. 4, Aug. 1981, pp. 412-413.
[11] F.N. Toth, H.M.M. Kerkvliet, G.C.M. Meijer, "Ultra-linear, low-cost measurement system for multi-electrode pF-range capacitor," in Proc. IEEE, IMTC/95, Boston, USA, Apr. 1995, pp. 512-515.
[12] J. van Drecht, "Relaxatie oscillator," Pat. Appl. 91.01076, The Netherlands, 1991.
[13] G.C.M. Meijer, J. van Drecht, P.C. de Jong and H. Neuteboom, "New concepts for smart signal processors and their application to PSD displacement transducers," Sensors and Actuators, vol. A35, 1992, pp. 23-30.
[14] F. van der Goes, "Low-cost smart sensor interfacing," Ph.D. Thesis, Delft University of Technology, Apr. 1996.
[15] F. van der Goes, "A novel low-cost capacitive-sensor interface," IEEE Trans. Instrum. Meas., vol. 45, no. 2, April 1996, pp. 536-540.
[16] G.W. de Jong, "Data sheet CapCo selector chip set for interfacing capacitive sensors," Technical report, Delft University of Technology, March 1995.
[17] X. Li, G.W. de Jong, F.N. Toth, F.M.L. van der Goes and G.C.M. Meijer, "Low-cost CMOS interface for capacitive sensors and its application in a capacitive angular encoder," to be published in Analog Integrated Circuits and Signal Processing, Special issue on smart sensor interfaces, 1997.

[18] —, "The Design Center, version 5.3," MicroSim Corporation, Jan. 1993.
[19] X. Li and G.C.M. Meijer, "A new method for the measurement of very low speeds using a multiple-electrode capacitive sensor," in Conference Digest, CPEM'96, Braunschweig, Germany, June, 1996, pp. 349-350.
[20] X. Li, G.C.M. Meijer and G.W. de Jong, "A new method for the measurement of low speed using a multiple-electrode capacitive sensor," IEEE Trans. Instrum. Meas., vol. 46, no. 2, April 1997.

Chapter 5

Capacitive Angular-Position Sensor

5.1 Introduction

In previous papers [1–12], it has been shown that with capacitive sensing elements rather high accuracy can be obtained. The remaining inaccuracy is mainly caused by the electric-field-bending effect and mechanical errors. The use of guarding electrodes is very important to reduce the influence of the electric-field bending and also of external interfering signals [1– 8]. However, guarding electrodes cannot completely eliminate the influence of the electric-field bending. Even when using well-designed guarding electrodes, the electric-field-bending effect is still one of the major reasons for the remaining nonlinearity of capacitive position sensors. A symmetrical and redundant structure of the sensing element can drastically reduce the mechanical errors, such as the nonflatness, obliqueness and eccentricity of the electrodes [5 – 9, 11].

This chapter presents a low-cost, high-performance smart capacitive angular-position sensor with a full circle measurement range. This novel design includes a modified sensing element, a special algorithm and the high-performance signal processor described in Chapter 4. Major error sources of the capacitive sensor, such as the electric-filed-bending effect and nonflatness, eccentricity, pattern error and obliqueness of the electrodes, are discussed in detail to show how an optimum sensing element structure can be obtained. The application of an advanced self-calibration technique [13, 25] further reduces the remaining systematic inaccuracy.

5.2 Basic principle of smart capacitive linear and angular position sensors

5.2.1 Systematic structure of a smart capacitive sensor

As described in Chapters 2 and 3 for the smart sensor, Figure 5.1 shows a schematic diagram of the smart capacitive position sensor. It is mainly composed of three parts: the capacitive sensing element, a signal processor and a microcontroller.

The capacitive sensing element is a multiple-electrode structure the capacitor values of which are sensitive to the position to be measured.

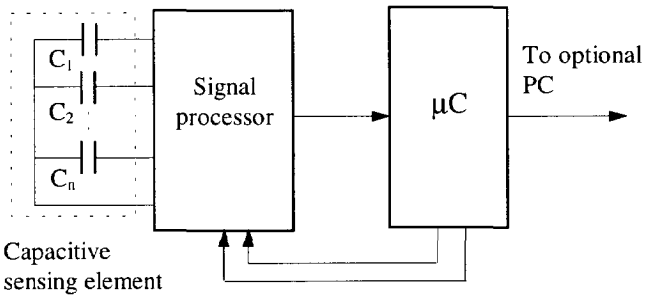

Figure 5.1 Schematic diagram of the smart capacitive position sensor.

The signal processor has a multiple-capacitance input and a single period-modulated output, and includes a nearly linear capacitance/period converter, which linearly converts the capacitor's values of the sensing element to period-modulated signals.

The microcontroller performs the measurement of the periods of the output signal of the capacitance/period converter, the position calculation and the calibration. It also enables the communication with the outside digital world.

5.2.2 Capacitive sensing element

As discussed in Chapter 3, and comparing the advantages of various electrode structures of capacitive sensing elements, the three-layered multiple-electrode structure is employed in our capacitive position sensor. Figure 5.2 shows a schematic drawing of the capacitive sensing element with a multiple-segment electrode structure [6, 8].

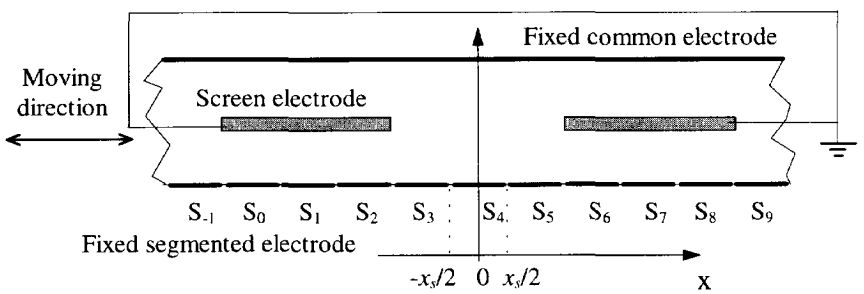

Figure 5.2 A schematic drawing of the capacitive sensing element with a multiple-segment electrode structure.

It mainly consists of three electrodes:

- a fixed common electrode with a single conductor,
- a fixed segmented electrode with multiple segments which have the same linear (or angular) width (x_s),
- a grounded moving screen electrode, the position of which is to be measured.

The capacitors are formed between the common electrode and the segmented electrode. The grounded moving screen electrode shields certain electrode segments from the common electrode and so decreases the capacitance between these electrodes significantly. Change in these capacitances is a measurement to determine the position (x_p) of the grounded moving electrode. Grounding of the moving screen electrode can be achieved by using a sliding contact.

5.2.3 Measurement procedure

To explain the measurement procedure, we suppose that the moving screen electrode is in the position shown in Figure 5.2. The relation between the measured position x_m, the capacitances and the measurand x_p is represented by the equation [6, 8]

$$\frac{x_m}{x_s} = \frac{(C_{s5} + C_{s6}) - (C_{s2} + C_{s3})}{2(C_{s4} - C_{s1})} \cong \frac{x_p}{x_s} \qquad (-\frac{1}{2} \le \frac{x_m}{x_s} \le \frac{1}{2}), \tag{5.1}$$

where x_s is the width of one segment, and $C_{s1} \cdots C_{s6}$ are respectively the capacitances between the common electrode and six adjacent electrode segments ($S_1 \cdots S_6$).

The measurement using formula (5.1) is called *an accurate fine measurement*. In this relationship, because of the use of the **R**atio of **T**wo **L**inear **C**ombinations of the **C**apacitances (RTLCC), the first-order term of the electric-field-bending effect is completely eliminated, and its second-order term is also partly eliminated. In addition to this, its advantages are:

- additive (offset) errors, spatial drift and spatial low-frequency noise in the capacitances ($C_{s1} \cdots C_{s6}$) are eliminated or at least significantly reduced.
- common multiplicative errors (gain errors) in the numerator and denominator are eliminated.

If the nonidealities of the sensing element and the electric-field-bending effect are neglected, then $x_m = x_p$.

The validity of formula (5.1) is limited to the measurement range of a single segment width (x_s). Outside this range, other appropriate capacitors are selected. With these capacitors, the position is calculated in a similar way. The procedure for selecting the appropriate capacitors is called *the first coarse measurement* which determines where is the center of the window of the moving screen electrode. Consequently, the resolution of this coarse measurement is only $\pm x_s/2$.

In the practical measurement of the position, firstly, the capacitances of the sensing element are converted to output periods of the signal processor, then these periods are measured by the microcontroller. The measured position is calculated from these measured periods [8]. As the signal processor described in Chapter 4, let us suppose that the signal processor has a linear transfer function for capacitance C to period T, which can be denoted by

$$T = kC + T_{off}, \tag{5.2}$$

where T_{off} is the period of the output signal of the signal processor when no capacitance is connected to be measured and k is the linear-transfer coefficient. Then from

equations (5.1) and (5.2), the relation between the measured position and the measured periods is represented by:

$$\frac{x_m}{x_s} = \frac{(T_{s5} + T_{s6}) - (T_{s2} + T_{s3})}{2(T_{s4} - T_{s1})}, \qquad (-\frac{1}{2} \le \frac{x_m}{x_s} \le \frac{1}{2}). \tag{5.3}$$

It is shown that the measured position is immune to the multiplicative errors, offset, drift and low-frequency noise caused by the signal processor also.

The operational principle described above is suited to be applied to highly accurate capacitive-both linear and angular-position sensors with a wide measurement range.

In remaining part of this chapter, we focus our attention in particular on the angular sensors.

5.3 Electrode structure of an angular-position sensing element

5.3.1 Structure of the sensing element

A simplified structure of the capacitive angular sensing element, which consists of three parallel discs, is shown in Figure 5.3.

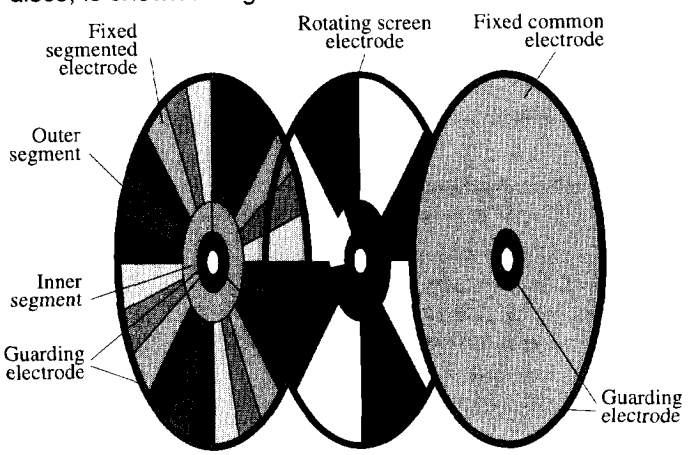

Figure 5.3 A simplified structure of the sensing element.

The common electrode is a single conductor. The segmented electrode is composed of 24 identical outer segments with a width of 15°, and three identical inner segments with a width of 120°. The rotating screen electrode is equipped with four outer windows and one inner window. The angular position of this screen electrode is to be measured.

The inner window is connected to one of the outer ones, forming the specially shaped opening shown in Figure 5.3. The four outer windows are equidistant in

angle and have the same area. The four outer windows on the screen electrode, which interact with the 24 outer segments on the segmented electrode, are used for *a very accurate fine measurement*, and *a first coarse measurement*. The resolution of the first coarse measurement amounts to $\pm x_s/2 = \pm 7.5°$.

The inner window, which corresponds to the three inner segments on the segmented electrode, is used for *a second coarse measurement* which has a resolution of $\pm 4x_s = \pm 60°$.

The 24 outer segments on the segmented electrode are divided into six groups with four segments each. The four segments in each group, which in Figure 5.3 have the same gray level, have a mutual pitch of a quarter of a circle. These four segments are connected, resulting in six group capacitors between the common electrode and outer segments on the segmented electrode, corresponding to the capacitances ($C_{s1} \cdots C_{s6}$) in formula (5.1).

The use of these cross-quad group capacitors significantly reduces the influence of both the stochastic mechanical errors and the systematic mechanical errors, such as the eccentricities, the nonflatness and the obliqueness of the electrodes. This technique has earlier been described in [5, 6]. However, the measurement range was limited to only 90°. Therefore, in the new sensor described here, the three inner segments on the segmented electrode, and one inner window on the rotating screen electrode, are applied for *a second coarse measurement* to determine in which quadrant the inner window is positioned. This extends the measurement range to the full circle (360°). Three additional capacitors (C_{c1}, C_{c2}, and C_{c3}) are formed between the common electrode and three inner segments on the segmented electrode.

As a consequence, three other capacitances (C_{c1}, C_{c2}, and C_{c3}) have to be measured. Therefore, in total, nine capacitances are measured in order to obtain an absolute angular position over the full measurement range of 360°. These nine capacitors' values are converted to nine periods by the signal processor. The microcontroller measures these nine periods and calculates the position to be measured.

5.3.2 Electric model of the sensing element

The diagram of the electric model of the sensing element structure is shown in Figure 5.4.

The capacitances C_{sisj} ($i, j = 1, 2, \cdots n$) represent the capacitances between the segments on the segmented electrode. The capacitances C_{sig} ($i = 1, 2, \cdots n$) are the capacitances between the segments on the segmented electrode and the ground. The capacitance C_{cg} is the capacitance between the common electrode and the ground.

In practical measurements, the capacitances (C_{si} ($i = 1, 2, \cdots n$)) are sequentially measured one by one. If one of them is measured, other segments will be electrically grounded. These grounded segments now play the part of the guarding electrodes. Then a two-port configuration for capacitance C_{si} is formed, as shown in Figure 5.5.

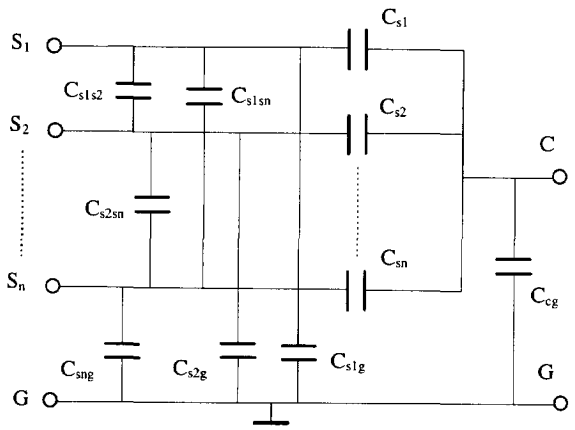

Figure 5.4 The diagram of the electrical model of the sensing element.

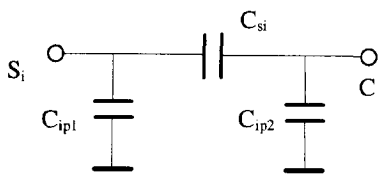

Figure 5.5 A simplified electric model of capacitance (C_{si}) to be measured.

The two parasitic capacitances are

$$C_{ip1} = C_{sig} + \sum_{j=1}^{n} C_{SiSj} \quad (j \neq i), \tag{5.4}$$

$$C_{ip2} = C_{cg} - C_{Si} + \sum_{j=1}^{n} C_{Sj}. \tag{5.5}$$

Generally, the values of these parasitic capacitances are much larger than the capacitance C_{si}. Their influences can be obviated by applying the two-port measurement technique and the appropriate measurement circuit as described in Chapter 4.

5.4 Nonidealities

The sources of the nonidealities in the sensor system described in Sections 5.2 and 5.3 can be divided into four categories:

- physical errors in the sensing element,
- mechanical errors in the sensing element,

- geometrical errors in the sensing element, which are caused by nonidealities in the etching process,
- electronic measurement system errors.

The physical errors are embodied in the electric-field-bending effect. Due to this effect, the capacitances between the completely shielded segments and the common electrode are not zero, and the capacitances between the nonshielded segments and the common electrode are less than in the case of a homogeneous field.

By applying a guarding technique and using an appropriate algorithm, the influence of the electric-field-bending effect can be reduced. Although the algorithm described by formula (5.1) can reduce the influence of the electric-field-bending effect, this effect can be further reduced by modifying formula (5.1) into:

$$\frac{x_m}{x_s} = \frac{(C_{s5} + C_{s6}) - (C_{s2} + C_{s3})}{2(C_{s4} - C_{s1}) + \alpha(C_{s2} + C_{s4} + C_{s6} - C_{s1} - C_{s3} - C_{s5})}, \quad (-\frac{1}{2} \le \frac{x_m}{x_s} \le \frac{1}{2}), \tag{5.6}$$

where α is called the fine-tuning factor ($0 \le \alpha << 1$).

Here, the appropriate fine-tuning factor will minimize the influence of the electric-field-bending effect. In our application, this optimal value for α amounts to 0.0328, which is found by a semi-empirical trial-and-error method.

The mechanical errors mainly consist of the nonflatness of the surface of the electrodes in the sensing element, the eccentricity, the obliqueness of the electrodes and the deformation of the moving screen electrode. The influence of these systematic mechanical errors as well as the influence of the stochastic mechanical errors, are significantly reduced by using the cross-quad configuration in the sensing element (see Figure 5.3).

Moreover, the sensitivities of the nonlinearity due to the electric-field-bending effect for certain geometrical parameters of the sensing element, such as electrode distance, position of the rotating screen electrode in the vertical direction and the radial sizes of the electrodes, are the opposite of those due to the nonflatness [8, 9, 10]. Thus, it is possible to optimize the geometry for the effect of electric-field bending and the nonflatness in order to minimize the total inaccuracy of the sensor.

The geometrical errors occur in the geometrical structure of the sensing element in the etching process. These errors may originate from: the pattern errors and frayed edges of the electrodes, and the presence of gaps and vias on the electrodes.

In Sections 5.6, 5.7 and 5.8, we discuss in detail the influences of these nonidealities on the accuracy of the capacitive sensor.

5.5 The measurement algorithm

The microcontroller is used to measure the periods of the output signal of the processor, to calculate the position, and to communicate with the outside digital world. The calculation of the absolute angular position from the measured nine periods is performed in three steps: an accurate fine measurement over a range of 15°, and a first and a second coarse measurement over ranges of 90° and 360°, respectively. To

measure the position, we can apply direct algorithm which needs nine measurements or indirect algorithm which needs seven measurements.

5.5.1 The direct 9-measurement algorithm

In direct 9-measurement algorithm, by direct measurement of six periods ($T_{s1} \cdots T_{s6}$) corresponding to the capacitances ($C_{s1} \cdots C_{s6}$), the accurate fine measurement is performed using formula (5.3) without fine tuning, or (5.6) with fine tuning. With the first coarse measurement it is found in which circle segment i (i = 0, 1, ··· 5) the angular position is situated. This is done by comparing the six measured values of the periods ($T_{s1} \cdots T_{s6}$). After the first coarse measurement, the position is accurately known over a range of 90°. The second coarse measurement determines in which quadrant q (q = 0, 1, ··· 3) the angular position is situated by comparing the three measured values of the periods ($T_{c1} \cdots T_{c3}$). Finally, the measured absolute angular position φ_m is found using the equation

$$\varphi_m = (\frac{\varphi_{mi}}{\varphi_s} + i + \frac{1}{2}) \times 15° + q \times 90°, \tag{5.7}$$

where φ_{mi}/φ_s is the result of the accurate fine measurement within one segment width. The variable φ is used to represent the angular dimension in the angular position sensor, but variable x can have both linear and angular dimensions. Figure 5.6 shows the procedure of this measurement algorithm.

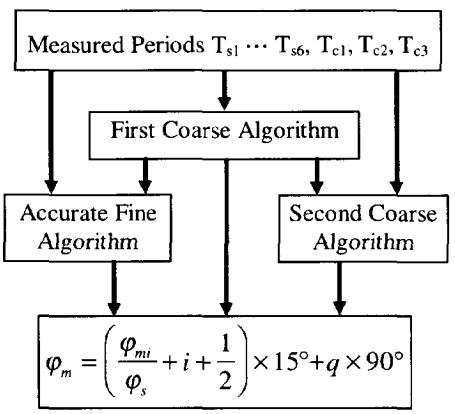

Figure 5.6 The procedure to perform the direct 9-measurement algorithm.

5.5.2 The indirect 7-measurement algorithm

In the indirect 7-measurement algorithm, groups of capacitors are measured in certain combinations. The accurate fine measurement is performed by measuring only four periods ($T'_{s1} \cdots T'_{s4}$) corresponding to the capacitances $C_{s1}+ C_{s2}+ C_{s3}$, $C_{s3}+ C_{s4}+ C_{s5}$, $C_{s5}+ C_{s6}+ C_{s1}$ and $C_{s2}+ C_{s4}+ C_{s6}$, and using formula (5.8) without fine tuning or formula (5.9) with fine tuning.

$$\frac{\varphi_m}{\varphi_s} = \frac{T'_{s3} - T'_{s1}}{T'_{s2} + T'_{s4} - T'_{s1} - T'_{s3}} \qquad (-\frac{1}{2} \le \frac{\varphi_m}{\varphi_s} \le \frac{1}{2}), \tag{5.8}$$

$$\frac{\varphi_m}{\varphi_s} = \frac{T'_{s3} - T'_{s1}}{(T'_{s2} + T'_{s4} - T'_{s1} - T'_{s3}) + \alpha'(3T'_{s4} - T'_{s1} - T'_{s2} - T'_{s3})}, \quad (-\frac{1}{2} \le \frac{\varphi_m}{\varphi_s} \le \frac{1}{2}), \tag{5.9}$$

where the periods $(T'_{s1} \cdots T'_{s4})$ are:

$$\begin{aligned} T'_{s1} &= k(C_{s1} + C_{s2} + C_{s3}) + T_{off} \\ T'_{s2} &= k(C_{s3} + C_{s4} + C_{s5}) + T_{off} \\ T'_{s3} &= k(C_{s5} + C_{s6} + C_{s1}) + T_{off} \\ T'_{s4} &= k(C_{s2} + C_{s4} + C_{s6}) + T_{off} \end{aligned}, \tag{5.10}$$

and

$$\alpha' = \alpha / 2. \tag{5.11}$$

The measurement to be selected for these multiple capacitances is easily performed by using the selector chip described in Chapter 4.

The first coarse measurement is performed by comparing the four measured values of the periods $(T'_{s1} \cdots T'_{s4})$. For the second coarse measurement, the procedure is the same as that in the direct 9-measurement algorithm.

Apart from the advantages of the direct 9-measurement algorithm, the 7-measurement algorithm offers some additional advantages:

- fewer measurements,
- avoidance of small capacitance measurement,
- more reduction of the electric-field-bending effect.

5.6 The influence of various geometrical parameters that occurs due to the electric-field-bending effect

5.6.1 Introduction

It can be shown that, by applying new concepts, with capacitive sensor elements a rather high degree of accuracy can be obtained. However, the electric-field-bending effect is still one of the major reasons for the remaining inaccuracy of capacitive sensors, even though well-designed guarding electrodes are used.

In this section, for the capacitive angular-position sensor described in Section 5.3, the influences of geometrical parameters on the nonlinearity, which originates from the electric-field-bending effect, are discussed in detail by analyzing the physical properties of the capacitive elements. The discussion is limited to the accurate fine measurement where we only consider the outer segments on the segmented electrode (Figure 5.3). The influence of small asymmetry of the inner part in the sensing element is ignored. It is shown that it is very helpful to predict the influences

of geometrical nonidealities and how to optimize the geometrical parameters of the sensing element [10, 14].

For a proper analysis of the relation between the capacitances and the geometrical parameters, a physical model and mathematical tools are required. Therefore, the analysis in this section starts with a physical model of the capacitive angular-position sensor. Next, a complete description of potentials, charge densities and capacitances for a complex symmetrical electrostatic system is obtained by solving Laplace's equation. A numerical analysis of the influence of geometrical parameters on the nonlinearity of the capacitive angular-position sensor is presented.

5.6.2 Physical model of the sensing element

Generally, it is difficult to find an analytical solution for a three-dimensional electrostatic-field problem. However, when the potential distribution in the geometry depends only on two-dimensional coordinates, and when there is a homogeneous permittivity inside, an analytical solution can usually be found [1, 15].

Fortunately, the electrode configuration which is shown in Figure 5.3 can be simplified to a two-dimensional structure, and the electrostatic-field problem in polar coordinates is transformed into one in rectangular coordinates.

If the dimensions of the segmented and common electrodes in the radial direction are much larger than the electrode distances and larger than the dimensions of the electrodes in the tangent direction, we can simplify the electrostatic-field problem by supposing that the potential is not directly affected by the radial dimension r at all, the effect of the radial dimension r on the potential is indirectly taken into account via the tangent dimension [6]. A two-dimensional model in rectangular coordinates corresponding to the three-dimensional structure shown in Figure 5.3 is shown in Figure 5.7, which is symmetrical with the y-axis.

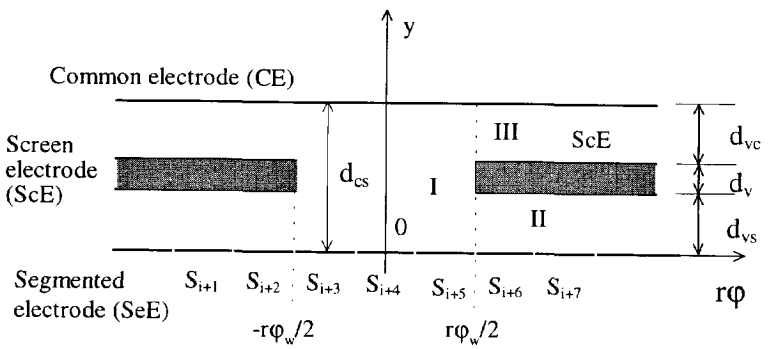

Figure 5.7 A cross-view of a part of the sensing element.

In this figure, φ_w is the angular width of the screen windows, d_{cs} the distance between the common and the segmented electrodes, d_v the thickness of the screen electrode, d_{vs} the distance between the screen and the segmented electrodes, d_{vc} the distance

between the common and the screen electrodes. Now, the parameter r is supposed to be constant. Then $r\varphi$ is the coordinate in the tangent direction at a radial distance r. Thus only the two-dimensional Laplace's equation has to be solved in rectangular coordinates.

In order to calculate the capacitance between the common electrode (CE) and the segmented electrode (SeE), we choose the common electrode as the transmitting electrode with potential U_0 and the segmented electrode as the receiving electrode with potential 0 (is grounded). The effect of the gap between two adjacent segments on the segmented electrode is neglected. The screen electrode (ScE) is also connected to ground.

For the total solution of this two-dimensional electrostatic-field problem, the configuration is divided into three areas I, II and III (see Figure 5.7) with generally different boundary conditions. For both $\varphi = \varphi_w/2$ and $\varphi = -\varphi_w/2$ within the range $0 < y < d_{cs}$, we assume that the potential is a continuous piecewise-linear potential, taken as a basic triangular-shaped function. The accuracy of this approximation is verified by the numerical calculation described in Section 5.6.5. The potential function is shown in Figure 5.8.

Figure 5.8 The piecewise-linear approximation for the potential at $\varphi = \varphi_w/2$.

In this model, the potential U_0 represents the potential of the transmitting electrode. The potentials U_1, U_2 and positions d_1, d_2 are auxiliary variables which are determined by the potential U_0, the geometrical parameters (d_{cs}, d_v, d_{vs} and d_{vc}) and the width of the screen windows φ_w. In the following section, we give the solution of the two-dimensional electrostatic-field problem and discuss the relations between U_1, U_2, d_1, d_2 and the geometrical parameters.

5.6.3 The solution of the two-dimensional electrostatic-field problem

By solving Laplace's equation in the areas I, II and III and according to Gauss flux theorem [4], for the distribution of the surface charge density σ_l[C/m^2] on the surface of the receiving electrode (SeE) ($y = 0$) it can be found that

$$\sigma_r = \begin{cases} -\varepsilon \dfrac{U_0}{d_{cs}} + \varepsilon U_0 \sum\limits_{n=1}^{\infty} \dfrac{n\pi}{d_{cs}} f_1(n) \dfrac{\cosh(\lambda_1 r\varphi)}{\cosh(\lambda_1 r \varphi_w / 2)}, & -\dfrac{\varphi_w}{2} < \varphi < \dfrac{\varphi_w}{2} \\ -\varepsilon U_0 \sum\limits_{n=1}^{\infty} \dfrac{n\pi}{d_{vs}} f_2(n) e^{-\lambda_2 r(\varphi - \varphi_w/2)}, & \dfrac{\varphi_w}{2} < \varphi \end{cases}, \tag{5.12}$$

where

$$f_1(n) = \frac{2d_{cs}}{(n\pi)^2} \left\{ \frac{\sin(\lambda_1 d_2)}{d_{cs} - d_2} + \frac{U_1}{U_0} \left[\frac{\sin(\lambda_1 d_{vs})}{d_{vs} - d_1} - \frac{d_{vs} \sin(\lambda_1 d_1)}{(d_{vs} - d_1) d_1} \right] + \frac{U_2}{U_0} \left[\frac{\sin \lambda_1 (d_{vs} + d_v)}{(d_2 - d_{vs} - d_v)} - \frac{d_{vc} \sin(\lambda_1 d_2)}{(d_2 - d_{vs} - d_v)(d_{cs} - d_2)} \right] \right\}, \tag{5.13}$$

$$f_2(n) = \frac{2U_1 d_{vs}^2}{U_0 (n\pi)^2} \frac{\sin(\lambda_2 d_1)}{d_1 (d_{vs} - d_1)}, \tag{5.14}$$

$$\lambda_1 = n\pi / d_{cs}, \quad \lambda_2 = n\pi / d_{vs}, \tag{5.15}$$

while n is an integer. The variables U_1, U_2, d_1 and d_2 can be found from the common boundary conditions at boundary $\varphi = \varphi_w/2$ or $\varphi = -\varphi_w/2$:

If two y values in the range $0 < y < d_{vs}$ and two y values in the range $d_{vs}+d_v < y < d_{cs}$ are arbitrarily selected, then four equations with the variables U_1, U_2, d_1 and d_2 are obtained. The relations between the variables U_1, U_2, d_1 and d_2 and the geometrical parameters can be found by solving these four equations. In order to make the theoretical results optimally coincide with the practical results, we select four y values that are respectively the points between d_1 and 0, d_1 and d_{vs}, $d_{vs}+d_v$ and d_2, and d_2 and d_{cs} namely:

$$y = 2d_1 / 3, \quad y = (2d_1 + d_{vs}) / 3, \quad y = (2d_2 + d_{vs} + d_v) / 3, \quad y = (2d_2 + d_{vc}) / 3. \tag{5.16}$$

According to the definition of a capacitance, the capacitances between the segments on the segmented electrode and common electrode can be obtained from formula (5.12). They are:

$$\begin{aligned} C_{s4} - C_{s1} &= \varepsilon \frac{\varphi_s (r_2^2 - r_1^2)}{2d_{cs}} \left(1 + \frac{\delta_s(\varphi_p)}{\varphi_s} \right) \\ (C_{s5} + C_{s6}) - (C_{s2} + C_{s3}) &= \varepsilon \frac{\varphi_p (r_2^2 - r_1^2)}{d_{cs}} \left(1 + \frac{\delta_p(\varphi_p)}{\varphi_p} \right), \\ C_{s5} - C_{s2} &= \varepsilon \frac{\varphi_s (r_2^2 - r_1^2)}{2d_{cs}} \left(1 + \frac{\delta_{25}(\varphi_p)}{\varphi_s} \right) \end{aligned} \tag{5.17}$$

where φ_p is the angular position to be measured, φ_s is the angular width of an electrode segment ($\varphi_s = 15°$), the parameters r_1 and r_2 are respectively the inner and outer radii of

the outer segments on the segmented electrode (see Figure 5.3), $\delta_p(\varphi_p)$, $\delta_s(\varphi_p)$ and $\delta_{25}(\varphi_p)$ are nonlinear terms caused by the electric-field-bending effect. For these terms it holds that:

$$d_s(\varphi_p) = -\frac{2d_{cs}}{r_2^2 - r_1^2}\left[2\sum_{n=1}^{\infty} f_1(n)\int_{r_1}^{r_2}\frac{\cosh(\lambda_1 r\varphi_p)\sinh(\lambda_1 r\varphi_s/2)}{\cosh(\lambda_1 r\varphi_w/2)}dr + \sum_{n=1}^{\infty} f_2(n)\int_{r_1}^{r_2} e^{\lambda_2 r(\frac{5}{2}\varphi_s - \frac{1}{2}\varphi_w - \varphi_p)}(1 - e^{-\lambda_2 r\varphi_s})dr\right], \tag{5.18}$$

$$\delta_p(\varphi_p) = -\frac{d_{cs}}{r_2^2 - r_1^2}\left[2\sum_{n=1}^{\infty} f_1(n)\int_{r_1}^{r_2}\frac{\cosh(\lambda_1 r\varphi_s/2)\sinh(\lambda_1 r\varphi_p)}{\cosh(\lambda_1 r\varphi_w/2)}dr + 2\sum_{n=1}^{\infty} f_2(n)\int_{r_1}^{r_2} e^{-\lambda_2 r(\frac{5}{2}\varphi_s - \frac{1}{2}\varphi_w)}\sinh(\lambda_1 r\varphi_p)dr\right], \tag{5.19}$$

$$\delta_{25}(\varphi_p) = -\frac{2d_{cs}}{r_2^2 - r_1^2}\left[2\sum_{n=1}^{\infty} f_1(n)\int_{r_1}^{r_2}\frac{\cosh(\lambda_1 r(\varphi_s - \varphi_p))\sinh(\lambda_1 r\varphi_s/2)}{\cosh(\lambda_1 r\varphi_w/2)}dr + \sum_{n=1}^{\infty} f_2(n)\int_{r_1}^{r_2} e^{-\lambda_2 r(\frac{3}{2}\varphi_s - \frac{1}{2}\varphi_w + \varphi_p)}(1 - e^{-\lambda_2 r\varphi_s})dr\right]. \tag{5.20}$$

5.6.4 The influence of the electric-field-bending effect on the accuracy

Substituting the capacitance functions that are described by formula (5.17) into the formula (5.6), results in an equation of the form:

$$\varphi_m = \frac{\varphi_p + \delta_p(\varphi_p)}{1 + \delta_s(\varphi_p)/\varphi_s + \delta_c(\varphi_p)/\varphi_s}, \tag{5.21}$$

where φ_m is the measured angular position, $\delta_c(\varphi_p)$ is the fine-tuning compensative term for the electric-field-bending effect. For this term it holds that:

$$\delta_c(\varphi_p) \cong \alpha(\varphi_p - \frac{\varphi_s}{2}). \tag{5.22}$$

With equation (5.21), it is found that the systematic nonlinearity $\varepsilon_e = \varphi_m - \varphi_p$ caused by the electric-field-bending effect can be approximated by:

$$\varepsilon_e \cong \delta_p(\varphi_p) - \frac{\varphi_p}{\varphi_s}\delta_s(\varphi_p) - \frac{\varphi_p}{\varphi_s}\delta_c(\varphi_p). \tag{5.23}$$

This nonlinearity is not only a function of the position φ_p to be measured but also of the geometrical parameters (d_{vs}, d_v, d_{vc}, d_{cs}, r_1, r_2, φ_w, φ_s) and the fine-tuning factor α.

5.6.5 Numerical solution of the problem

In order to verify the validity of the analytical solutions, the distribution of the charge density on the surface of the receiving electrode (SeE) and the potential at $\varphi = \varphi_w/2$ (see Figure 5.7) have been numerically calculated by using an existing Maxwell software package [16]. Figure 5.9 shows a scheme of a part of a cross-section view of the sensor which has a symmetrical configuration with the line A-A'. The dimensional and conditional parameters of this configuration are: $w_1 = w_2 = 0.1$ mm, $d_v = 0.2$ mm, $d_{vs} = d_{vc} = 0.9$ mm, $d_{cs} = 2$ mm, $r\varphi_w = 15$ mm, a potential on the common electrode $U_0 = 1$ V, and the screen electrode and segmented electrode are grounded.

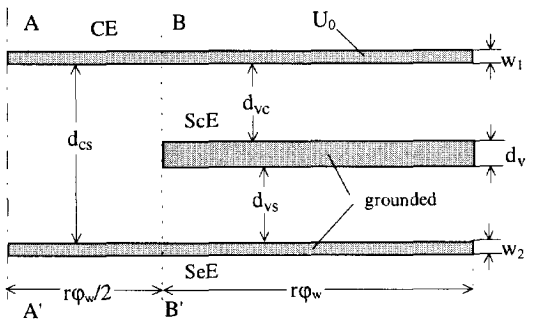

Figure 5.9 The model used for a numerical verification of the analysis.

In the calculation, about 3000 triangle meshes were used. Figure 5.10 shows the numerically and analytically calculated distributions of the charge density on the surface of the receiving electrode (SeE) and of the potentials along the line B-B' in Figure 5.9. The analytical results for the distributions of the charge density are described by the equations (5.12).

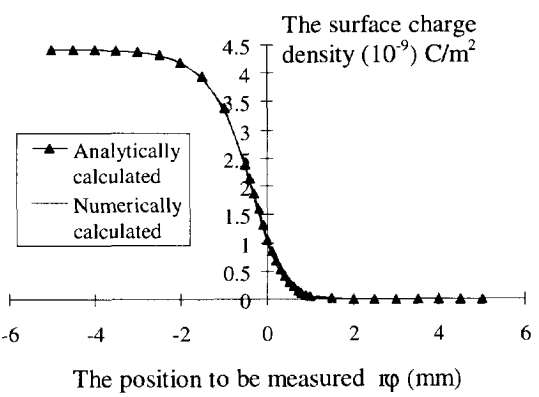

(a)

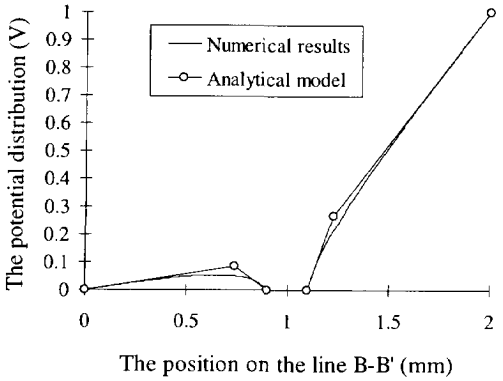

(b)

Figure 5.10 The distributions of the charge-density and potential analytically and numerically calculated.

From Figure 5.10, it can be concluded that the analytical and the numerical results for distributions of the charge density and potential are in good agreement. The numerical analysis is mainly used to verify the validity of the approximations in the analytical one. However, to predict the influence of small nonidealities, the analytical analysis is much more suited than the numerical one, because this kind of analysis consumes much less calculation time for the same level of accuracy. These nonidealities are discussed in the following section.

5.6.6 The influence of the geometrical parameters on the nonlinearity of the sensor

According to equation (5.23), the influence of the geometrical parameters d_{cs}, d_{vs}, d_{vc}, d_v, r_1, r_2, φ_s and φ_w on the nonlinearity of the sensor can be found. Because the relation between the nonlinearity and the geometrical parameters, as described by equation (5.23), is very complex, it is difficult to calculate the relation of the nonlinearity and the geometrical parameters in a direct way. The variables U_1, U_2, d_1 and d_2 are also a function of the geometrical parameters and there is an optimum fine-tuning factor α_{op}, which minimizes the influence of the electric-field bending for every sensing element structure. Therefore, firstly the variables U_1, U_2, d_1 and d_2 have been calculated, secondly, the optimum fine-tuning factor (α) and the corresponding nonlinearity have been calculated, using a trial-and-error method.

Figure 5.11 shows the nonlinearity, caused by the electric-field-bending effect, over a single-segment range for $\alpha = 0$ and $\alpha = 0.051$ (optimum value), respectively, for the geometrical parameters listed in Table 5.1.

Table 5.1 The geometrical parameters of the sensing element.

parameters	notation	unit	values
electrode distance	d_{cs}	mm	3.0
thickness of the screen electrode	d_v	mm	0.3
position of the screen electrode	d_{vc}/d_{vs}	-	1.0
inner radix of the electrode	r_1	mm	10.0
outer radix of the electrode	r_2	mm	21.5
width of the segment electrode	φ_s	degree	15
width of the screen electrode	φ_p	degree	45

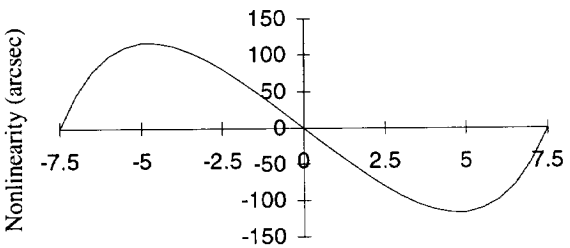

The angular position to be measured for one segment (degree)

(a)

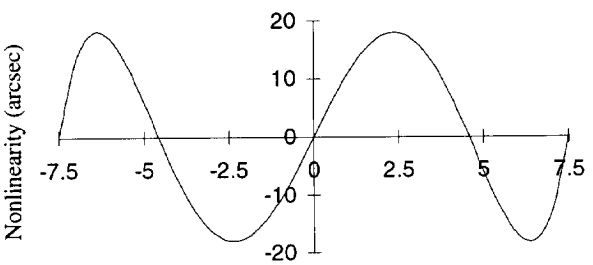

The angular position to be measured for one segment (degree)

(b)

Figure 5.11 The nonlinearity of the sensor for (a) $\alpha = 0$ and (b) $\alpha = 0.051$.

The nonlinearity is a periodic function with a period of the width of one segmented electrode. By using a fine-tuning factor $\alpha > 0$, the nonlinearity of the sensor caused by the electric-field-bending effect can be improved by a factor of 6.5.

Figure 5.12 shows the maximum nonlinearity as a function of the vertical geometrical parameters of the sensing element (d_{cs}, d_v and d_{vc}/d_{vs}) and corresponding optimum fine-tuning factor, respectively.

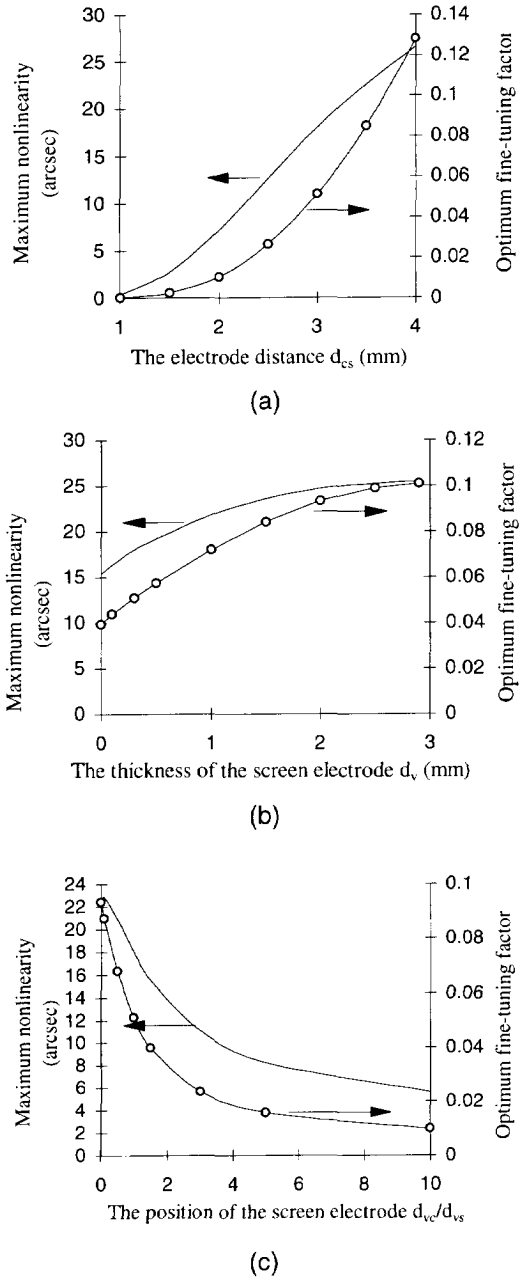

Figure 5.12 The influence of the electric-field bending on the nonlinearity as function of the geometrical parameters. The electrode structure itself is assumed to be ideal.

In this figure, the maximum nonlinearity is the absolute value of the peak nonlinearity in the range $-\varphi_s/2 - \varphi_s/2$ (see Figure 5.11(b)).

It is, obviously, shown that, when the distances between electrodes is short and the screen electrode is thin and there is a large ratio d_{vo}/d_{vs} (the screen electrode is near to the segmented electrode), there is only a small degree of nonlinearity obtained. It should be noted here that for accurate sensors a small nonlinearity is not the only requirement. Amongst the other requirements are a low sensitivity of the angular-position measurement to mechanical tolerances and nonidealities, such as mechanical vibration, nonflatness, obliqueness and eccentricity of the electrodes, a low temperature coefficient and insensitivity to pollution and humidity. These requirements can be better fulfilled by employing longer electrode distances and thickness, and smaller ratio d_{vo}/d_{vs}. The optimum structure is found as a compromise between these conflicting requirements.

Figure 5.13 shows the relations of the maximum nonlinearity and the dimensions of electrodes in the radial direction (r_1, r_2-r_1), and the corresponding optimum fine-tuning factor.

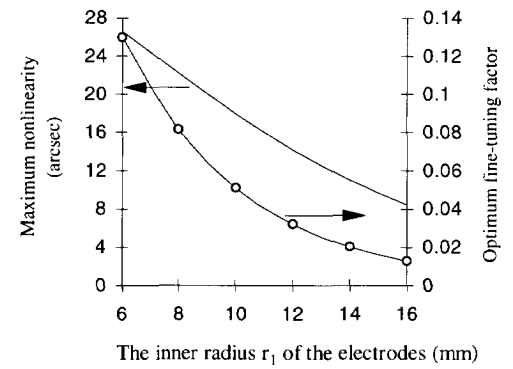

(a)

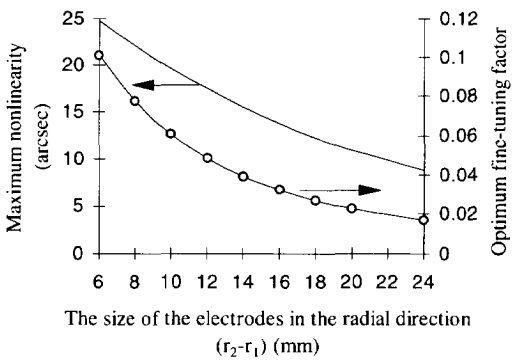

(b)

Figure 5.13 The influence of the radii of the electrodes on the nonlinearity. (a) $r_2 - r_1$ is constant, (b) r_1 is constant.

The larger the dimensions of electrodes in the radial direction are, the smaller is the nonlinearity that is found. This effect is because of the larger width ($r\varphi_s$) of the segments. The influence of the electric-field-bending effect in cylinder coordinates is equivalent to that in rectangular coordinates with a segment width of $x_s = (r_2+r_1)\varphi_s/2$ being the average width of one cylindrical segment. Both Figure 5.12 and Figure 5.13 show that a large electric-field-bending effect requires a large value of the fine-tuning factor to make the nonlinearity as low as possible. The fine-tuning factor is more effective for the large electric-field-bending effect.

Due to the electric-field-bending effect, Figure 5.14 shows that the optimum window width of the screen electrode is slightly larger than $3\varphi_s$, which amounts to about 52°.

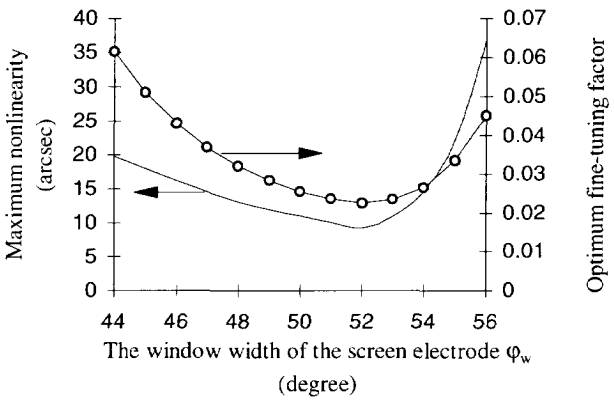

Figure 5.14 The optimum window width of the screen electrode.

5.6.7 Conclusions

Analytical expressions for the distributions of the potential and charge density in a capacitive angular-position sensor with three electrode discs in an axis-symmetrical configuration have been found by using an appropriate physical model and solving Laplace's equation.

These analytical expressions are very useful to calculate the influence of electric-field bending on the nonlinearity in the capacitive angular- or linear-position sensor. It has been shown that the nonlinearity is significantly reduced by using an additional parameter in the retrieving algorithm, the "fine-tuning factor". Optimal values for the fine-tuning factor have been calculated for a variety of geometrical parameters. The results of the analysis are very useful in finding the optimal geometrical parameters with respect to the accuracy of the sensing element structure. This optimum will depend on the electric-field-bending effect on the one hand and on the influences of the nonflatness, mechanical stability and sensitivity to pollution and humidity on the other hand.

5.7 The influence of the mechanical errors

5.7.1 Introduction

The systematic mechanical errors are the most important error components of any measurement system for mechanical measurands. They determine the advantages and disadvantages of the system over its competitors in a certain field. During the design of a smart angular-position sensor, the cheapest mechanical solution is aimed for, as the mechanical part of the sensor is most often the most expensive part. Then, the question arises as to how high the acceptable level of the systematic mechanical errors is. Therefore, the influence of systematic mechanical errors on one implementation of the capacitive angular-position sensor will be derived. Unavoidable errors can be compensated for. These errors can also be eliminated by calibration.

5.7.2 The influence of the eccentricity of the electrodes

The eccentricity of the electrodes is only for the angular-position sensor. In the practical implementation of the capacitive angular-position sensing element, the common electrode and segmented electrode are mounted in the same housing. The outer and inner radii of the common electrode are, respectively, larger and smaller than that of the segmented electrode. Then, a margin δ_m between the common electrode and the segmented electrodes is formed (see Figure 5.15(a)). If the eccentricity between the common electrode and the segmented electrode is smaller than this margin, the inaccuracy will not be directly affected by this eccentricity. Only a very small inaccuracy is created by the electric-field-bending effect due to this eccentricity. In the following, we discuss the influence of the eccentricity of the screen electrode.

We suppose the common electrode and the segmented electrode are concentric and that the rotating screen electrode is excentral to them.

Figure 5.15(b) shows the top view of the electrode structure of the sensing element where there is an eccentricity between the screen electrode and the segmented electrode (the common electrode).

In the new coordinate, the original point of which is the center of the screen electrode, the inner and outer radius of the segmented electrode are, respectively,

$$\begin{aligned} r'^2_1 &= r_1^2 - 2r_1\delta R\cos(\varphi - \varphi_0) + \delta R^2 \\ r'^2_2 &= r_2^2 - 2r_2\delta R\cos(\varphi - \varphi_0) + \delta R^2 \end{aligned}, \tag{5.24}$$

where δR and φ_0 represent, respectively, the amplitude and the direction of the eccentricity, r_1 and r_2 are, respectively, the inner and outer radii of the outer segments on the segmented electrode.

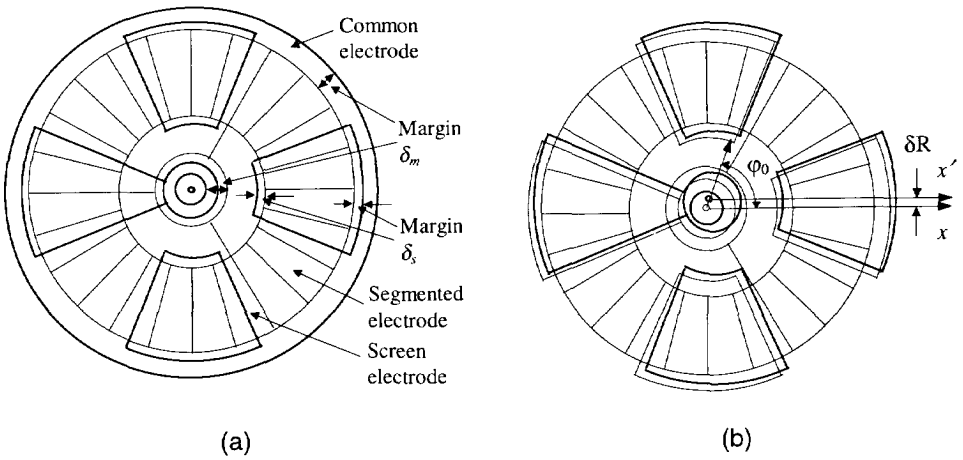

Figure 5.15 (a) A top view of the capacitive angular-position sensor. (b) A top view of the capacitive angular-position sensor with eccentricity of the electrodes.

When the outer and inner radii of the screen electrode are, respectively, larger and smaller than that of the segmented (common) electrode, and the electric-field-bending effect is ignored, the capacitance between the common electrode and the segmented electrode is

$$C_{si} = \frac{\varepsilon}{d_{cs}} \int_{r_1'}^{r_2'} \int_{\varphi_1}^{\varphi_2} r\,dr\,d\varphi = \int_{\varphi_1}^{\varphi_2} \left[\frac{1}{2}\left(r_2^2 - r_1^2\right) - \left(r_2 - r_1\right)\delta R\cos\left(\varphi - \varphi_0\right) \right] d\varphi . \tag{5.25}$$

By using appropriate integration limitation and some calculations, we find that:

$$\begin{aligned} \left(C_{s5} + C_{s6}\right)_i - \left(C_{s2} + C_{s3}\right)_i &= \frac{\varepsilon}{d_{cs}} \left[\left(r_2^2 - r_1^2\right) - \delta R\left(r_2 - r_1\right)\sin\varphi_0 \right] \\ 2\left(C_{s4} - C_{s1}\right)_i &= \frac{\varepsilon}{d_{cs}}\left(r_2^2 - r_1^2\right) \end{aligned} , \tag{5.26}$$

where i = 1, 2, 3, 4, which, respectively, represent four quarter circles. Because of the cross-quad configuration of the sensing element, the measured angular position is

$$\frac{\varphi_m}{\varphi_s} = \frac{\sum_{i=1}^{4} \left[\left(C_{s5} + C_{s6}\right)_i - \left(C_{s2} + C_{s3}\right)_i \right]}{2\sum_{i=1}^{4} \left(C_{s4} - C_{s1}\right)} = \frac{\varphi_p}{\varphi_s} . \tag{5.27}$$

This means that the influence of the eccentricity between the screen electrode and the segmented (common) electrode can be completely eliminated for the small eccentricity.

However, when the electrode distances of the four corresponding segments on the cross-quad position are not equal, for instance due to the effect of the

obliqueness of the electrode, then the effect of the eccentricity cannot be completely eliminated. Now, the maximum effect of the eccentricity on the measured position is [6]:

$$|\delta\varphi_m|_{\max} = 6\sqrt{2}\sqrt{2+\sqrt{2}} \cdot \varphi_s \frac{\delta R}{\pi(r_1+r_2)} \frac{\delta d_{cs}}{d_{cs}}, \tag{5.28}$$

where d_{cs} and δd_{cs} are the mean value and the deviation of the electrode distance, respectively. With φ_s = 15°, δR = 0.1 mm peak, δd_{cs} = 10 μm peak, d_{cs} = 2 mm, r_2 = 22.5 mm and r_1 = 7.5 mm, this results in $|\delta\varphi_m|_{\max}$ = 4.5″ peak.

5.7.3 The influence of the obliqueness of the electrodes

Figure 5.16 shows a simple model of the obliqueness of the common electrode. The screen electrode is ideally parallel to the segmented electrode. The obliquity is represented by the angle α. Thus, the distance d'_{cs} between the common electrode and the segmented electrode is a function of the coordinate x, it is

$$d'_{cs}(x,y) = d_{cs} + x \cdot \tan(\alpha). \tag{5.29}$$

In the polar coordinate, the equation (5.29) can be written as

$$d'_{cs}(r,\varphi) = d_{cs} + \tan(\alpha) r\cos(\varphi - \varphi_0), \tag{5.30}$$

where φ_0 is the angle direction which causes the maximum obliqueness.

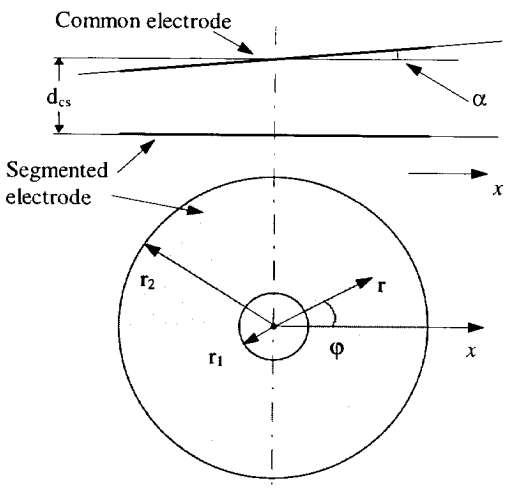

Figure 5.16 The model of the obliqueness.

Under the condition of ignoring the electronic field-bending effect, according to the definition of the capacitance of the parallel-plane capacitor [4], the capacitance density C'_s between the common electrode and the segmented electrode is

$$C_s' = \frac{\varepsilon}{d_{cs}}\left[1 - \frac{r\tan(\alpha)}{d_{cs}}\cos(\varphi - \varphi_0) + \frac{r^2\tan^2(\alpha)}{d_{cs}^2}\cos^2(\varphi - \varphi_0)\right]. \tag{5.31}$$

Because $\tan(\alpha)$ is always very small, the effects, which are higher than the second-order terms, are ignored here.

By using appropriate calculations, we find that:

$$\begin{aligned}\sum_{i=1}^{4}\left[\left(C_{s5} + C_{s6}\right)_i - \left(C_{s2} + C_{s3}\right)_i\right] &= \frac{\varepsilon}{d_{cs}}\left[4\left(r_2^2 - r_1^2\right) + \frac{\tan^2(\alpha)}{d_{cs}^2}\left(r_2^4 - r_1^4\right)\right]\varphi_p \\ \sum_{i=1}^{4}\left(C_{s4} - C_{s1}\right)_i &= \frac{\varepsilon}{d_{cs}}\left[2\left(r_2^2 - r_1^2\right) + \frac{\tan^2(\alpha)}{2d_{cs}^2}\left(r_2^4 - r_1^4\right)\right]\varphi_p\end{aligned}. \tag{5.32}$$

Therefore, the measured position is:

$$\frac{\varphi_m}{\varphi_s} = \frac{\sum_{i=1}^{4}\left[\left(C_{s5} + C_{s6}\right)_i - \left(C_{s2} + C_{s3}\right)_i\right]}{2\sum_{i=1}^{4}\left(C_{s4} - C_{s1}\right)} = \frac{\varphi_p}{\varphi_s}. \tag{5.33}$$

Formula (5.33) shows that the influence of the obliqueness between the common electrode and the segmented electrode can completely be eliminated to the second order. However, for the combination of the obliqueness and eccentricity, the first-order term of the obliqueness will affect the accuracy of the measured position (see Section 5.7.2).

5.7.4 The influence of deformation of the screen electrode

5.7.4.1 The model of deformation of the screen electrode

The screen electrode is made of very thin metal plate in a practical sensor, so it is prone to deformation. For the sensing element structure depicted in Figure 5.3, there are various deformations of the screen electrode. Now, a worst case of the deformation

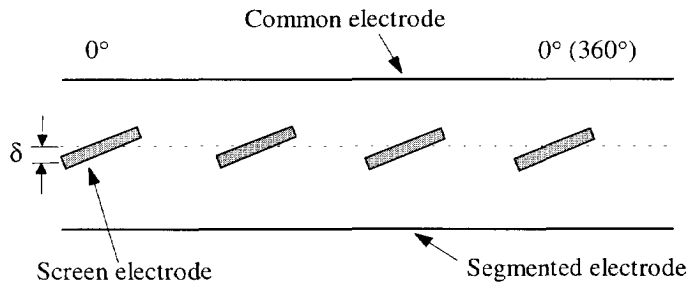

Figure 5.17 A worst-case model of the deformation.

is discussed, and shown in Figure 5.17 where δ is the deformation of the screen electrode.

5.7.4.2 The influence of deformation of the screen electrode

The influence of the deformation of the screen electrode on the accuracy of the sensor is mainly created via the electric-field-bending effect. By using the results in Section 5.6, the influence of the deformation can be found (see Figure 5.18 and Table 5.2).

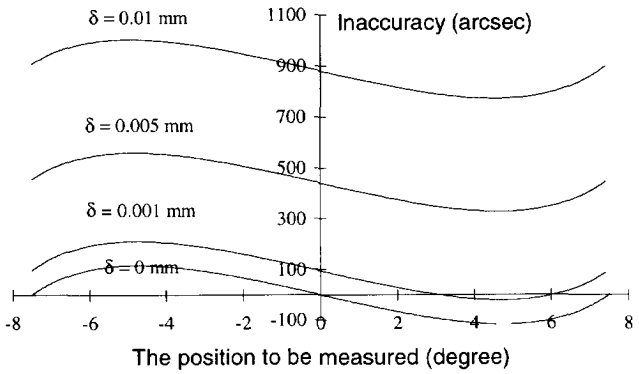

Figure 5.18 The influence of the deformation of the screen electrode.

Table 5.2 The influence of the deformation.

δ (mm)	0.0	0.001	0.005	0.01	0.05
P_{offset} (arcsec)	0.0	94.2	439.6	879.2	4367
Max. Nonlinearity (arcsec)	116.5	117.2	120.4	124.2	153.2
Min. Nonlinearity (arcsec)	-116.5	-115.7	-112.6	-108.7	-76.8

where the inaccuracy (in Figure 5.18) is the difference between the measured angular position and the angular position to be measured ($= \varphi_m - \varphi_p$), Variable P_{offset} is the offset of the measured angular position, which is caused by the deformation, the nonlinearity is the difference between the errors and the offset. Figure 5.18 and Table 5.2 show that the deformation of the screen electrode not only affects the linearity of the sensor but that it also causes an offset which is approximately in linear relation with the value of the deformation δ and is not a function of the position to be measured. The offset is automatically eliminated during calibration, after assembling the encoder in its mechanical environment.

5.7.5 The influence of the nonflatness

For capacitive sensors based on the variation of the electrode-plate surface, such as the angular encoder, the influences of the nonflatness and the roughness of the electrode surface are relatively serious. Although the use of extremely flat electrode surfaces will reduce this influence, it will also increase the costs of the sensor.

In this section, the influence of the nonflatness of the electrode surfaces on the nonlinearity of the capacitive angular-position sensor described in Section 5.3, is discussed by using a simple and effective model of the nonflatness. The influences of geometrical parameters, which originate from the nonflatness, are discussed in more detail. The analytical results are very helpful in optimizing the sensing element structure in connection with other effects, such as the electric-field-bending effect.

5.7.5.1 A simple model of the nonflatness

A simple model of the nonflatness of the electrodes is shown in Figure 5.19. In the x direction, the nonflatness is a cosine distribution. In the y direction, the nonflatness is constant. When the nonflatness distributions of the common electrode and the segmented electrode are inverse, the influence of the nonflatness will be the most serious (worst case). This case is here considered in detail.

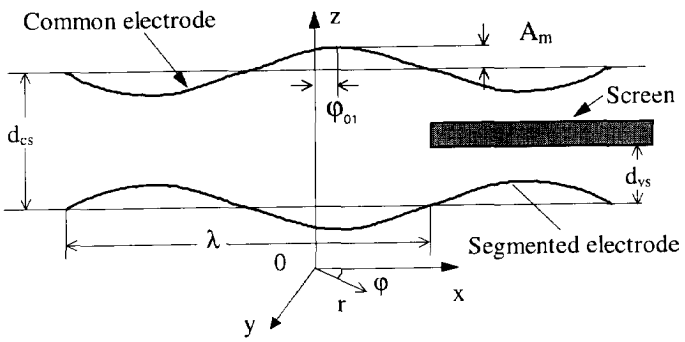

Figure 5.19 The model of the nonflatness of the electrode surface.

The distance between the common electrode and the segmented electrode in the polar coordinate is

$$d'_{cs}(r,\varphi) = d_{cs} - 2A_m \cos\left[\frac{2\pi}{\lambda} r\cos(\varphi - \varphi_0) - \varphi_{01}\right], \tag{5.34}$$

where A_m is the peak value of amplitude of the nonflatness, λ the spatial wavelength of the nonflatness wave, φ_{01} the phase shift between the center of the electrodes and the nonflatness waves. d_{cs} is the mean electrode distance.

5.7.5.2 The influence of the nonflatness

It is supposed that the surface of the screen electrode is an ideal plane and the electric-field-bending effect is ignored. According to the definition of capacitance for the biplane capacitor, the capacitance density C'_s between the common electrode and the segmented electrode in the polar coordinate is

$$C_s' = \frac{\varepsilon}{d_{cs}}\left\{1+\frac{2A_m}{d_{cs}}\cos\left[\frac{2\pi}{\lambda}r\cos(\varphi-\varphi_0)-\varphi_{01}\right] - \frac{4A_m^2}{d_{cs}^2}\cos^2\left[\frac{2\pi}{\lambda}r\cos(\varphi-\varphi_0)-\varphi_{01}\right]\right\}. \tag{5.35}$$

Because $A_m << d_{cs}$, the effects, which are higher than the second-order terms, have been ignored here. Then, for the capacitances between the common electrode and the segmented electrode, it holds that:

$$(C_{s5}+C_{s6})-(C_{s2}+C_{s3}) = \frac{\varepsilon}{d_{cs}}\left[4\left(r_2^2-r_1^2\right)\left(1-\frac{2A_m^2}{d_{cs}^2}\right)\varphi_p+\Delta_{pc56}-\Delta_{pc23}\right], \tag{5.36}$$

$$(C_{s4}-C_{s1}) = \frac{\varepsilon}{d_{cs}}\left[2\left(r_2^2-r_1^2\right)\left(1-\frac{2A_m^2}{d_{cs}^2}\right)\varphi_s+\Delta_{sc4}\right], \tag{5.37}$$

for $-1/2 \le \varphi_p/\varphi_s \le 1/2$. Where Δ_{pc56}, Δ_{pc23} and Δ_{sc4} are, respectively, the nonlinear terms of the capacitances ($C_{s5}+C_{s6}$, $C_{s2}+C_{s3}$ and C_{s4}), which are caused by the nonflatness. These nonlinear terms can be calculated by using the following formula and the integration limits shown in Table 5.3.

$$\Delta = \frac{2A_m}{d_{cs}}\int_{r_1}^{r_2}\int_{\varphi_1}^{\varphi_2}\left[\cos\left(\frac{2\pi}{\lambda}r\cos(\varphi-\varphi_0)-\varphi_{01}\right) - \frac{A_m}{d_{cs}}\cos\left(\frac{4\pi}{\lambda}r\cos(\varphi-\varphi_0)-2\varphi_{01}\right)\right]r\,dr\,d\varphi. \tag{5.38}$$

Table 5.3 The integrated limits of the capacitances.

Capacitors	φ_1	φ_2
$C_{s5}+C_{s6}$	$\varphi_s/2$	$\varphi_w/2+\varphi_p$
$C_{s2}+C_{s3}$	$-\varphi_w/2+\varphi_p$	$-\varphi_s/2$
C_{s4}	$-\varphi_s/2$	$\varphi_s/2$

Therefore, the measured angular position φ_m is

$$\frac{\varphi_m}{\varphi_s} = \frac{(C_{s5}+C_{s6})-(C_{s2}+C_{s3})}{2(C_{s4}-C_{s1})} = \frac{\varphi_p+\dfrac{d_{cs}^2(\Delta_{pc56}-\Delta_{pc23})}{4(r_2^2-r_1^2)(d_{cs}^2-2A_m^2)}}{\varphi_s+\dfrac{d_{cs}^2\Delta_{sc4}}{2(r_2^2-r_1^2)(d_{cs}^2-2A_m^2)}}, \quad -\frac{1}{2}\le\frac{\varphi_m}{\varphi_s}\le\frac{1}{2}. \tag{5.39}$$

With this equation, the systematic measurement error $\varepsilon_e = \varphi_m - \varphi_p$ can be calculated, with

$$\varepsilon_e(\varphi_p, r_1, r_2, d_{vs}, d_v, d_{vc}, d_{cs}, \varphi_w, \varphi_s, \lambda, A_m, \varphi_0, \varphi_{01}) = \frac{d_{cs}^2}{4(r_2^2-r_1^2)(d_{cs}^2-2A_m^2)}\left(\Delta_{pc56}-\Delta_{pc23}-2\frac{\varphi_p}{\varphi_s}\Delta_{sc4}\right), \tag{5.40}$$

as a function of the position φ_p to be measured, the geometrical parameters of the sensor (d_{cs}, r_1, r_2, φ_w, φ_s) and the nonflatness parameters (λ, A_m, φ_o, φ_{01}).

Formula (5.40) shows that although a symmetrical and redundant structure of the sensing element is used, the nonflatness on the surface of the electrodes still affects the accuracy of the sensor. In the following, we discuss in detail the influence of the various parameters on the nonlinearity due to the nonflatness.

5.7.5.3 The numerical analysis of the influence of the nonflatness

Because of the complicated relationships between the nonlinearity and various parameters as described by equation (5.40), it is very difficult to find the analytical solution in a direct way. However, the numerical solution can be obtained according to equation (5.40). Table 5.4 shows the various used parameters of the sensing element structure and the nonflatness. Using these parameters, the nonlinearity of the sensor has been calculated (see Figure 5.20)

Table 5.4 The parameters of the nonflatness model and sensing element structure.

parameter	notation	unit	values
amplitude	A_m	mm	0.01
spatial wavelength	λ	mm	60.0
phase shift	φ_{01}	degree	0.0
electrode distance	d_{cs}	mm	2.0
position of screen electrode	d_{vs}	mm	0.9
width of segment electrode	φ_s	degree	15
width of screen electrode	φ_w	degree	45
inner radii of electrode	r_1	mm	5.0
outer radii of electrode	r_2	mm	22

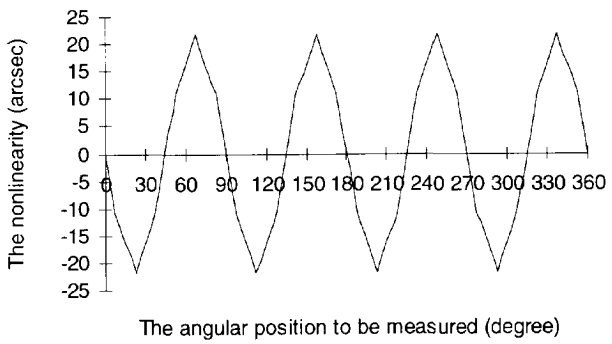

Figure 5.20 The influence of the nonflatness on the linearity of the sensor.

Figure 5.20 shows that the nonlinearity of the sensor is a period function with a period of a quarter circle, where there are the maximum and minimum values (peak value). The period performance of the nonlinearity is due to the cross-quad configuration of the sensing element.

5.7.5.3.1 The influence of the nonflatness parameters

The nonflatness parameters are mainly the spatial wavelength, the phase shift and the amplitude of the nonflatness wave. Under the conditions listed in Table 5.4, the influences of these parameters on the nonlinearity of the sensor are shown in Figure 5.21.

In Figure 5.21, the nonlinearity represents the peak value of the nonlinearity shown in Figure 5.20. Figure 5.21 shows that a maximum nonlinearity is caused on the certain spatial wavelength of the nonflatness, and, for the small nonlinearity, the amplitude A_m of the nonflatness should be small. It is also shown that the nonlinearity is maximum when the phase shifts between the center of the electrodes and the nonflatness waves are noninverse ($n\lambda$, n = 0, 1, ⋯).

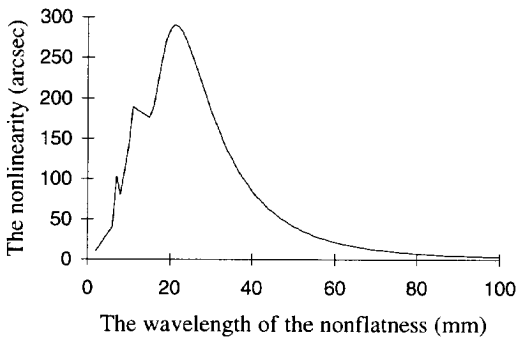

(a)

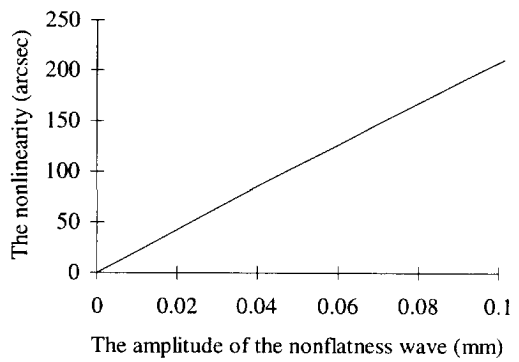

(b)

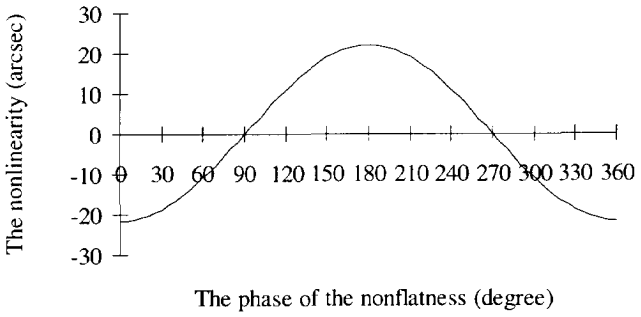

(c)

Figure 5.21 The influence of the parameters of the nonflatness.

5.7.5.3.2 The influence of the geometrical parameters of the sensing element

Because of the influence of the nonflatness, the measured position is sensitive to the geometrical parameters of the sensing element, such as the electrode distance d_{cs}, the width of the segment φ_s and the radial dimensions of the electrode. For the parameters listed in Table 5.4, the influences of the geometrical parameters on the nonlinearity of the sensor are shown in Figure 5.22.

It is, obviously, shown that a small nonlinearity is obtained with long electrode distances and small radial dimensions. Thus, the requirements for a small nonlinearity are opposite to those for a small electric-field-bending effect.

5.7.5.3.3 The relation between λ, which causes a maximum nonlinearity, and the radial dimensions

Figure 5.21(a) shows that there is a worst spatial wavelength of the nonflatness. This worst spatial wavelength is almost unrelated to the vertical dimensions, such as the electrode distance, the thickness of the rotating electrode, but it is related to the radial dimensions of the sensing element (see Figure 5.23).

In Figure 5.23, the maximum nonlinearity is the maximum of the nonlinearity shown in Figure 5.21(a), the worst spatial wavelength is that corresponding to the maximum nonlinearity. It is shown that the worst spatial wavelength is linearly related to the radial dimensions of the sensing element (r_1, r_2-r_1).

5.7.5.4 Conclusion

The influence of the nonflatness of the electrodes on the nonlinearity of the capacitive sensor have been discussed in detail. A model of the nonflatness of the electrode surface has been created. According to this model, the influence of the parameters of the nonflatness and the structure of the sensing element on the nonlinearity of the sensor have been derived theoretically.

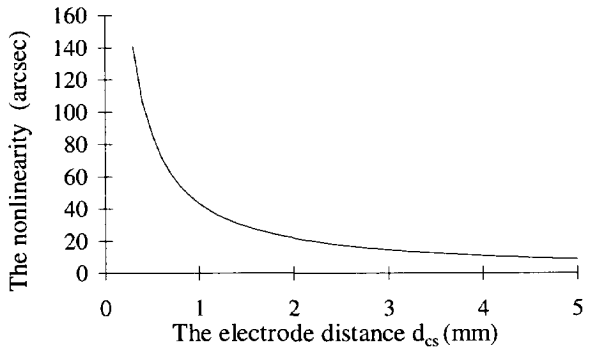

(a)

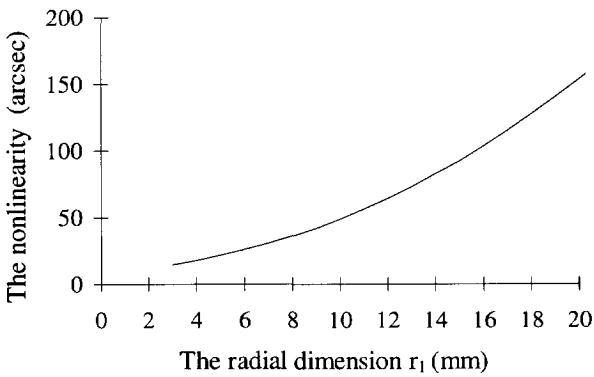

(b)

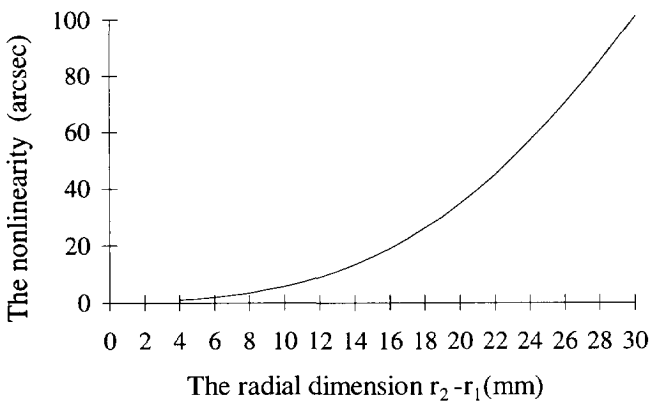

(c)

Figure 5.22 The influence of the geometrical parameters of the sensing element.

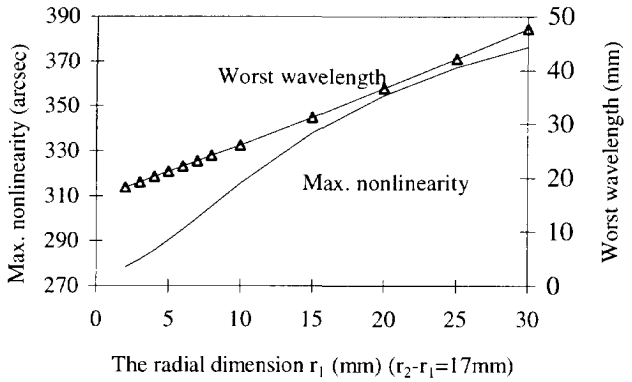

(a)

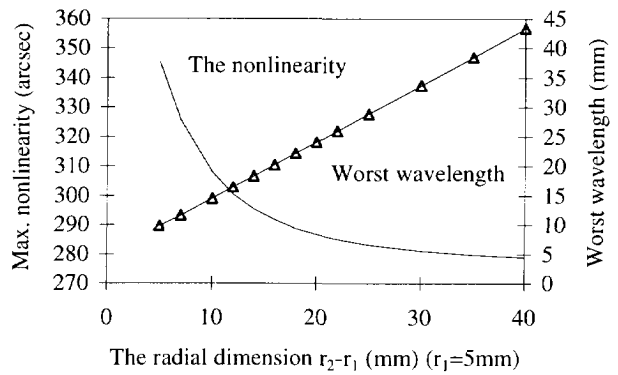

(b)

Figure 5.23 The relations between the worst spatial wavelength and the radial dimensions of the sensing element.

5.8 The influence of other geometrical errors

5.8.1 The influence of the pattern errors of the electrodes

We suppose that the electrode distance and the segment width φ_s are the same for each segment, and that differences in the capacitance values are only due to differences in the radial sizes of the segments, and that the electric-field-bending effect can be ignored. Then, after some calculations using formula (5.1) or formula (5.6), the inaccuracy ε_i caused by the pattern error of the segmented electrodes on the measured angular position is:

$$\varepsilon_i = \varphi_m - \varphi_p \cong \begin{cases} \dfrac{C_{i+1,\max} - C_{i-1,\max}}{2C_{i,\max}}\varphi_s + \dfrac{C_{i+2,\max} + C_{i-1,\max} - 2C_{i,\max}}{2C_{i,\max}}\varphi_p, & \dfrac{\varphi_s}{2} \geq \varphi_m > 0 \\ \dfrac{C_{i+1,\max} - C_{i-1,\max}}{2C_{i,\max}}\varphi_s + \dfrac{C_{i+1,\max} + C_{i-2,\max} - 2C_{i,\max}}{2C_{i,\max}}\varphi_p, & -\dfrac{\varphi_s}{2} < \varphi_m \leq 0 \end{cases}, \quad (5.41)$$

for the measurement range of one segment width. Where $C_{i,max}$ (i = 1, 2, ···, 6) represents the capacitance between the outer segments on the segmented electrode and the common electrode without the rotating electrode.

This formula will be used for the calibration of systematic inaccuracy in capacitive angular position sensor and results in a piecewise self-calibration technique. The calibration technique is discussed in detail in Section 5.9.

5.8.2 The influence of the gaps and vias on the electrodes

To obtain an infinitely small gap between two adjacent electrodes in a capacitive sensor is impossible. Meanwhile, printed-circuit boards are often used as carriers of the electrodes in low-cost capacitive sensors. Then, the vias are used for the electrical connection between the electrodes and signal wires. In previous papers [17, 18, 24], the influence of the finite gaps on the capacitance has been calculated. This effect can be described by using the effective gap width.

As an example, for the electrode structure shown in Figure 5.24, the effective gap width can be numerically calculated by using an existing Maxwell software package [16] (see Figure 5.25).

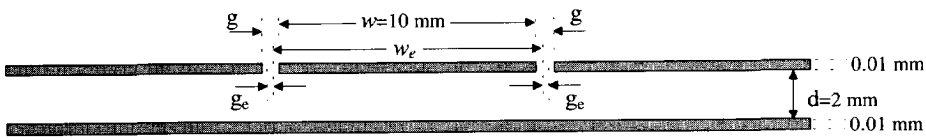

Figure 5.24 A cross-section of the electrode structure used for numerical simulation of the effective gap.

After some calculations using formula (5.1), the influence of the finite gap width on the accuracy of the capacitive position sensor described in Figure 5.3 can be obtained. It holds that

$$\frac{\varphi_m}{\varphi_s} \cong \frac{\varphi_p}{\varphi_s}\left(1 + \frac{g_e}{(r_2 + r_1)\varphi_s}\right) - \frac{1}{2}\frac{g_e}{(r_2 + r_1)\varphi_s}\left(1 + \frac{g_e}{(r_2 + r_1)\varphi_s}\right), \quad (5.42)$$

where g_e is the effective gap width. It is shown that the finite gap not only affects the linearity but also causes an offset. The offset can be automatically eliminated during calibration, after assembling the encoder in its mechanical environment.

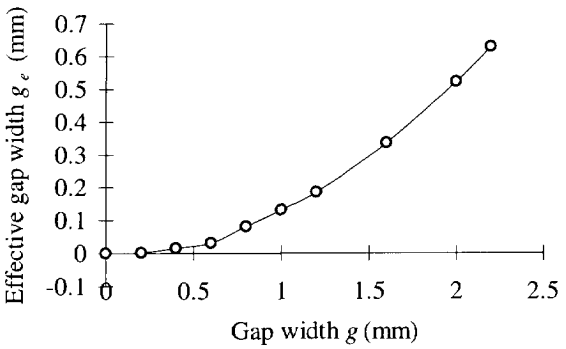

Figure 5.25 The simulated effective gap width.

Similarly, the influence of the vias on the accuracy of the capacitive position sensor can be obtained, it is

$$\frac{\varphi_m}{\varphi_s} \cong \frac{\varphi_p}{\varphi_s}\left(1+\frac{\pi r_{ve}^2}{A_s}\right), \tag{5.43}$$

where A_s is the area of segment electrode, r_{ve} is effective radius of the via.

For example, for a gap width of 0.15 mm and via radius of 0.3 mm, according to Figure 5.25, the effective gap width and effective via radius are about 0.9 μm and 0.02 mm, respectively. Then, the nonlinearities caused by these effects on the measured position amount to 2.9″ and 0.7″, respectively.

5.8.3 The influence of the frayed edges

In order to discuss the influence of the frayed edges of the electrodes, the dominating edges in the sensing element should first be defined. After we have done this, the influences of these dominating edges will be discussed. Figure 5.26 gives a top view of the capacitive sensing element shown in Figure 5.3.

It is, obviously, shown that for the capacitances between the segmented electrode and the common electrode the important edges are:

- the radial edges of the screen electrode,
- the radial edges of the segmented electrode,
- the tangential edges of the segmented electrode.

We call these edges the dominating edges. Only the quality and the position of these dominating edges are of importance.

One way of describing the frayed edge is by using Fourier transformations [6]. Figure 5.27 shows the common area, burdened with frayed edges in the tangential direction, of a segment and the opposite common electrode.

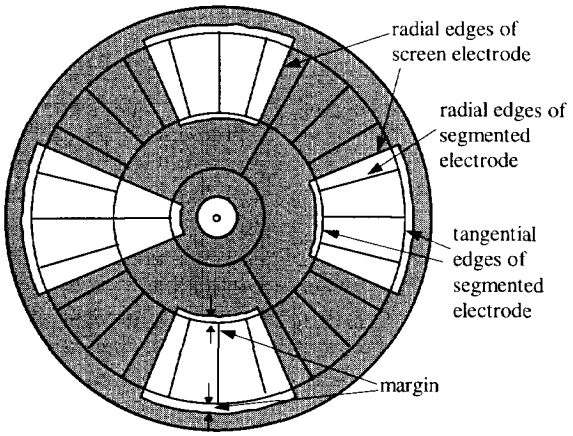

Figure 5.26 A top view of the capacitive angular-position sensing element.

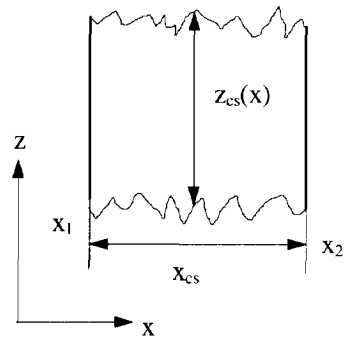

Figure 5.27 Common area, burdened with frayed edges in the z direction, of a segment.

If we assume that:

- the electric field is homogeneous,
- $Z_{cs}(x)$ is a summation of an average term $\overline{Z_{cs}}$ and a fluctuating term $\tilde{Z}_{cs}(x)$ (fluctuating with x) such that $Z_{cs}(x) = \overline{Z_{cs}} + \tilde{Z}_{cs}(x)$,
- $\tilde{Z}_{cs}(x)$ is approximated by a summation of sine or cosine terms. We consider the effect of one of the terms (Bennet approximation) such that $\tilde{Z}_{cs}(x) = \hat{Z}_{cs} \cos\left[2\pi\left(x - x_1\right)/\lambda\right]$, where λ is the spatial wavelength in the x-direction,

then, the capacitance between the segmented electrode and the common electrode is given by the following equation:

$$C_{sc} = \frac{\varepsilon}{d_{cs}} \int_{x_1}^{x_2} Z_{cs}(x)\mathrm{d}x = \varepsilon \frac{x_{cs}\overline{Z_{cs}}}{d_{cs}} + \varepsilon \frac{\lambda \hat{Z}_{cs}}{2\pi d_{cs}} \sin\left(\frac{2\pi x_{cs}}{\lambda}\right). \tag{5.44}$$

From this equation, it can be concluded that the transfer from $\tilde{Z}_{cs}(x)$ to C_{sc} is a sine function in the spatial frequency domain. Such a function acts like a low-pass filter and therefore tends to suppress higher spatial frequencies in the frayed edges.

Additionally, as shown in ref.[6] page 65, if the electric field is not homogenous, there is an additional low-pass action in the form of the smoothing of the surface charge density in the spatial domain with a spatial -3dB roll-off frequency of $(2\pi d_{cs})^{-1}$. The corresponding transfer function has a roll-off with a very steep slope which increases with the spatial frequency.

When we suppose that the average term $\overline{Z_{cs}}$ is equal for all segments and apply these results to the capacitive angular-position sensor, from equations (5.1) and (5.44) we find

$$\frac{\varphi_m}{\varphi_s} \cong \frac{\varphi_p}{\varphi_s} + \frac{\hat{r}_{21}}{\varphi_s \overline{r_{21}}} \frac{\lambda}{\pi} \sin\left(\frac{2\pi}{\lambda}\varphi_p\right), \tag{5.45}$$

where the second term in the right-hand part of the equation represents the effect of the frayed edges. Now, the unit of λ is the same as that of φ_m. The parameters $\overline{r_{21}}$ and $\hat{r}_{21}$ are, respectively, the average term and the amplitude of the fluctuating term of the radial dimension $(r_2\text{-}r_1)$. For example, with $\varphi_s = 15°$, $\hat{r}_{21} = 0.1$ mm peak, $\overline{r_{21}} = 11$ mm and $\lambda = 0.4°$, this results in a maximum inaccuracy $|\delta\varphi_m|_{max} = 4.2''$.

5.9 Piecewise self-calibration technique

5.9.1 Introduction

Usually, the conventional sensors are manually adjusted using, for instance, trim potentiometer adjustments to remove the offset errors and gain variations [16, 17], while temperature compensation is accomplished with dedicated temperature compensating elements or networks. However, this method is not suited for a sensor array or a complex sensor with multiple sensing elements, such as capacitive sensors with multiple-electrodes [6, 7, 8]. In smart sensors using microcontrollers, an alternative means of calibration and compensation is more suitable. By determining the relationship between the values indicated by the sensor under controlled conditions and a reference sensor, a correction array for each sensor is obtained. This correction array is loaded in the EPROM of the microcontroller for later use, to compensate for offset and gain errors in real-time by a combination of the software/hardware corrections during signal acquisition and processing.

With respect to the calibration techniques, two methods are in common use: When the acquisition speed is critical, the fastest approach is the use of a look-up table requiring little or no calculation overhead to produce the correction voltage, but this is at the expense of the need for a large EPROM capacity [21, 22]. The second

and slower technique is to apply a higher-order polynomial fit to the data obtained from the measurement [23]. This approach requires much less EPROM capacity, but at the expense of longer data-processing time.

Recently, a calibration technique has been presented [13, 25] which consists of a combination of the two calibration techniques mentioned above, i.e., the use of a relatively simple piecewise-linear-fit formula. The advantages of this technique are:

- fast data processing,
- the moderate use of memory, because only a few correction data are stored in the EPROM.

An important and remarkable property of this technique, called piecewise self-calibration, is that it does not need an accurate reference. Even temperature compensation can also be accomplished in real time without using an additional temperature sensor.

5.9.2 Basic concepts of the calibration technique

Calibration is required to obtain a higher degree of accuracy. The new calibration technique presented in this section is very suitable for this purpose:

The conventional fast look-up table calibration would require the microcontroller to have a large-size memory, or an external memory. However, the curve-fit calibration would need a complex time-consuming calculation. Furthermore, both of the conventional methods would need a very accurate reference for the calibration. The piecewise calibration presented in this section offers a compromise between the memory size of the microcontroller and the complexity of the calculations. In this calibration technique, a relatively simple fit calculation is used to perform the calibration in a certain piecewise measurement range. Only a small correction data array is required for the piecewise fit calculation over the full measurement range.

Figure 5.28 shows the inaccuracy of possible measurement results in a sensor and its piecewise linearized approximation.

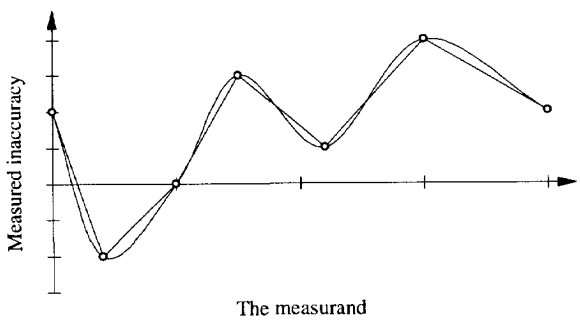

Figure 5.28 The measured systematic inaccuracy for a sensor system and its piecewise linearized approximation.

In this figure, the smooth curve represents the actually measured systematic inaccuracy of the sensor. This inaccuracy can be approximated by using N linear

pieces. Thus, in order to compensate for this inaccuracy, only N simple linear fit formulas and 2(N+1) correction data (measurand and measured inaccuracy data) are required under certain conditions. These linear fit formulas and data are stored in the EPROM of the microcontroller. In the conventional applications of this calibration technique, a very accurate reference is always needed. Under certain conditions, the described calibration technique can be performed without using an accurate reference. This will be shown for the special case of a smart sensor with multiple sensing elements.

In a smart sensor with multiple sensing elements, the correction data can be obtained by performing some additional measurements for some sensing elements under certain conditions. Sometimes, an accurate reference is not needed for such a calibration. Moreover, temperature compensation can be accomplished simultaneously if the correction data can be obtained in real time.

As a general example, Figure 5.29 shows the transfer functions from the measurand x to the output signals y of the sensing elements in a sensor system with multiple sensing elements for a large measurement range. For a capacitive sensor, the output signal y of the sensing element is the capacitance.

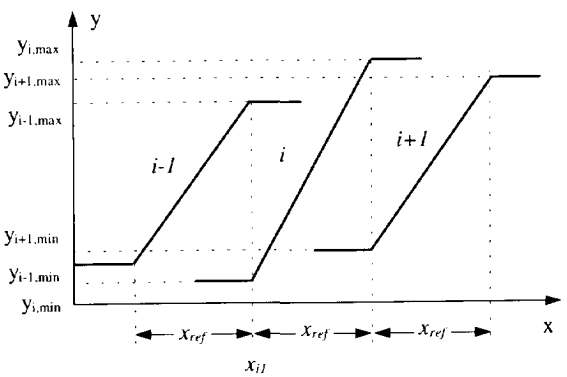

Figure 5.29 The transfer function of the sensing elements in a sensor system with multiple sensing elements.

The transfer functions in the x_{ref} zones of the curves represent the valid transfer relations between the output signals of the sensing elements and the measurand. For one sensing element, outside these regions, the output signal cannot validly report the change of the measurand. Then, generally, the valid region x_{ref} is used to measure the measurand. If the transfer function within the x_{ref} region is linear, we have:

$$y_i = \frac{\left(y_{i,\max} - y_{i,\min}\right)}{x_{ref}}\left(x - x_{i1}\right). \tag{5.46}$$

The parameter x_{i1} is the start point of the x_{ref} zone of a particular sensing element. This formula is only valid in the measurement range of x_{ref} for sensing element i.

Extension of the measurement range can be performed by using other sensing elements, for instance *i-1*, *i+1*, etc.

Because of the mismatch of the sensing elements, the ranges of the maximum values and minimum values ($y_{i,max}$ - $y_{i,min}$) and the slopes of the transfer functions for the various sensing elements can be different. This will result in a systematic error of the sensor system if we only use one formula to represent the transfer relations of all sensing elements.

Because these maximum values and minimum values are insensitive to the measurand in a certain range, it is possible to measure them with a relatively high degree of accuracy without using an additional reference sensor. Then, the systematic error caused by the different values of ($y_{i,max}$ - $y_{i,min}$) can be calibrated by using different parameters ($y_{i,max}$ - $y_{i,min}$) in formula (5.46) for different sensing elements. This calibration technique is very suitable for the sensor system with multiple sensing elements or multiple sensors. An interesting application of this technique is described in the following section.

5.9.3 Application in the capacitive angular-position sensor

The described calibration technique has been successfully implemented in the smart capacitive angular-position sensor with multiple-electrodes shown in Figure 5.3. Although the effect of the mechanical errors is strongly reduced by using a symmetrical and redundant configuration in the sensing element [5 – 9], some mechanical errors, for instance, the nonflatness, and the pattern errors of the segmented electrode will still affect the equality of the segment capacitance values between the outer segments and the common electrode. Here, the influence of the nonflatness of the electrode surface is a mean over the area of one segment. This results in a systematic inaccuracy with a period of six segment widths (90°) on the measured angular position, because the outer window on the rotating electrode repeats itself after six segment widths.

By eliminating the inaccuracy described by formula (5.41) from the measured position described in formula (5.1), or formula (5.6), the measured position is obtained:

$$\frac{\varphi_m}{\varphi_s}=\begin{cases}\left(1-\dfrac{C_{i+2,\max}+C_{i-1,\max}-2C_{i,\max}}{2C_{i,\max}}\right)\dfrac{\varphi_m(C_i)}{\varphi_s}-\dfrac{C_{i+1,\max}-C_{i-1,\max}}{2C_{i,\max}}, & \dfrac{\varphi_s}{2}\geq\varphi_m>0\\ \left(1-\dfrac{C_{i+1,\max}+C_{i-2\max}-2C_{i,\max}}{2C_{i,\max}}\right)\dfrac{\varphi_m(C_i)}{\varphi_s}-\dfrac{C_{i+1,\max}-C_{i-1,\max}}{2C_{i,\max}}, & -\dfrac{\varphi_s}{2}<\varphi_m\leq 0\end{cases} \quad (5.47)$$

for the measurement range of one segment width. Where $\varphi_m(C_i)/\varphi_s$ represents the relationship described by formula (5.1), or formula (5.6). Formula (5.47) shows that the multiplicate and offset calibrations are performed simultaneously. This is used as linear piecewise fit formula for the calibration. Thus, the values of six capacitors ($C_{i,max}$, $i = 1, 2, \cdots, 6$) should be measured beforehand for applying the calibration.

Although formula (5.47) is obtained under some limitation conditions, it also contribute to compensate the effects of the electrode distance errors and the segment width φ_s errors. This calibration is called a self-calibration now, because an accurate reference is not needed for this calibration.

5.9.4 Calibration procedures

In practical measurement of the angular position, first, the capacitances of the sensor are converted to output periods of the signal processor, then these periods are measured by the microcontroller. The measured angular position is calculated from these measured periods. From equations (5.47) and (5.2), the relation between the measured position and the measured periods is represented as:

$$\frac{\varphi_m}{\varphi_s} = \begin{cases} \left(1 - \dfrac{T_{i+2,\max} + T_{i-1,\max} - 2T_{i,\max}}{2(T_{i,\max} - T_{off})}\right)\dfrac{\varphi_m(T_i)}{\varphi_s} - \dfrac{T_{i+1,\max} - T_{i-1,\max}}{2(T_{i,\max} - T_{off})}, & \dfrac{\varphi_s}{2} \geq \varphi_m > 0 \\ \left(1 - \dfrac{T_{i+1,\max} + T_{i-2,\max} - 2T_{i,\max}}{2(T_{i,\max} - T_{off})}\right)\dfrac{\varphi_m(T_i)}{\varphi_s} - \dfrac{T_{i+1,\max} - T_{i-1,\max}}{2(T_{i,\max} - T_{off})}, & -\dfrac{\varphi_s}{2} < \varphi_m \leq 0 \end{cases} \quad (5.48)$$

for the measurement range of one segment width. Where $\varphi_m(T_i)/\varphi_s$ represents the relationship described by the formula (5.3) or formula (5.6).

An important property of formula (5.48) is that many undesired nonidealities, such as, multiplicative errors and offsets, of both the sensing element and the processing circuit are eliminated or significantly reduced.

Here, in order to apply the self-calibration technique in the measurement of the position, seven periods ($T_{i,max}$, (i = 1, 2, ···, 6), and T_{off})) should be measured, and the measured values are stored in the microcontroller in advance.

In a practical sensor structure, the widths of the window and the shield on the rotating electrode are relatively large in comparison with the electrode distance. Thus, when the rotating electrode is in the position where equation (5.3) is equal to zero, the influence of the electric-field-bending effect on the capacitances C_i and C_{i-3} can be ignored. Then, it is found that the maximum value $T_{i,max}$ is:

$$T_{i,\max} \cong T_i \quad (5.49)$$

and the offset period of the signal processor T_{off} can be obtained by:

$$T_{off} \cong T_{i-3}\,. \quad (5.50)$$

That means no additional signal processing circuit is required for the measurement of these seven correction data.

To obtain these seven correction data ($T_{i,max}$, (i = 1, 2, ···, 6), and T_{off}), the screen electrode should be rotated at least 90°. Under stable conditions, for instance, when the changes of temperature and humidity are within a certain limited range, these correction data are valid and can be used for the calibration of the systematic errors according to equation (5.48). When environment temperature is significantly changed, these correction data should be upgraded. It is possible to measure the seven correction data for various temperatures and to store them in the memory. This would require a large memory. Moreover, the long-term drift of the correction data can offer a problem. Therefore, it would be a considerable advantage to upgrade these correction data in real time. For the method presented here, this is possible when both of the following conditions are met:

- the change of temperature is small during the time that the seven data are collected, while the screen electrode is rotated over 90°,
- the rotating speed of the screen electrode is not too high, so the correction data can accurately be measured.

The recalibration procedure can be fully automated and, for instance, repeated when a significant temperature change is observed or after a certain period of time.

The attractive features of this self-calibration technique are its simplicity: only a few correction data are required and an accurate reference is not required. To apply this technique, only seven periods for the correction are required to be measured beforehand. The correction is performed according to the algorithm of equation (5.48). When the seven correction periods can be measured in real time, the temperature compensation can be accomplished simultaneously.

In summarizing the results of the described technique, it can be concluded that this technique offers a good trade-off between the memory size of the microcontroller and the calculated complexity by combining the look-up table calibration and the curve-fit calibration. The application of this technique in a smart capacitive angular-position sensor results in a piecewise self-calibration which does not need an accurate reference. For the multiplicate and offset calibrations of the inaccuracy caused by the mechanical errors and the pattern errors of the electrodes, only three simple linear fit formulas and seven correction data are required.

5.10 Experimental results

5.10.1 Realization of the sensor system

5.10.1.1 Mechanical structure

An angular-position sensor based on the structure described in Figure 5.3 has been built and tested. A distance of 2.5 mm between the common electrode and segmented electrode with a diameter of 50 mm was found to be an optimum to minimize the effect of electric-field bending and mechanical errors. The common electrode and segmented electrode were made using simple printed-circuit-board technology. The capacitance between each of the nonshielded segments and the common electrode amounts to about 0.15 pF. Guarding electrodes, surrounding the segmented electrode and the common electrode, were used to reduce the influence of the electric-field bending and of electromagnetic interference. The rotating electrode with a thickness of 0.2 mm was made out of stainless steel by spark erosion technology and is grounded by a sliding contact. All the electrodes are mounted in a metal housing, with a diameter of 57 mm, which is connected to ground and shields against external interference.

5.10.1.2 Electronic part

One version of the signal processor was implemented with discrete components, and powered by a single 5 V supply voltage. The frequency of the oscillator is about 8.0 kHz, and the applied range of the oscillator frequency is about 4 kHz - 8 kHz. The nine

periods were measured in a total measurement time of about 140 ms. The microcontroller directly gives a digital output signal representing the measured position.

5.10.1.3 The organic whole of the smart sensor

In addition, an advanced version of the smart capacitive angular-position sensor has been realized by using the smart signal processor described in Chapter 4. A cross-section drawing of the entire sensor is shown in Figure 5.30.

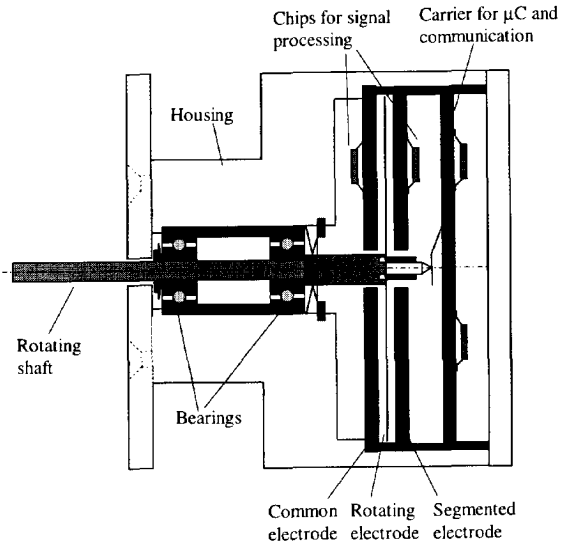

Figure 5.30 A cross-section drawing of the entire sensor.

Here, double-side printed-circuit boards are used as the carriers of both the electrodes and the ICs. Some important advantages of this compact way of assembling are:

- reduction of the influence of the parasitic capacitances of the wiring,
- low-cost manufacturing and material,
- high reliability and stability,
- reduction of EMI problems.

5.10.2 Measurement set-up

A manually driven angular table with a resolution of ±5″ and a measurement range of a full circle (360°) is used as reference sensor. The measurement set-up with a separated signal processor is depicted in Figure 5.31.

A special mechanical coupling is used to couple the shaft of the angular table and the shaft of the capacitive angular-position sensor in order to meet the misalignment (radial shift and radial rotation) between both shafts. The angular table is driven by hand and read out with the naked eye. The electrodes of the capacitive sensing element and the processing circuit are connected via the thin cables.

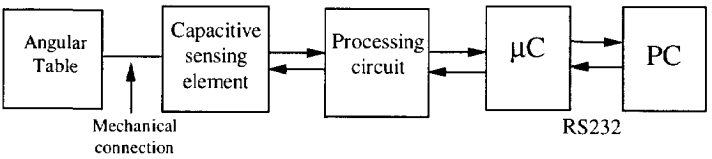

Figure 5.31 The measurement set-up.

The applied microcontroller is of the type 87C51FB. An additional RS232 interface chip is applied to enable communication between the microcontroller and the personal computer.

5.10.3 Measurement results

5.10.3.1 The resolution of the smart sensor system

Figure 5.32 shows the measured noise of the smart sensor system. The measurement time amounted to 580 ms for a single measurement of the angular position. The noise includes the noise of the processing circuit and the sensing element (mechanical and electronic), and the sampling noise of the period measurement.

From the measured noise, the resolution of the entire sensor system is found to be 0.58″ and 1.41″, respectively, when the shaft of the capacitive angular-position sensor is free or is not free from the shaft of the angular table (see Figure 5.32).

Figure 5.33 shows the relation between the noise of the sensor system and the measurement time. When the time of one complete measurement is shorter than 76 ms, increasing measurement time is very effective to reduce the measurement noise. However, for longer measurement times, no noise reduction is found. This is due to the mechanical noise. The measurement noise even increases with very long measurement times. For noise, the optimum range of measurement time is about 160 ms to 1230 ms.

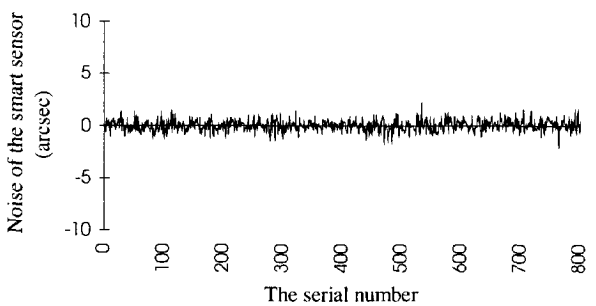

(a)

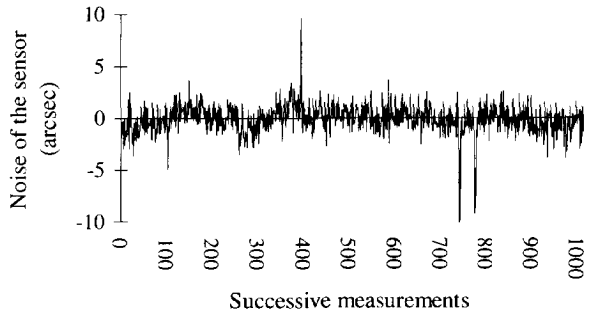

(b)

Figure 5.32 The measured noise of the capacitive angular-position sensor, for a series of measurements performed under identical conditions in a fixed position of the rotating electrode. Each measurement takes about 580 ms. a) The shaft of the capacitive angular-position sensor is free from the shaft of the angular table, (b) The shaft of the capacitive angular-position sensor is not free from the shaft of the angular table.

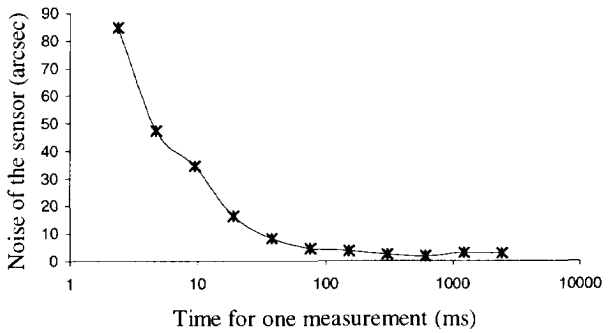

Figure 5.33 The relation between the measured noise of the sensor and the measurement time.

5.10.3.2 Reproducibility

The reproducibility of the measurement set-up and the capacitive angular-position sensor is defined as the angular-position inaccuracy, relative to the angular position measured by the angular table, where the same angular position is reproduced several times. The measured reproducibility amounts to 2.54″ (see Figure 5.34).

5.10.3.3 Repeatability

The repeatability is defined as the difference between two successive measurements of the angular position by the capacitive angular-position sensor. For the two

successive measurements, the angular position to be measured is monitored by the angular table. The measured repeatability amounts to 3.56″ (see Figure 5.35).

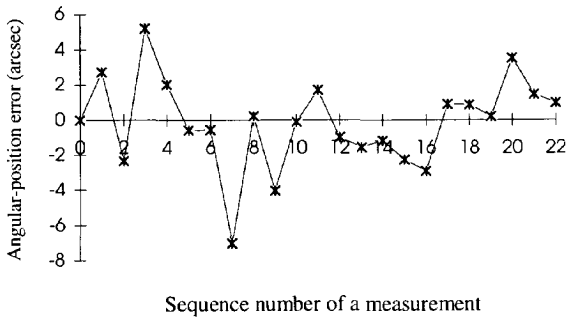

Figure 5.34 The angular-position inaccuracy, relative to the angular position measured by the angular table (read-out error of ±5″), where the same angular position is reproduced 23 times.

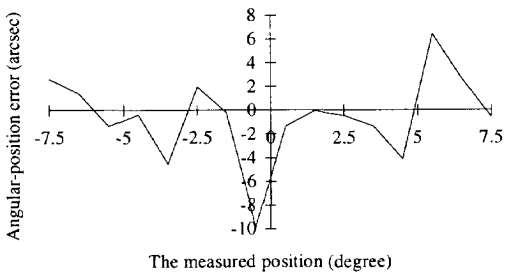

Figure 5.35 The repeatability of the sensor system.

5.10.3.4 Inaccuracy of the sensor

The measured absolute inaccuracy of the entire sensor system over the measurement range of a full circle (360°) amounts to 123.1″ *without fine tuning* (α = 0) (see Figure 5.36(a)) and 57.7″ *with fine tuning* (α = 0.0328) (see Figure 5.36(b)).

5.10.3.5 Measured inaccuracy in relation to the electrode distance

Figure 5.37 shows the relations between the measured inaccuracy of the angular-position sensor and the electrode distance, without and with fine tuning. Meanwhile, the relation between the optimum values of the fine-tuning factor and the electrode distance are also shown.

From this figure, an optimum electrode distance can be obtained because the inaccuracy caused by the electric-field-bending effect is proportional to the electrode

distance and the inaccuracy caused by the nonflatness of the electrode surface is inversely proportional to the electrode distance.

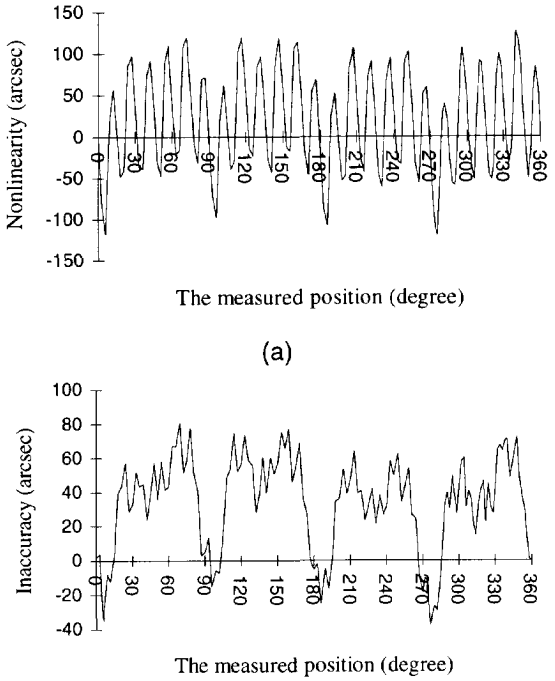

Figure 5.36 The measured inaccuracies of the sensor system. (a) without fine tuning ($\alpha = 0$), (b) with fine tuning ($\alpha = 0.0328$).

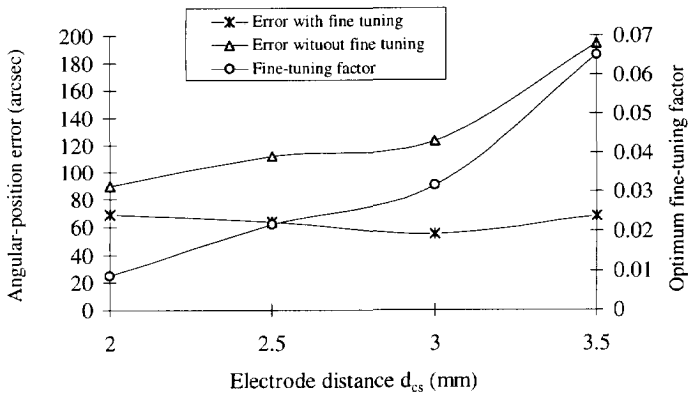

Figure 5.37 The relations of the measured inaccuracy and optimum fine-tuning factor with the electrode distance.

5.10.4 Discussion

5.10.4.1 The noise

The noise shown in Figure 5.32(a) originates mainly from the noise of the processing circuit and the capacitances of the sensing element, and the sampling noise of the period measurement. From Figure 5.32(a) and (b), the mechanical noise, which originates from the sensing element and the mechanical coupling, is found to be:

$$\sqrt{1.41^2 - 0.58^2} = 1.29''.$$

It is concluded that the overall resolution, including the sensing element and measurement set-up, is dominated by the mechanical part.

5.10.4.2 Electric-field-bending effect and the fine-tuning-factor effect

In Figure 5.36(a), where no fine tuning is applied, it is shown that the angular-position inaccuracy of the sensor consists mainly of two periodic parts: one with a period of one segment width (15°) is caused by the electric-field-bending effect, and another one with a period of 90° is caused by the mechanical errors, such as the nonflatness, obliqueness, eccentricity, pattern errors of the segmented electrode.

In Figure 5.38(a), the inaccuracy caused by the electric-field-bending effect over one segment width is shown to be about 84.2″ without fine tuning ($\alpha = 0$). When fine tuning is applied ($\alpha = 0.0314$), the remaining error is only 14.4″ and has a period of half the width of one segment (7.5°) (see Figure 5.38(b)). The fine tuning correction is very effective in reducing the electric-field-bending effect. By applying the fine tuning, the improvement in the nonlinearity caused by the electric-field-bending effect amounts to a factor of 5.8. This measured result is in good agreement with the simulated results presented in Section 5.6.

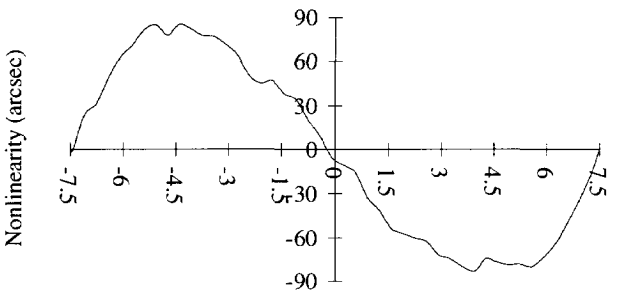

(a)

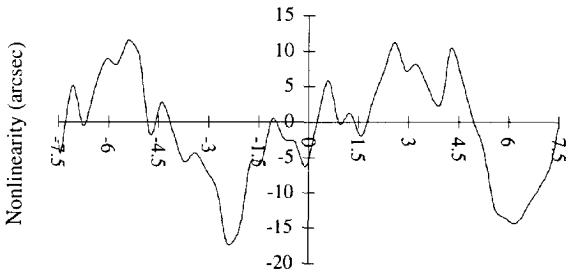

(b)

Figure 5.38 The measured angular-position error over one segment width; without fine tuning ($\alpha = 0$), (b) with fine tuning ($\alpha = 0.0314$).

5.10.4.3 The influence of the eccentricity

The inaccuracy caused by the hole of the rotating electrode for the coarse measurement in combination with the eccentricity is about 8.5″ (see Figure 5.39).

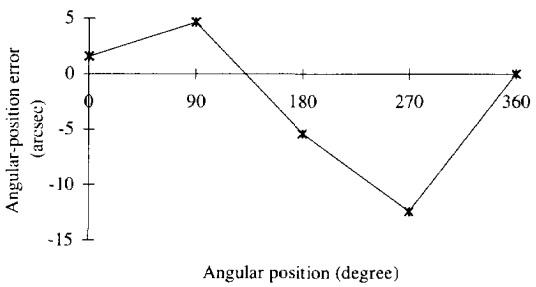

Figure 5.39 The measured angular-position inaccuracy due to the nonsymmetrical configuration. Each value in the figure is an average of five measurements taken to reduce the electrical noise of the sensor.

5.10.4.4 Pattern error and calibration

Figure 5.40 shows the measured capacitances between the segmented electrodes and the common electrodes. The errors are due to pattern errors and nonflatness. These errors cause a systematic inaccuracy of 39.3″ with a period of 90° on the measurement angular position. This inaccuracy can further be reduced by using the self-calibration technique described in Section 5.9. After fine-tuning correction and the self-calibration technique are applied, the angular-position inaccuracy of the sensor is reduced to 26.2″ (15.5 bits) (see Figure 5.41). The improvement in the inaccuracy of the sensor by using the self-calibration technique amounts to a factor of 2.2.

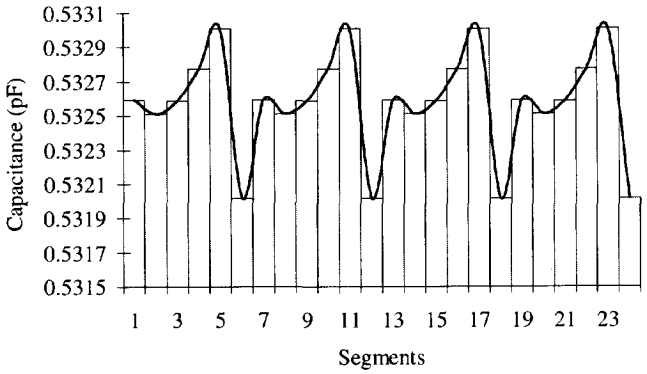

Figure 5.40 The measured capacitances between the segmented electrodes and the common electrodes.

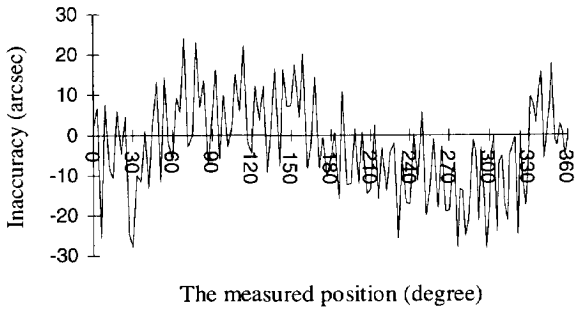

Figure 5.41 The inaccuracy of the sensor after fine-tuning correction and self-calibration.

In Figure 5.41, the remaining inaccuracy originates mainly from the noise of the sensor system, the remaining nonlinearity caused by the electric-field-bending effect, and the inaccuracy caused by the hole in the rotating electrode for the coarse measurement in combination with eccentricity. The last two inaccuracies can be reduced by decreasing the electrode distance d_{cs} and increasing the margin between the rotating electrode and segmented electrode in the radial dimension. This means that the optimum electrode distance will decrease when self-calibration is applied.

5.10.5 Conclusions

The inaccuracy shown in Figure 5.36(a) consists mainly of two periodic parts: one with a period of one segment width (15°) and the other with a period of six segment widths (90°). The effect of the electric-field bending causes mainly an inaccurate component with a period of one segment width (15°), because of the repeatability of one

segment width for the accurate fine measurement. The mechanical errors, such as the nonflatness, the obliqueness, the eccentricity, and the pattern errors of the electrodes cause mainly an inaccuracy with a period of six segment widths (90°), because the measurement with the outer electrodes repeats itself after six segment widths. From Figure 5.36(b), it is concluded that the effect of fine-tuning is very effective in reducing the influence of the electric-field-bending effect. The remaining inaccuracy after fine tuning mainly originates from the mechanical errors and the pattern errors of the electrodes, and can be further reduced by applying the self-calibration technique.

5.11 Conclusions

A low-cost, high-performance smart capacitive angular-position sensor with a full-circle measurement range has been presented. The symmetrical and redundant structure of the sensing element drastically reduces the mechanical errors, such as the nonflatness, obliqueness, eccentricity and pattern errors of the electrodes. The applied algorithm eliminates or strongly reduces the influences of many systematic nonidealities of the sensing element and the signal processor, such as the electric-field-bending effect and mechanical errors, in a very effective way. The sensor's geometrical structure is optimized by analyzing the influences of various error sources. The use of a smart signal processor and a microcontroller makes it very easy to accurately measure small multiple capacitances. Meanwhile, the microcontroller performs self-calibration to further reduce the remained systematic inaccuracy after applying fine-tuning. A prototype of the sensor has been built using low-cost material. The inaccuracy of this smart capacitive angular-position sensor is less than ±26.2″ over the measurement range of 360° for a measurement time of about 140 ms.

References

[1] W. Chr. Heerens, "Review article: application of capacitance techniques in sensor design," J. Phys. E: Sci. Instrum., vol. 19, 1986, pp. 897-906.
[2] F. Zhu, J.W. Spronck and H.F. van Beek, "A capacitive absolute position transducer," In Proc. of the 7th International Precision Engineering Seminar, Kobe, Japan, 1993.
[3] F.N. Toth and G.C.M. Meijer, "A low-cost, smart capacitive position sensor," IEEE Trans. Instrum. Meas., vol. 41, no. 6, Dec. 1992, pp.1041-1044.
[4] W. Chr. Heerens, "Multi-terminal capacitor sensors," J. of Phys. E: Sci. Instrum., Vol. 15, 1982, pp. 137-141.
[5]. G.W. de Jong, G.C.M. Meijer, K. van der Lingen, J.W. Spronck, A.M.M. Aalsma and Th. D.A.J.M. Bertels, "A smart capacitive absolute angular-position sensor," Sensors and Actuators, vol. A41-A42, 1994, pp. 212-216.
[6] G.W. de Jong, " Smart capacitive sensor (physical, geometrical and electronic aspects)," Ph.D. Thesis, Delft University of Technology, April 1994.
[7] X. Li, G.C.M. Meijer and G.W. de Jong, "An accurate smart capacitive angular-position sensor with a full circle range, " in Proc. IMTC/95, Watham, USA, April 24-26, 1995, pp. 80-83.

[8] X. Li, G.C.M. Meijer, G.W. de Jong and J.W. Spronck, "An accurate low-cost capacitive absolute angular-position sensor with a full-circle range," IEEE Trans. Instrum. Meas., vol. 45, no. 2, April 1996, pp. 516-520.
[9] X. Li and G.C.M. Meijer, "A high-performance capacitive absolute angular encoder," in Proc. National Conference on Sensor Technology, Delft, The Netherlands, March 1996, pp.151-154.
[10] X. Li, "Design of smart capacitive sensor with full-circle measurement range," Internal report, Faculty of Electrical Engineering, TU Delft, Aug. 1994.
[11] G. Brasseur, "A robust capacitive angular position sensor," in Proc. of the IEEE IMTC/96, Brussels, Belgium, June 1996, pp. 1081-1086.
[12] M.H.W. Bonse, "Capacitive position transducers, theoretical aspects and practical applications," Ph.D. Thesis, Delft Univ. of Technology, Faculty of Mechanical Engineering and Marine Technology, Dec. 1995.
[13] X. Li and G.C.M. Meijer, "A self-calibration technique for a smart capacitive angular-position sensor," in Proc. IEEE IMTC/96, Brussels, Belgium, June 1996, pp. 774-777.
[14] X. Li, G.W. de Jong and G.C.M. Meijer, "The application of the capacitor's physics to optimize capacitive angular-position sensors," IEEE Trans. Instrum. Meas., vol. 46, no. 1, Feb. 1997, pp. 8-14.
[15] W. Chr. Heerens, "Multi-terminal capacitor sensors," Journal of Physics E: Sci. Instrum., vol. 15, 1982, pp. 137-141.
[16] Ansoft Corp., "Maxwell 2D Field Simulator," Version 4.3x Release Notes, Pittsburgh, USA, June 1991.
[17] IEC 1969, Publication No. 250, Geneva: IEC.
[18] ASTM 1986, Publication D 150, Philadelphia: ASTM.
[19] G.C.M. Meijer and A.W. van Herwaaden "Thermal sensors," IOP, Bristol, 1994.
[20] G. Erdi, "A precision trim technique for monolithic analog circuits," IEEE J. Solid-State Circuits, vol. 10, 1975, pp. 412-416.
[21] Paul T. Kolen, "Self-calibration/compensation technique for microcontroller-based on sensor arrays," IEEE Trans. Instrum. Meas., vol. 43, no. 4, Aug. 1994, pp. 620-623.
[22] J. Brignell, "Software techniques for sensor compensation," Sensors and Actuators, vol. A25-A27, 1991, pp. 29-35.
[23] P. Hille, R. Hohler and H. Strack, "A linearisation and compensation method for integrated sensors," Sensors and Actuators, vol. A44, 1994, pp. 95-102.
[24] D.G.W. Goad and H.J. Wintle, "Capacitance corrections for guard gaps," Meas. Sci. Technol. vol.1, no.9, Sept. 1990, pp. 965-969.
[25] X. Li, G.C.M. Meijer and G.W. de Jong, "A microcontroller-based self-calibration technique for a smart capacitive angular-position sensor," IEEE Trans. Instrum. Meas., vol. 46, no. 3, June. 1997.

Chapter 6

Contactless Potentiometric Position Sensor

6.1 Introduction

Consisting of a single wire with a sliding contact, the conventional resistive potentiometer is one of the simplest and most efficient position sensors. However, its disadvantages are low accuracy and low linearity. Moreover, the long-term stability of this system is bad, since the sliding contact is directly in contact with the resistive element of the potentiometer. The position-sensitive detector (PSD) which is an optical potentiometer [1, 2, 3] is an interesting alternative which is suitable to be implemented as an integrated circuit. However, this system can only measure displacement over a narrow range (3 mm), and the cost and energy consumption of the PSD and the LED are rather high. These drawbacks are overcome in the novel contactless potentiometers which are described in ref. [6 – 9]. The modified potentiometer is used as a sensing element for a low-cost smart contactless position sensor.

The smart contactless position sensor is suitable to replace both linear and circular potentiometers. In this chapter, we limit ourselves to the discussion of an angular position sensor for the measurement range of 270°.

6.2 Basic principle

Figure 6.1 shows the entire contactless position sensor system.

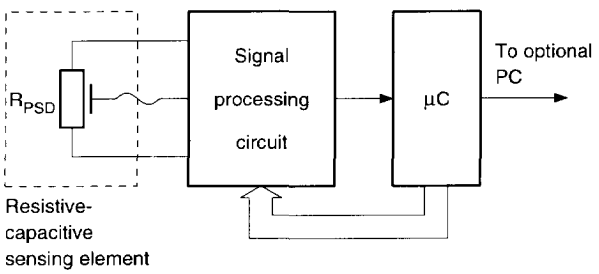

Figure 6.1 An overview of a contactless position sensor for a linear potentiometer.

The contactless sensing element is a modified potentiometer with a sliding contact which is not directly in contact with the resistive layer of the conventional potentiometer.

The slide forms an electrode which is capacitively coupled to the resistive layer. The advantages are low cost, high long-term stability and a wide measuring range [6, 7, 8].

The signal processor described in Chapter 4 or a modified Martin oscillator can be used in this case. The use of the three-signal approach, as presented in Chapter 3 and ref. [1, 5] , will eliminate many nonidealities. The period-modulated output signal of the signal processor, of which the period is linearly related to the position, is directly read out by a microcontroller.

6.3 Electrode structure

The contactless sensing element consists mainly of two parts: a rotating electrode and a resistive layer. A simple equivalent model of the contactless position sensor is shown in Figure 6.2.

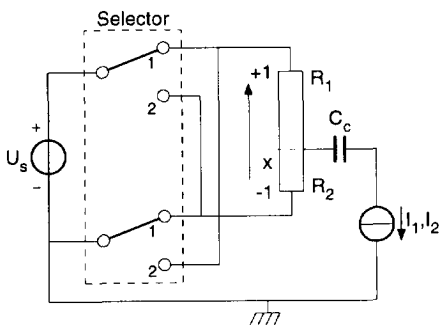

Figure 6.2 A simple equivalent model of the contactless sensing element.

The capacitor C_c represents the equivalent capacitance between the sliding electrode and the resistive layer. The sum of the resistances R_1 and R_2 is the resistance R_{PSD} of the resistive layer. When I_1 and I_2 represent the currents through C_c in the position "1" and "2" of the switches respectively, then it holds that

$$I_1 = \frac{j\omega C_c U_s}{R_1 + R_2 + j\omega R_1 R_2 C_c} R_2, \tag{6.1}$$

$$I_2 = \frac{j\omega C_c U_s}{R_1 + R_2 + j\omega R_1 R_2 C_c} R_1. \tag{6.2}$$

When we denote the relative position by a number x, which varies from -1 for the bottom position to +1 for the top position, then we find that

$$x = \frac{R_2 - R_1}{R_1 + R_2} = \frac{I_1 - I_2}{I_1 + I_2}. \tag{6.3}$$

The position x is only the function of the resistances R_1 and R_2 and is not related to capacitance C_c. This is an important property because it means that the measurement is

immune to the electrode distance and the mechanical tolerances which result from deviations or nonuniformity of the electrode distance.

Figure 6.3 shows the simplified structure of the contactless angular sensing element. It is mainly composed of two parts: a nonmoving part formed by the resistive layer, and a rotating part formed by the sliding electrode which is capacitively coupled with the resistive layer.

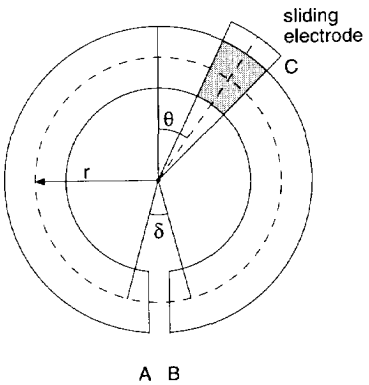

Figure 6.3 The simplified structure of the sensing element of the angular position sensor.

The radius r is the average radius of the resistive layer. The relation of the angle θ to the resistors R_1 and R_2 is

$$\theta = (180 - \delta/2)\frac{R_2 - R_1}{R_1 + R_2} = K\frac{R_2 - R_1}{R_1 + R_2} = Kx, \tag{6.4}$$

where K = 180-δ/2 (degree) is a constant, which represents half of the angular measurement range. It is not necessary to use a small sliding electrode. In fact, the width of this electrode is only limited by the wish to make the measuring range as large as possible. It can easily be shown that the measured position x corresponds to the position of the center of the sliding electrode.

6.4 Signal processing

In order to obtain the position x or the angle θ, the three currents I_1, I_2 and I_0 have to be measured. The current I_0 is permitted to be zero. The three currents can be converted into period-modulated signals, using a capacitance-controlled oscillator which generates square-wave output signals where periods T_{pi} are related to the current by the linear equation

$$T_{pi} = aI_i + b \quad (i = 0,\ 1,\ 2). \tag{6.5}$$

When I_0= 0, we find

$$\frac{T_{p1}-T_{p2}}{T_{p1}+T_{p2}-2T_{p0}}=\frac{I_1-I_2}{I_1+I_2}=x. \tag{6.6}$$

In this result, the influence of the unknown offset *b* and the unknown gain *a* of the capacitance-controlled oscillator is also eliminated.

Figure 6.4 shows the electronic circuitry for the smart contactless position sensor system [6, 7, 8].

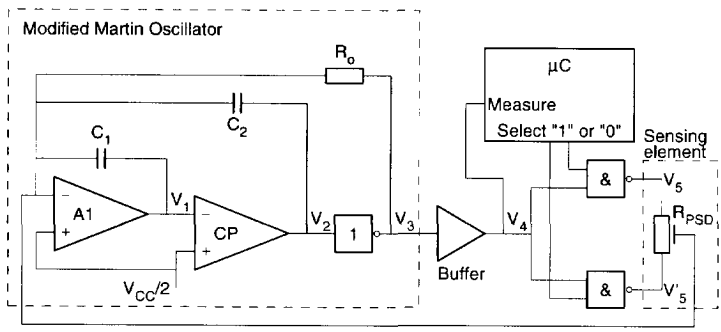

Figure 6.4 The electronic circuitry of the smart contactless position sensor system.

The modified Martin oscillator [4, 5] is composed of an operational amplifier A_1, a comparator CP, an inverter, the capacitances C_1, C_2 and a resistance R_0. The microcontroller can directly read out the period-modulated signals from V_4 and control the selector (two NAND gates). A noninverting buffer is used between the oscillator and the selector to eliminate undesired interactions.

6.5 Nonidealities

In ref. [1] it is shown that the system is immune to most of the nonidealities of the opamp and the comparator, such as slewing, limitations of bandwidth and gain, offset voltages and input bias currents. These nonidealities cause only additive or multiplicative errors which are eliminated by the three-signal method. However, some effects cannot be eliminated by the three-signal method in this system, as we discuss now:

6.5.1 The effect of two NAND gates which have different ON resistances R_{ON}

The output stages of two NAND gates shown in Figure 6.4 will have an influence on the measured position. Figure 6.5 shows the output stages of two NAND gates and their equivalent models with different ON or OFF conditions.

The resistances R_{PON1}, R_{NON2}, R_{PON3} and R_{NON4} represent, respectively, the ON resistances of M_1, M_2, M_3 and M_4. Further, it is assumed that this includes the parasitic resistances between the output terminals of the NAND gates and the connectors of the

resistive layer respectively. The M_1 and M_2, M_3 and M_4 are, respectively, the output transistors of two NAND gates.

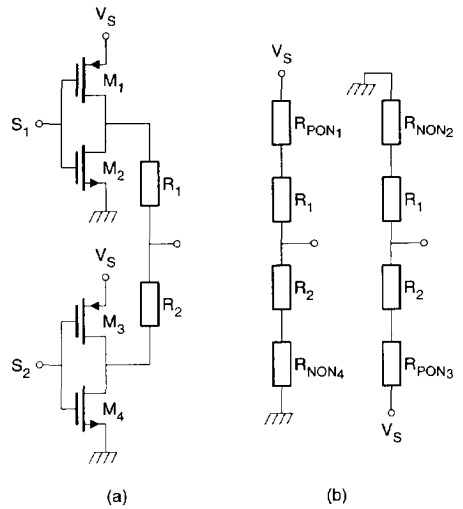

Figure 6.5 The output stages of two NAND gates and their equivalent models.

A straightforward calculation of the inaccuracy of R_{ON} for the measured position can be approximated by:

$$\frac{T_{p1}-T_{p2}}{T_{p1}+T_{p2}-2T_{p0}} \cong x\left[1-\left(R_{NON1}+R_{NON2}\right)/R_{PSD}\right] + x^2\left(R_{PON1}-R_{PON2}+R_{NON2}-R_{NON1}\right)/2R_{PSD} + \left(R_{PON2}-R_{PON1}+R_{NON2}-R_{NON1}\right)/2R_{PSD} \quad (6.7)$$

Formula (6.7) shows that the ON resistances of the NAND gates not only cause an offset and a gain error but also the nonlinearity. Usually, the offset and gain errors can easily be eliminated during the installation and calibration of the angular position sensor in its final set-up. The maximum influence of R_{ON} occurs at $x = \pm 1$. When, for example, $R_{NON} = 40\ \Omega$, $\Delta R_{NON} = 4\ \Omega$, $R_{PON} = 50\ \Omega$, $\Delta R_{PON} = 5\ \Omega$ and $R_{PSD} = 100\ k\Omega$, then both the maximum nonlinearity and the offset amount to 0.0045% (which corresponds to 21.1 arcsec).

6.5.2 The effect of the parasitic capacitances

The parasitic capacitors of the smart angular position sensor are shown in Figure 6.6. The effects of the parasitic capacitors C_{p1}, C_{p1}' and C_{p3} can be neglected, where the C_{p1}, C_{p1}' and C_{p3} include the cable capacitances. The parasitic capacitances C_{p2} and C_{p2}' are also composed of two parts: the parasitic capacitances between the sliding electrode and the terminals of the resistive layer, and the parasitic capacitances between the outputs of the selector and the inverting input of the integrator in the measuring circuit.

The influence of the parasitic capacitances C_{p2} and C_{p2}' on the measured position can be expressed by the following equation:

$$\frac{T_{p1}-T_{p2}}{T_{p1}+T_{p2}-2T_{p0}} \cong \frac{x+\left(C_{p2}-C'_{p2}\right)/C_c}{1+\left(C_{p2}+C'_{p2}\right)/C_c}. \tag{6.8}$$

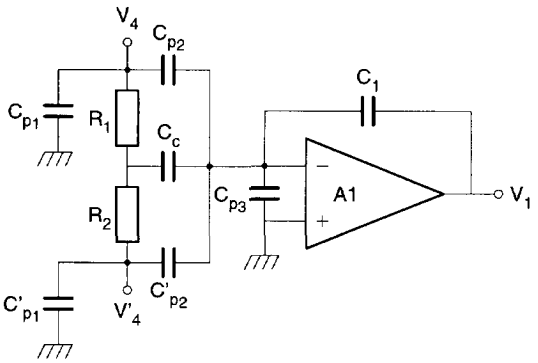

Figure 6.6 The parasitic capacitances of the sensor.

Formula (6.8) shows that the measured position is related to the capacitance C_c, due to the effect of the parasitic capacitances.

Since the capacitor C_c is very small (about 2.2 pF), the parasitic capacitors C_{p2} and C_{p2}' can cause a large error in the position measurement. This error will change with the position x (or angle θ) since the capacitor C_c and the parasitic capacitors C_{p2} and C_{p2}' depend on the position x. Therefore, the parasitic capacitances C_{p2} and C_{p2}' have to be minimized in the design of the sensing element and measuring system.

6.6 Experimental results

The system has been built and tested using a contactless angular sensor, a signal-processing circuit and a microcontroller of the type INTEL D87C51FA. The signal-processing circuit uses a modified Martin oscillator [4, 5] which has been implemented with a simple dual OPAMP (TLC272AC) and two CMOS NAND gates according to the circuit shown in Figure 6.4. The structure of the sensing element is shown in Figure 6.7. The resistive potentiometer R_{PSD} is approximately 100 kΩ.

The electrodes were made using printed-circuit-board technology. The sliding electrode has an effective area of 61 mm^2. The distance between the sliding electrode and the resistive layer is about 0.2 mm, and the equivalent capacitance C_c is about 2.2 pF. In order to eliminate the influence of the parasitic capacitors and the electromagnetic interference, guarding electrodes were made all around the sliding electrode, and shielding is used.

The measuring system is powered by a single 5V supply voltage. The frequency of the oscillator is about 7.0 kHz, and the applied range of the oscillator frequency is about 3.3 kHz – 7.0 kHz. The three periods T_{p0}, T_{p1}, T_{p2} are measured in a total measurement time of about 100 ms. The noise of the signal processor, which includes the sampling noise, is shown in Figure 6.8.

The measured nonlinearity of the entire smart sensor system over the measurement range of -135° to +135° is less than ±0.3% (see Figure 6.9). This nonlinearity is mainly due to the nonlinearity of the resistive layer and the effect of the parasitic capacitors.

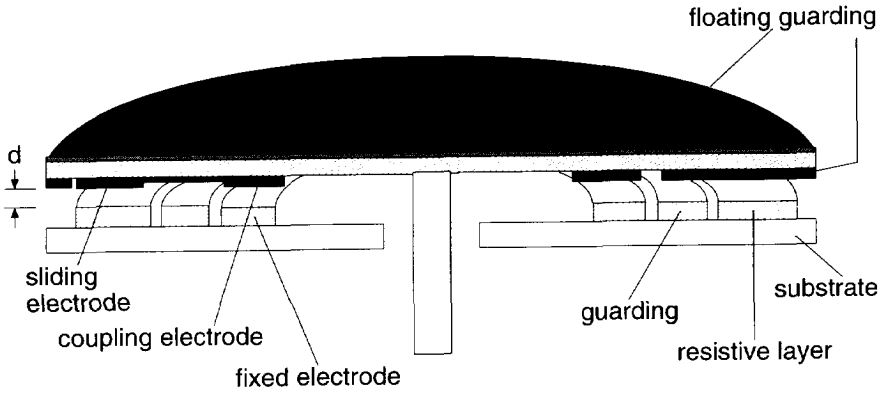

Figure 6.7 The physical structure of the sensing element.

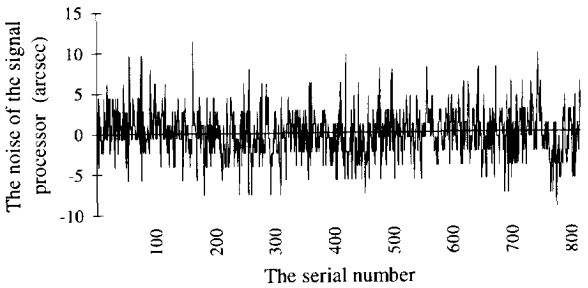

Figure 6.8 The noise of the signal processor. The result of a series of 800 measurements performed under identical conditions. Each measurement takes about 100 ms.

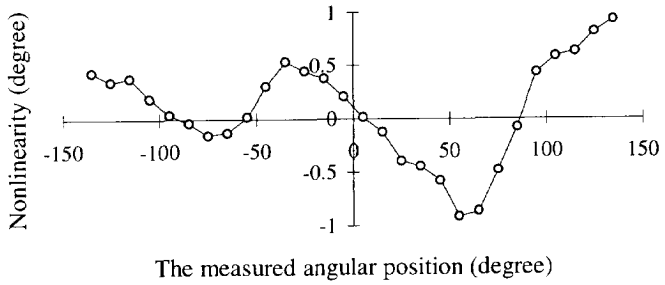

Figure 6.9 The experimental results for the nonlinearity of the complete smart sensor.

6.7 Conclusions

A novel contactless position sensor has been presented. The signal-processing circuit is simple and can be implemented as a single-chip CMOS integrated circuit. A prototype of the system has been built and tested. The nonlinearity amounts to 0.3%. The main causes of this nonlinearity are the parasitic capacitors in the sensing element and the nonlinearity of the resistive layer.

References

[1] G.C.M. Meijer, Jaap van Drecht, Paul C. de Jong and Harry Neuteboom. "New concepts for smart signal processors and their application to PSD displacement transducers", Sensors and Actuators, vol. A35, 1992, pp. 23-30.

[2] G.C.M. Meijer and R. Schrier, "A linear high-performance PSD displacement transducer with microcontroller interfacing", Sensors and Actuators, vol. A21-A23, 1990, pp. 538-543.

[3] Y.Z. Xing and W.J. Lian, "A novel integrated optical potentiometer", Proc. 4th Int. Conf. Solid-State Sensors and Actuators (Transducers'87), Tokyo, Japan, June 2-5, 1987, pp. 427-430.

[4] K. Martin, "A voltage-controlled switched-capacitor relaxation oscillator", IEEE J. Solid-State Circuits, vol. 16, no. 4, Aug. 1981, pp. 412-413.

[5] F.N. Toth and G.C.M. Meijer, "A low-cost, smart capacitive position sensor", IEEE Trans. on Instr. and Meas. , vol. 41, no. 6, Dec. 1992, pp.1041-1044.

[6] X. Li and G.C.M. Meijer, "A smart resistive-capacitive position sensor," in Proc. Dutch conference on Sensor Technology, Enschde, The Netherlands, Feb. 1994, pp. 135-139.

[7] X. Li and G.C.M. Meijer, "A novel smart resistive-capacitive angular PSD", Proceedings of the IEEE, IMTC '94, May 1994, Hamamastu, Japan, pp. 308-311.

[8] X. Li and G.C.M. Meijer, "A novel smart resistive-capacitive position sensor," IEEE Trans. Instrum. Meas., vol. 44, no. 3, June 1995, pp.768-770.

[9] —, "Non-contacting potentiometer opens up new perspectives," NovoTechnik, 1996.

Chapter 7

Capacitive Sensor for Low-Speed Measurement

7.1 Introduction

Many methods to measure speed have been presented in the previous papers [1, 2, 3]. They can be classified into two typical categories:

- the spatial filter method,
- the digital measurement method.

As an example of the spatial filter method, assuming a light source moving behind parallel-slit reticules with a speed magnitude ϑ, a viewer positioned in front will observe a blinking phenomena (see Figure 7.1). The frequency of this blinking f will be proportional to the magnitude of the speed of the moving light source. This relationship can be written as

$$\vartheta = p / T = p \cdot f \tag{7.1}$$

where p is the pitch of the parallel-slit reticules and T is the period of the blinking. Therefore, by measuring f, we can calculate the magnitude of the speed of the moving object. This technique for measuring speed-magnitude is termed the "spatial filter method".

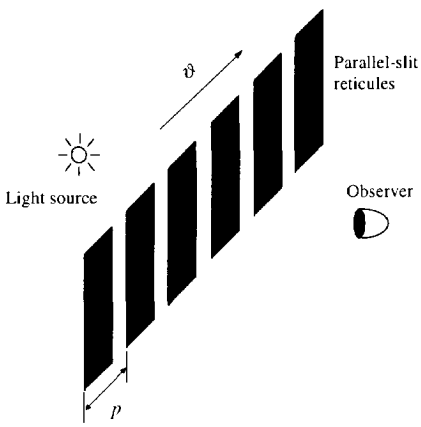

Figure 7.1 A speed measurement model using the spatial filter method.

The frequency of the blinking can be measured by modeling the parallel-slit reticules as the spatial impulse response of the system, and convolving this response with the moving light source as the spatial input signal. The blinking effect implies that the output signals of the spatial filter system are in the time domain, i.e., the output signals stretch or contact in the time domain with corresponding changes in the speed of the moving light source.

In the digital speed measurement method, a shaft encoder (optical) or magnetic pick-up are usually used to detect angular speed. The output of the shaft encoder provides electric pulses. The frequency of these pulses is proportional to the rotational speed. A speed signal is obtained by processing the pulses from the encoder by using an additional electronic circuit. The direction of the speed can be evaluated by using two quadrature pulses from the encoder.

Several methods can be used to derive the speed signal from the encoder pulses. The typical methods are:

- direct pulse counting,
- single pulse time measurement,
- constant elapsed time,
- pulse time measurement using a variable number of counted pulses.

When using the digital speed measurement method, it will take a relatively long time to perform a single low-speed measurement. A simple alternative and relatively fast method for the measurement of very low speed can be obtained by using a potentiometer as the sensing element [4]. When using this method, an accuracy of 0.8 percent has been reported for a speed of 1 rpm in a measurement time of 200 ms. However, since the sliding contact is directly in contact with the resistive element of the potentiometer, the long-term stability is poor and there is a hysteresis problem when the speed is changed. Two speed measurement methods using capacitive sensor have been presented in ref. [6], see Section 4.5. However, these methods are only suitable to measure high and middle speed.

In this chapter, a new method for the measurement of low speed by using the multiple capacitive sensing element described in Section 5.3 (see Figure 5.3) is presented. Then, it is possible to measure both angular position and low speed using one capacitive sensor. The processing circuit for the angular-position measurement can also be used to convert the time-variable capacitance to a period-modulated signal which can directly be read out by a microcontroller. A new algorithm, which can eliminate or strongly reduce the influence of many nonidealities, is used to calculate the speed from the values of the measured capacitances. The measurement can be performed in a relatively short time. Meanwhile, the direction of rotation can also be indicated.

7.2 Measurement principles

When the value of a capacitor linearly varies with the position, this phenomenon can be used for the measurement of low speed. The relation between the speed ϑ to be measured and the capacitance can be described as:

$$\vartheta = \frac{\partial C_s / \partial t}{\partial C_s / \partial x} = \frac{1}{K} \cdot \frac{\partial C_s}{\partial t} . \tag{7.2}$$

Where K is the slope that capacitance changes with the position, which only depends on the structure of the capacitive sensing element, and for which it holds that:

$$K = \frac{C_{smax} - C_{smin}}{x_{se}}. \tag{7.3}$$

In this equation, x_{se} is the effective segment width of the capacitive sensing element.

Figure 7.2 shows a simple capacitive low-speed sensor system [5, 7]. The sensing element for the speed is the capacitor C_s, whose value is linear with the position. A simple signal processor described in Chapter 6 is employed to measure the time-variant capacitance.

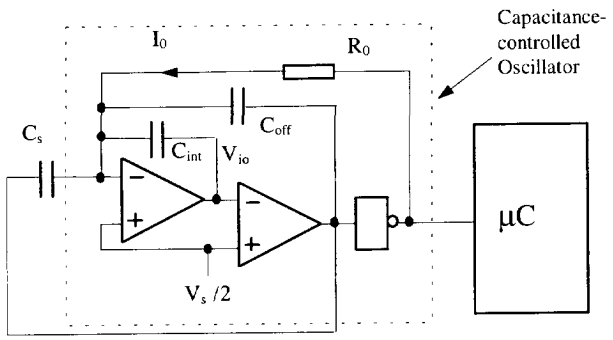

Figure 7.2 An overview of the measurement system for low speed.

At any instant, the time-variant capacitance C_s can be converted into a period-modulated signal by using a capacitance-controlled oscillator which generates square-wave output signals. This period-modulated signal can be directly read out and processed by a microcontroller.

Figure 7.3 shows the waveform of voltage V_{io} at the integrator output of the oscillator, for the case where the moving electrode of the capacitive sensing element is moving.

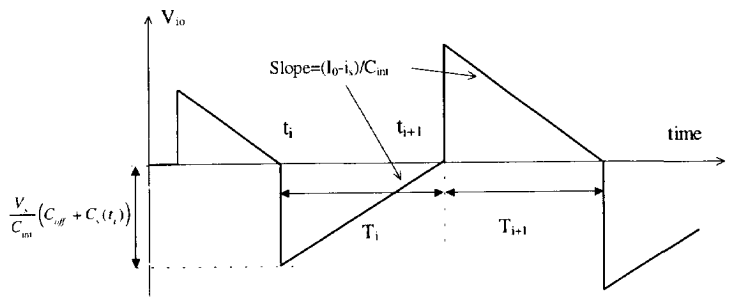

Figure 7.3 The waveform of V_{io} of the oscillator.

According to the principle of the oscillator, two adjacent charge and discharge time intervals T_i and T_{i+1} amount to

$$T_i = \frac{V_s\left[C_s(t_i) + C_{off}\right]}{I_0 - i_s}, \tag{7.4}$$

$$T_{i+1} = \frac{V_s\left[C_s(t_{i+1}) + C_{off}\right]}{I_0 - i_s}, \tag{7.5}$$

where V_s is the supply voltage and i_s is a current which is caused by the change of the capacitance with time. For the current i_s it holds that

$$i_s = V_s \frac{\partial C_s(t)}{\partial t} = V_s K \vartheta . \tag{7.6}$$

For a constant speed, the relation between capacitances $C_s(t_i)$ at moment t_i and $C_s(t_{i+1})$ at moment t_{i+1} can be written as :

$$C_s(t_{i+1}) = C_s(t_i) + \frac{\partial C_s}{\partial t} T_i . \tag{7.7}$$

From the equations (7.4) – (7.7), the average speed ϑ_{av} over time T_i+T_{i+1} is obtained, which yields:

$$\vartheta_{av} = \frac{I_0}{KV_s} \cdot \left(1 - \frac{T_i}{T_{i+1}}\right) \tag{7.8}$$

By measuring two adjacent half-periods T_i and T_{i+1}, and using equation (7.8), the average speed over time T_i+T_{i+1} can be calculated. However, this measuring method has the following disadvantages,

- there are errors caused by the delay time t_d of the oscillator,
- the serious influence of offset voltage and bias current of the OPAMPs in the oscillator,
- the considerable sampling noise due to the very short measuring time (T_i+T_{i+1}).

These disadvantages can be overcome by measuring many full periods. Suppose that T_{s1} and T_{s2} represent two adjacent measurement time intervals for N full periods of the oscillator, according to:

$$T_{s1} = \sum_{i=1}^{2N} T_i , \tag{7.9}$$

$$T_{s2} = \sum_{i=2N+1}^{4N} T_i . \tag{7.10}$$

Then, after some calculations using equations (7.2) – (7.10), for the measured average speed ϑ_{av} over time $T_{s1}+T_{s2}$, it is found that:

$$\vartheta_{av} = \frac{I_0}{V_s K} \cdot \left[1 - \left(\frac{T_{s1}}{T_{s2}}\right)^{1/2N}\right] = \frac{2Nx_{se}}{T_{\max} - T_{\min}} \cdot \left[1 - \left(\frac{T_{s1}}{T_{s2}}\right)^{1/2N}\right], \tag{7.11}$$

where

$$T_{max} - T_{min} = 4R_0N(C_{smax} - C_{smin}). \tag{7.12}$$

By measuring the two adjacent time intervals (T_{s1} and T_{s2}) for N full periods and periods T_{max}, T_{min}, the speed is calculated with formula (7.11). Meanwhile, the sign of the result of formula (7.11) indicates the direction of movement.

7.3 Capacitance in the sensing element

The capacitive sensing element described in Section 5.3 is used as a low-speed sensing element. By selectively connecting segments, a piecewise linear relation between the capacitances and position can be obtained (see Figure 7.4).

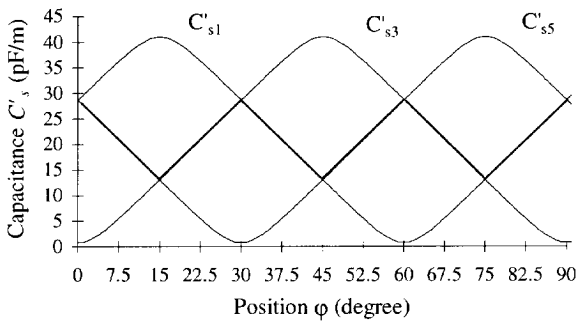

Figure 7.4 The distribution of the capacitance.

In this figure, $C'_{s1} = C_{s1}+C_{s2}+C_{s3}$, $C'_{s3} = C_{s3}+C_{s4}+C_{s5}$ and $C'_{s5} = C_{s5}+C_{s6}+C_{s7}$.

The linear parts, which are shown by the bold line in Figure 7.4, are selected for the measurement of low speed. This selection reduces the influence of the electric-field-bending effect (see Figure 7.4). The calculated results show that the nonlinearity of the linear parts is less than ±0.3% over the range 10° ~ 35° (see Figure 7.5).

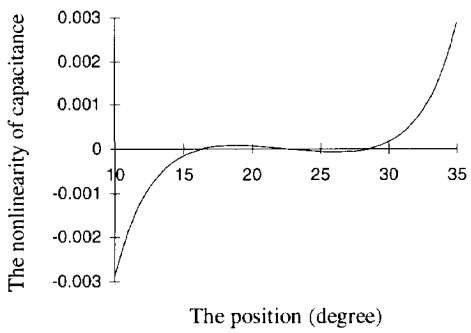

Figure 7.5 The nonlinearity of the capacitance with the position.

7.4 The measurement algorithm

Figure 7.4 has shown that the capacitances are piece-linearly related to the position over the full circle and this piece-linear part is composed of C'_{s1}, C'_{s3} and C'_{s5}. Thus, in the measurement process for low speed, the capacitor which is used as the sensing element for low speed should first be known, second, this capacitance is measured. Figure 7.6 shows a measurement process for low speed.

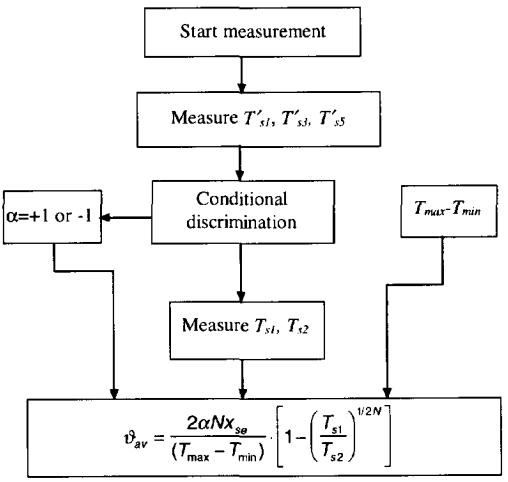

Figure 7.6 The measurement process for low speed.

In Figure 7.6, α is the factor of the moving direction. T'_{s1}, T'_{s3} and T'_{s5} are time intervals for N full periods of the oscillator corresponding to capacitances C'_{s1}, C'_{s3} and C'_{s5}, respectively.

The conditional discrimination is listed in Table 7.1. The C_s represents the capacitance whose linear-piecewise is used as a sensing element for the measurement of low speed. As seen from Table 7.1 and Figure 7.4 the middle value is always applied in further processing.

Table 7.1 The conditional discrimination.

Discrimination	C_s	α
$T'_{s5} > T'_{s1} > T'_{s3}$	C'_{s1}	+1
$T'_{s1} > T'_{s5} > T'_{s3}$	C'_{s5}	-1
$T'_{s1} > T'_{s3} > T'_{s5}$	C'_{s3}	+1
$T'_{s3} > T'_{s1} > T'_{s5}$	C'_{s1}	-1
$T'_{s3} > T'_{s5} > T'_{s1}$	C'_{s5}	+1
$T'_{s5} > T'_{s3} > T'_{s1}$	C'_{s3}	-1

7.5 The influence of nonidealities

7.5.1 The influence of some nonidealities of the signal processor

Figure 7.7 shows some of the signal processor's main nonidealities. In this figure, I_{bias} is the input bias current of the amplifier (integrator), V_{off1} and V_{off2} are, respectively, the input offset voltages of the amplifier and the comparator, and C_p represents a parasitic capacitance.

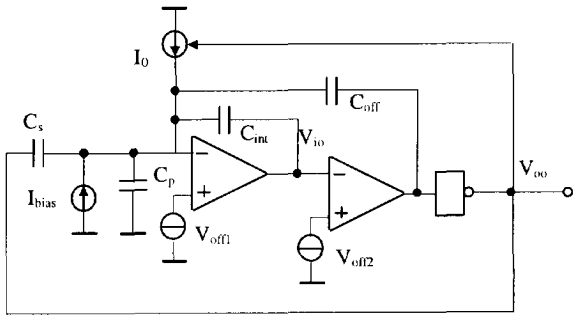

Figure 7.7 Some main nonideality sources in the signal processor.

The polarity of the current source I_0 is controlled by the output signal of the oscillator. If I_0 is an ideal current source, the input offset voltage V_{off1} of the amplifier causes only a d.c. level shift of the output signals without changing the period of the oscillator. If I_0 is a nonideal current source, the offset voltage V_{off1} causes an additional influence which is similar that of the bias current I_{bias}. However, the input offset voltage V_{off2} of the comparator causes only a d.c. level shift of some of the signals without changing the period of the oscillator whether I_0 is ideal or nonideal. Therefore, only the influences of the bias current I_{bias} and the time delay t_d of the integrator and the comparator are taken into account here. Figure 7.8 shows the output signals of the oscillator.

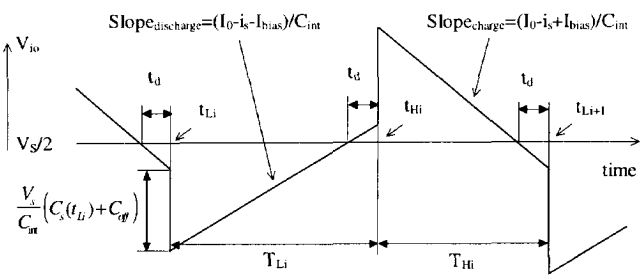

Figure 7.8 The output voltage of the integrator.

The current i_s is caused by the moving of the moving electrode. Extension of the basic equations (7.4) and (7.5) to include the effects of the delay time and the bias current enables us to find the relative error ε_{rel} which is defined as

$$\varepsilon_{rel} = \frac{\vartheta_{av} - \vartheta_{av0}}{\vartheta_{av0}}, \tag{7.13}$$

where ϑ_{av0} denotes the value of the average speed in the ideal case. For the relative deviation in the measured speed, after some straightforward calculations, it is found that:

$$\varepsilon_{rel} \cong -\frac{I_{bias}^2}{2\left(I_0^2 - I_{bias}^2\right)} \cdot \left[1 - \left(\frac{T_{s2}}{T_{s1}}\right)^{1/2N}\right]. \tag{7.14}$$

From formula (7.14), it can be concluded that the time delay t_d of the integrator and the comparator does not effect the measured speed and that the bias current I_{bias} only causes a second-order effect. A large current I_0 will reduce the influence of the bias current I_{bias}, but has the disadvantage that large capacitor values are required for a certain frequency and that the power dissipation increases.

7.5.2 The influence of the slew rate of the OPAMP

The relative deviation due to the finite slewing effect S_R of the OPAMP, is

$$\varepsilon_{rel} \cong \frac{I_0}{2S_R C_{\text{int}}\left(C_{off} + C_{\text{int}} + C_p\right)} \cdot \left[\frac{3C_{off}}{2N} \cdot \left(\frac{T_{s1}}{T_{s2}}\right)^{1/2N} + 2C_{off} + C_s\right]. \tag{7.15}$$

Formula (7.15) shows that to reduce this effect, the slew rate S_R of the OPAMP and the integration capacitance C_{int} should be as large as possible, and the current I_0 should be as small as possible. However, for the small I_0, the other effect will be increased. Therefore, the optimum value of I_0 is a compromise between conflicting requirements.

7.5.3 The influence of the bandwidth of the OPAMP

The relative deviation due to the finite bandwidth ω_1 of the OPAMP, is

$$\varepsilon_{rel} \cong \frac{I_0}{2\omega_1 C_{\text{int}} V_s} \cdot \left[1 - \left(\frac{T_{s1}}{T_{s2}}\right)^{1/2N}\right]. \tag{7.16}$$

Formula (7.16) shows that, to reduce this effect, the unity-gain frequency ω_1 of the OPAMP, the integration capacitance C_{int} and the voltage supply V_s should be as large as possible, and the current I_0 should be as small as possible.

7.6 Limitation of the measurement range

7.6.1 The minimum measurable speed

The minimum measurable speed is mainly limited by the choice of the maximum response time (measurement time) T_m, the maximum and minimum capacitances (C_{smax}, C_{smin}) between the common electrode and one segment, and the resolution of the signal processor. According to the measurement process described in Figure 7.6, the total time for one successive measurement is:

$$T_m = T'_m + T_{s1} + T_{s2}, \tag{7.17}$$

where T'_m is time for measuring capacitances C'_{s1}, C'_{s3} and C'_{s5}. The minimum measurable speed ϑ_{min} amounts to:

$$\vartheta_{min} \geq \frac{\delta C_{re}}{12(C_{smax} - C_{smin})(T_{s1} + T_{s2})}, \tag{7.18}$$

where δC_{re} is the resolution of the sensor system for capacitance measurement, which includes the sampling noise of the microcontroller.

For example, when δC_{re} = 50 aF, C_{smax} - C_{smin} = 0.15 pF and T_{s1}+T_{s2} = 10 ms, then ϑ_{min} ≥ 0.168 rpm.

7.6.2 The maximum measurable speed

The maximum measurable speed is mainly limited by the measurement time (T_{s1}+T_{s2}).

$$\vartheta_{max} \leq 1/36(T_{s1} + T_{s2}). \tag{7.19}$$

For example, when T_{s1}+T_{s2}= 10 ms, Then ϑ_{max}≤ 167 rpm.

Based on equations (7.18) and (7.19), Figure 7.9 shows the relations between the measurable speeds and the measurement times.

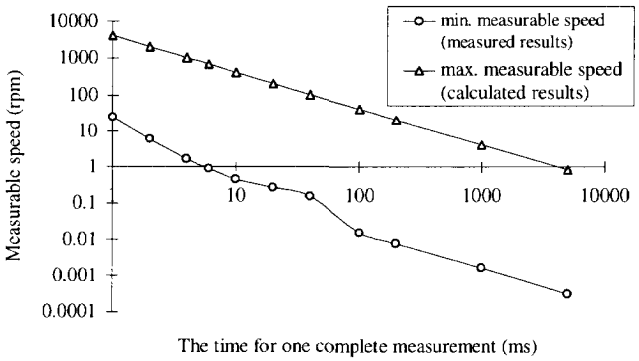

Figure 7.9 The relations between the measurable speeds and the measurement times.

For the minimum measurable speed, first, the resolution of the sensor system δC_{re} is measured in a fixed position of the rotating electrode ($\vartheta = 0$ rpm), then the minimum measurable speed is calculated by using equation (7.18). Of course, this minimum measurable speed can also be calculated by using formula (7.11) and measuring T_{s1} and T_{s2} in a fixed position of the rotating electrode.

It is shown that the increase of the measurement time results in the decrease of both the maximum and the minimum measurable speeds.

7.7 Experimental results

The performance of the speed sensor for the measurement of low speed was tested using a smart signal-processing circuit and a capacitive sensing element with a multiple electrode described in Chapter 5, and a microcontroller. The five time intervals T'_{s1}, T'_{s3}, T'_{s5}, T_{s1} and T_{s2} (see Figure 7.6) are measured in a total measurement time of about 100 ms. Figure 7.10 shows the measured noise of the sensor, including the noise of the signal processor, the sampling noise of the microcontroller and the noise of the sensing element for $\vartheta = 0$ rpm. The standard deviation of this noise amounts to 0.0168 rpm for the measurement time of 100 ms.

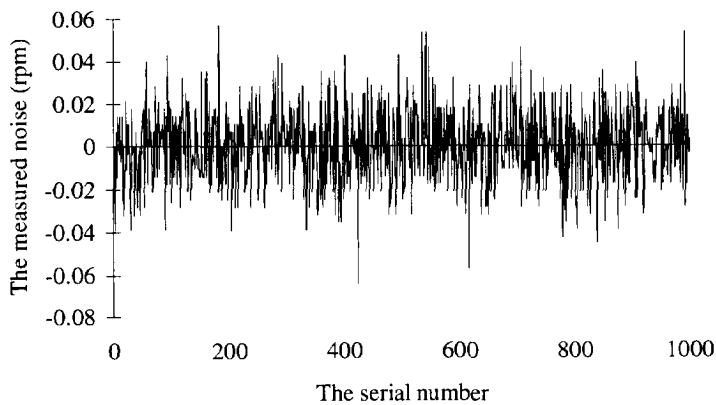

Figure 7.10 The measured noise of the system. The result of a series of 1000 measurements performed under identical conditions in a fixed position of the rotating electrode. Each measurement takes about 100 ms.

For a constant speed of 33 rpm, the measured deviation amounts to 0.45 rpm in a measurement time of 50 ms (see Figure 7.11). This deviation mainly originates from the deviation of the speed source, mechanical deviation of the sensing element, the noise of the signal processor and the sampling noise of the microcontroller.

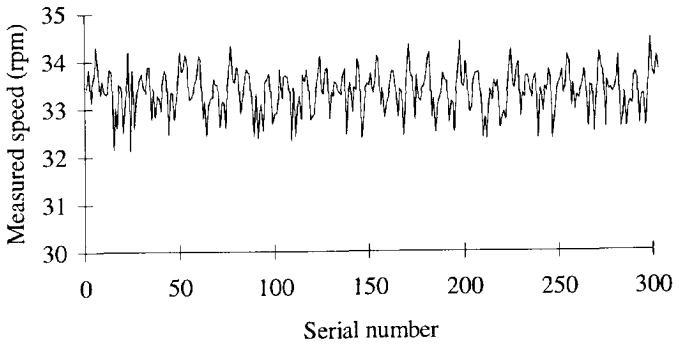

Figure 7.11 The measured result of a series of 300 measurements performed under a constant speed (ϑ = 33 rpm). Each measurement takes about 50 ms.

7.8 Conclusions

It has been show that the capacitive position encoder described in Chapter 5 can also be used to measure low speed, provided that the measurement algorithm is modified for this application. The proposed algorithm eliminates or strongly reduces the influences of many systematic nonidealities of the sensing element and the signal processor in an effective way. A microcontroller is used to measure time intervals, to calculate speed and to communicate with the outside digital world. A prototype discussed in Chapter 5 has been applied and tested for this application. The standard deviation of the noise (ϑ = 0 rpm) amounts to 0.0168 rpm for a measurement time of 100 ms. For a constant speed of 33 rpm, the measured accuracy amounts to 0.45 rpm in a measurement time of 50 ms. As compared to existing speed sensors, the main advantages of this novel capacitive low-speed sensor are its simplicity, low cost and the very low speed that can be measured with a relatively high resolution in a short measurement time. The sensor system also indicates the rotating direction.

References

[1] R. Bonert. "Design of a high performance digital tachometer with a microcontroller," IEEE Trans. Instrum. Meas., vol. IM38, Dec. 1989, pp. 1104-1108.
[2] Yasufumi Ameari and Isao Masuda, "Velocity sense detection based on the spatial filter method," IEEE Trans. Instrum. Meas., vol. IM39, Dec. 1990, pp.649-652.
[3] C.D. diCenzo, B. Szabados and N.K. Sinha, "Digital measurement of angular velocity for instrumentation and control," IEEE Trans. Ind. Electron. Contr. Instrum., vol. IECI-23, Feb. 1976, pp. 83-86.

[4] W. Ahmad and M. Ahmad, "A potentiometric transducer for the measurement of very low speeds," IEEE Trans. Instrum. Meas., vol. IM34, Sept. 1985, pp. 470-471.
[5] X. Li and G.C.M. Meijer, "A new method for the measurement of very low speeds using a multiple-electrode capacitive sensor," in Proc. IEEE CPEM/96, Braunschweig, Germany. June 1996, pp. 349-350.
[6] G. de Jong, "Smart Capacitive Sensors (physical, geometrical and electronic aspects)", Ph.D. Thesis, Delft University of Technology, April, 1994.
[7] X. Li and G.C.M. Meijer, "A new method for the measurement of low speed using a multiple-electrode capacitive sensor," IEEE Trans. Instrum. Meas., vol. 46, no. 2, April 1997.

Chapter 8

Contactless Potentiometric Sensor for Low-Speed Measurement

8.1 Introduction

A method for the measurement of low speed by using a multiple capacitive sensing element has been presented in Chapter 7. In this chapter, we discuss the application of this measurement method to low speed in the contactless resistive potentiometer. The use of the contactless devices can overcome the hysteresis problem of the conventional potentiometer [3].

8.2 Measurement principle and algorithm

Figure 8.1 shows the electronic circuitry of the contactless potentiometric speed sensor system. It consists mainly of a contactless resistive potentiometer, a selector, an oscillator and a microcontroller as described in Chapter 6.

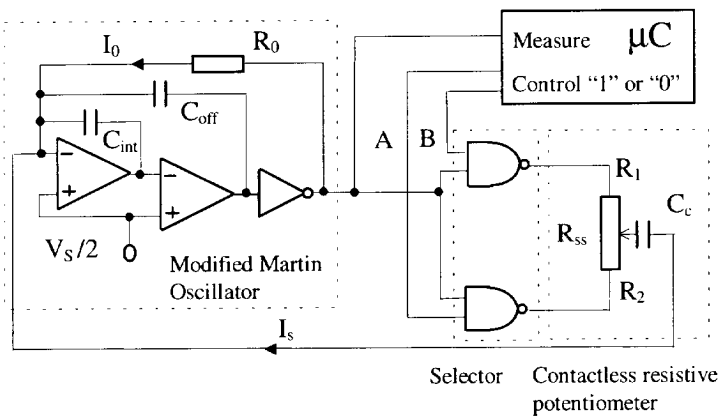

Figure 8.1 The principle of the contactless resistive potentiometric sensor.

The sensing element for low speed is the modified resistive potentiometer described in Chapter 6. The selector, which is formed by two NAND gates, is controlled by the microcontroller. Meanwhile, the microcontroller acquires the output data from the oscillator. The current I_s carries the information of the speed to be measured.

According to the measurement principle for low speed presented in Chapter 7, for the measured average speed ϑ_{av} over time interval $T_{11}+T_{22}$, it is found that [2]:

$$\vartheta_{av} = \frac{I_0 L_e}{V_s C_c} \cdot \left[1-\left(\frac{T_{11}}{T_{22}}\right)^{1/2N}\right] = \frac{L_e}{2R_0 C_c} \cdot \left[1-\left(\frac{T_{11}}{T_{22}}\right)^{1/2N}\right]. \tag{8.1}$$

where the coefficient L_e is the effective length of the linear resistive layer and V_s is the supply voltage. The T_{11} and T_{22} represent, respectively, two adjacent time intervals for N full periods of the oscillator when one fixed terminal of the resistive potentiometer is connected to the output of the oscillator and other fixed terminal is grounded, for instance, A is high level "1", B is low level "0".

By measuring the two adjacent time intervals T_{11} and T_{22}, the speed can be calculated with formula (8.1). Meanwhile, the sign of the result of formula (8.1) indicates the moving direction.

Formula (8.1) shows that the measured speed is not only related to the measured periods but also to the values of devices R_0 and C_c. By using two additional measurements of the periods T_{Cc} and T_{off}, the values of R_0C_c can be measured. The T_{Cc} represents the time interval for N full periods of the oscillator when two fixed terminals of the resistive potentiometer are connected to the output of the oscillator, for instance, A and B are high level "1". T_{off} represents the time interval for N full periods of the oscillator when two fixed terminals of the resistive potentiometer are grounded, for instance, A and B are low level "0". The values of the two periodic signals T_{Cc} and T_{off} do not change with the speed and the position of the moving electrode. They can be written

$$T_{Cc} = \frac{2NV_s(C_c + C_{off})}{I_0} = 4NR_0(C_c + C_{off}), \tag{8.2}$$

$$T_{off} = \frac{2NV_s C_{off}}{I_0} = 4NR_0 C_{off}. \tag{8.3}$$

The measurement for the time intervals T_{Cc} and T_{off} determines the value of R_0C_c.

It is concluded that four time intervals are required to be measured in different states of the selector in the measurement of the speed. The four possible output states of the selector, which provide alternation of the terminals of the sensing element and enable the offset measurements, are controlled by the output signals, A and B, of the microcontroller. Table 8.1 shows the controlled states in a complete measurement process.

Table 8.1 The controlled states in a complete measurement process.

Time interval to be measured	T_{11}	T_{22}	T_{Cc}	T_{off}
Corresponding control states A-B	1-0	1-0	1-1	0-0

The states 1-0 for T_{11} and T_{22} in the table correspond to the connection of the contactless resistive potentiometer as shown in Figure 8.1. As an alternative, the states 0-1 for T_{11} and T_{22} also could be used, but this does not offer any difference.

For the average speed ϑ_{av} over the complete measurement time $T_m=T_{11}+T_{22}+T_{Cc}+T_{off}$, it can be found that [2]:

$$\vartheta_{av} = \frac{2NL_e}{T_{Cc} - T_{off}} \cdot \left[1 - \left(\frac{T_{11}}{T_{22}}\right)^{1/2N}\right]. \tag{8.4}$$

From formula (8.4), it can be concluded that the measured speed ϑ_{av} is independent of the capacitance C_c. This is an important property, because it means that the measurement is immune to the electrode distance and the mechanical tolerances which result from deviations or nonuniformity of the electrode distance.

8.3 The influence of the parasitic capacitances

In Chapter 7, major influences of some nonidealities of the signal processor and the OPAMP have been discussed in detail. These discussions also apply to the contactless potentiometric speed sensor. A special influence in the potentiometric sensor is due to the parasitic capacitances [3].

The parasitic capacitors of the potentiometric sensor have been shown in Figure 6.6. For the low-speed measurement, the effect of the parasitic capacitor C_{p3} has been shown in formula (7.14). However, C_{p3} affects the periods of the oscillator due to the limited bandwidth of the OPAMP, so C_{p3} also affects the speed measured by the formula (7.15). The effects of the parasitic capacitors C_{p1} and C_{p1}', which include the cable capacitances, can be neglected. The parasitic capacitances C_{p2} and C_{p2}' are also composed of two parts: the parasitic capacitances between the sliding electrode and the terminals of the resistive layer, and the parasitic capacitances between the outputs of the selector and the inverting input of the integrator in the measuring circuit.

They exert an influence on the measured speed via the (T_{Cc} - T_{off}) in formula (8.4) only. When this effect is taken into account, then, for the measured speed ϑ_{av}, it is found that:

$$\vartheta_{av} = \left(1 + \frac{C_{p2} + C_{p2}'}{C_c}\right) \frac{2NL_e}{T_{Cc} - T_{off}} \cdot \left[1 - \left(\frac{T_{11}}{T_{22}}\right)^{1/2N}\right]. \tag{8.5}$$

Formula (8.5) shows that the measured speed is related to the capacitance C_c due to the effect of the parasitic capacitances. Therefore, the parasitic capacitances C_{p2} and C_{p2}' should be as low as possible.

8.4 Experimental results

The prototype presented in Chapter 6 for the angular-position sensing system has been used to sense angular speeds. It consists of a contactless resistive potentiometer, a signal-processing circuit and a microcontroller of the type INTEL D87C51FB. The signal-processing circuit uses a modified Martin oscillator as described in Chapter 6, which has been implemented with a simple dual OPAMP (TLC272AC) and two CMOS NAND gates according to the circuit shown in Figure 8.1.

The measuring system is powered by a single 5 V supply voltage. The frequency ($1/T_{off}$) of the oscillator during the offset measurement is about 7.0 kHz. During the other measurement phases, the oscillator frequency is in the range of about 3.3 kHz - 7.0 kHz. For the different measurement times, the measured noise of the angular-speed sensor, including the noise of the signal processor, the sampling noise of the microcontroller and the noise of the sensing element, is shown in Figure 8.2.

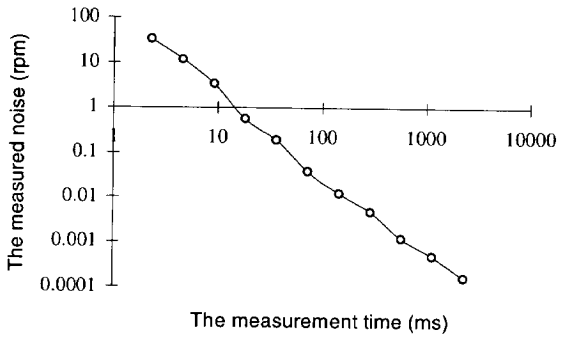

Figure 8.2 The measured noise of the angular-speed sensor at the different measurement times: The results of the measurements performed under identical conditions in a fixed position of the sliding electrode.

The implemented angular-speed sensor was employed to measure two constant rotating speeds of about 9.5 rpm and 33.5 rpm at the different measurement times. The measurement results are shown in Figure 8.3. The standard deviations from these speed measurements are also shown in Figure 8.3. It is concluded that the standard deviation at a short measurement time mainly originates from the sampling noise of the microcontroller, the standard deviation at a relatively long measurement time mainly originates from the mechanical noise of the sensing element and the inaccuracy of the speed source.

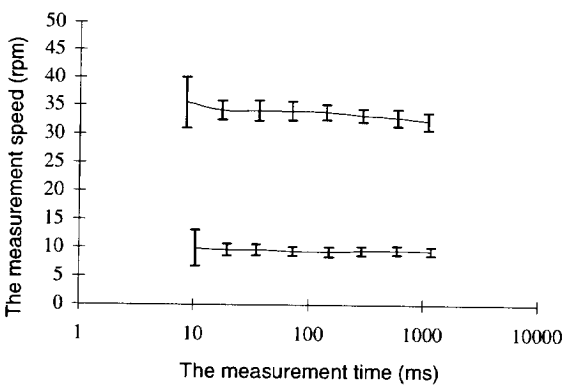

Figure 8.3 Measurement results for two constant speeds: showing the measured speeds and errors as function of the measurement times.

8.5 Conclusions

By applying an improved algorithm, the low moving speed as well as the position of the object can be measured by using a low-cost contactless resistive potentiometer with a relatively high resolution in a short measurement time. A prototype of the system has been built and tested. Compared to existing speed sensors, the main advantages of this novel low-speed sensor are its simplicity, low cost and the low speed that can be measured with a relatively high resolution in a short measurement time. The angular range is limited by the potentiometer geometry and the finite size of the sliding electrode, and typically amounts to about 270°.

References

[1] W. Ahmad and M. Ahmad, "A potentiometric transducer for the measurement of very low speeds," IEEE Trans. Instrum. Meas., vol. IM-34, no. 3, Sept. 1985, pp. 470-471.
[2] X. Li and G.C.M. Meijer, "A novel low-cost non-contact resistive potentiometric sensor for the measurement of low speed," to be submitted to IEEE Trans. Instrum. Meas..
[3] X. Li and G.C.M. Meijer, "A novel smart resistive-capacitive position sensor," IEEE Trans. Instrum. Meas., vol. 44, no. 3, June 1995, pp. 768-770.

Chapter 9

A Comparison Between Capacitive and Contactless Potentiometric Sensors

Based on the system approach and the mechatronic approach, two types of smart sensors, capacitive and contactless resistive-potentiometric sensors, have been developed. Both of them can be used to measure position and speed. Although similar signal processors and measurement methods are used for these two types of sensors, their specifications are different because of the different structures of the sensing elements. Some important specifications of these two sensors are listed in Table 9.1 and Table 9.2 for the measurements of the angular position and angular speed, respectively.

Table 9.1 A comparison between the two sensors for the measurement of angular position.

	Capacitive	Contactless potentiometric
Measurement range	360°	<360° (270°)
Accuracy	±26″	±2920″
Resolution*	4.2″	3.1″
Simplicity	+ -	+
Environment sensitivity	+	-
Costs	-	+

* Note: The resolutions are measured at a measurement time of 100 ms.

Table 9.2 A comparison between the two sensors for the measurement of angular speed.

	Capacitive	Contactless potentiometric	Conditions
Measurable speed	0.13 ~ 84 rpm	0.1 ~ 899 rpm	Measurement time: 50 ms
Standard deviation (resolution)	0.45 rpm	3.4 rpm	Measurement time: 50 ms Measured speed: 33 rpm
Simplicity	+ -	+	
Environment sensitivity	+	-	
Costs	-	+	

In the contactless potentiometric position sensor, the finite areas of the two fixed terminals of the resistive layer and the sliding electrode result in a measurement range of less than 360°. The nonlinearity of the resistive layer and presence of the parasitic capacitances are the main causes of the inaccuracy in the contactless potentiometric position sensor. However, in the capacitive sensor, the inaccuracy originates mainly from the noise of the sensor, the effect of the electric-field bending and the unsymmetrical structure of the rotating electrode.

For the measurement of low speed, the measurable-speed range of the contactless potentiometric sensor is larger than that of the capacitive sensor. This is due to the fact that the effective range of the resistive layer (about 270°) is larger than the width of one segment (15°). The relatively large mechanical tolerance in the contactless potentiometric sensing element causes a large error in the measurement speed.

The relative humidity is one of important environmental influence sources. As this has been discussed in Section 3.5.5, the influence of moisture (light humidity) can be eliminated by measuring the ratio of two capacitances if both capacitors are filled with air having the same permittivity. However, condensation can cause a conductive layer. The conductive layer will short-circuit the resistive layer in the contactless potentiometric sensor and then seriously affect the measured accuracy. Such a conductive layer can short-circuit the electrodes, which are connected to the input of the signal processor, with grounded guardings and can make the measurement impossible in both sensors.

Chapter 10

Conclusions and Recommendations

10.1 Conclusions

The main objective of this research work was to study low-cost, high-performance smart capacitive sensors for the measurement of position and speed following a "System" approach and a "Mechatronic" approach. Theoretical and experimental investigations have led to some significant results. The investigations were focused on the mechanical and physical aspects of the capacitive sensing element, the relationship between measurand and the capacitance, and the signal processors which can measure small capacitances using microcontrollers. In addition to the fundamental studies, two new types of smart capacitive sensors have been developed. Both smart sensors can measure position as well as speed.

Here, the contributions of this thesis can be classified into four fields:

- Design concepts for smart sensors.
- Sensing elements.
- Signal and information processing.
- New types of smart sensors.

Design concepts for smart sensors

- The system approach:

A smart sensor system has a hierarchical multiple-layered structure based on system theory. The three main layers are characterized as: signal processing in the lower layer, information processing in the middle layer and knowledge processing in the top layer.

- The mechatronic approach:

Mechatronics is defined as an integration of mechanical, electronic and information technology. The parts of a mechatronic system must be considered as an integrated overall system from the beginning of the design.

The most popular concept of a smart sensor is a microcontroller-based smart sensor which could be composed of a sensing element, a signal processor and a microcontroller. The sensing element is used to sense the measurand and converts the specific measurand to a usable and measurable output based on a basic physical principle. The signal processor transfers the signals of the sensing element

to a microcontroller-compatible signal. The microcontroller performs the measurement of the output signal of the signal processor, digital and algorithm signal processing, and making a digital output signal for the outside world.

Sensing elements

It is shown that the cost of the sensing element for the measurement of mechanical quantities forms a dominant part of the total sensor cost. Moreover, its nonidealities seriously affect the final results of the sensor. A multiple-electrode structure of the capacitive sensing element can effectively reduce the electric-field-bending effect and the effect of mechanical tolerances. Therefore, the use of such a structure can result in a high-performance, low-cost sensor.

A typical example of such a structure is the three-layered multiple-electrode structure of the capacitive sensing element. It is shown that the use of this structure results in a low sensitivity to many mechanical tolerances, such as the electrode distance, the position and thickness of the moving electrode. Further, the small influence of the electric-field-bending is also reduced. In addition, also the symmetrical structure of the electrodes eliminates or strongly reduces many mechanical nonidealities, for instance, the eccentricity, nonflatness of the electrode surface, and obliqueness. By theoretically analyzing and calculating, the optimum geometrical parameters of the sensing element with respect to the accuracy have been derived. This optimum depends on the nonlinearity caused by nonidealities and electric-field-bending effects on the one hand and on nonflatness, mechanical stability, and sensitivity to pollution and humidity on the other hand.

An alternative approach to realizing high-performance and low-cost sensors is found in the use of contactless potentiometric or "resistive-capacitive" sensing elements.

Signal and information processing

In the smart capacitive sensor system, two processings, signal and information processing, are performed by, for instance, the capacitance-controlled oscillator and the microcontroller. A signal processor, which consists of a linear capacitance-controlled oscillator and a multiplexer, can perform accurate processing of small multiple capacitances in a low-cost way. For the measurement of small capacitances with large parasitic capacitances, the two-port measurement technique is very effective in reducing the effect of the parasitic capacitances.

The use of the three-signal technique eliminates the unknown offset and unknown gain errors of the signal processor. An extension of the three-signal technique results in the *Ratio of Two Linear Combinations of the Capacitances (RTLCC)* technique in the multiple-electrode capacitive sensor. This technique eliminates many nonidealities in both the capacitive sensing element and the signal processor, such as the electric-field-bending effect, nonflatness, eccentricity, obliqueness, spatial drift and spatial low-frequency noise in the sensing element, and offset voltages, input bias currents, gain error and low-frequency drift and noise in the signal processor.

This advanced technique was performed by using a microcontroller with a memory. Further, the use of the microcontroller with a memory in the capacitive

sensor results in a piecewise self-calibration technique which eliminates the remaining systematic errors without the use of an accurate reference. The microcontroller also performs the situation control, signal measurement (Analog-to-Digital conversion) and communication with the digital world, such as a personal computer.

New types of smart sensors

By using the system and mechatronic approaches, the design of the capacitive sensor is optimized, which involves optimum sensor-system architecture, optimum structure of the capacitive sensing element, an optimum algorithm and an optimum signal processor for small capacitance measurement. This enables the realization of a low-cost and high-performance smart sensor. Thus, the development of two types of new smart sensors, capacitive and contactless potentiometric sensors, has been reported and described in this thesis. These two types of smart sensors are suitable to measure both angular position and low angular speed. The described operational principle is also suitable for linear position and speed measurement.

- *A capacitive sensor.* For the position measurement, a high degree of accuracy, of ±26″, was obtained over the measurement range of 360°. The resolution, repeatability and reproducibility of the prototype are better than 1.5″, 3.6″ and 2.5″ for a measurement time of 150 ms, respectively. Simply by changing the algorithm, the same capacitive sensing element and signal processor can be used to measure low speed. For a constant-speed measurement (30 rpm), the accuracy amounts to 0.45 rpm in a measurement time of 50 ms.
- *A contactless potentiometric sensor.* For the position measurement, an accuracy of ±0.3% was obtained over the measurement range, which is limited to 270°. Changing only the algorithm, the same sensing element and signal processor was used to measure low speed. For a constant speed measurement (30 rpm), the accuracy amounts to 3.4 rpm in a measurement time of 50 ms. This relatively large inaccuracy is due to the large mechanical tolerance in the contactless potentiometric sensing element and the inaccuracy of the speed source. It can be concluded that a simple sensing element with relatively large mechanical (dynamic) tolerance is not suited to measure speed accurately.

10.2 Recommendations

Considering the practical applications of the two types of smart sensors, capacitive and contactless potentiometric sensors, presented in this thesis, further investigations into the influences of temperature, humidity (moisture and condensation) and pollution on the electrode surfaces would be very worthwhile.

On improving the signal processor to increase the measurement speed, for instance, up to 1 kHz, the smart capacitive sensor will appear in the control systems as well as in the measurement systems.

In the capacitive angular-position sensor, a sliding contact was used to ground the moving electrode. Removing this sliding contact to derive a noncontact capacitive sensor will be a very interesting research.

It can be expected that the smart capacitive sensor with its multiple-electrode structure will be strongly competitive in the future market.

Summary

In Chapter 1 a short introduction to smart capacitive sensors and the aim of the work described in this thesis are given. Capacitors are used as sensing elements to directly or indirectly measure various physical and mechanical quantities. These elements offer the advantages of low energy consumption, high resolution and simple structure. However, practical applications of capacitive sensors in industry are limited due to some challenging physical, electrical and mechanical problems, such as the physical effects of electric-field bending, the accurate measurement of very small capacitance, nonlinearity, parameter drift, cross sensitivity, accuracy, stability and dynamic range. The smart capacitive sensor offers a solution to improving these imperfections. In this thesis, we define a smart sensor as a sensor whose functions include at least one of the following: a logic function, the bi-directional communication, and making a decision.

Chapter 2 contains a brief overview of position and speed sensors, and presents some general physical aspects of capacitive position and speed sensors. One attractive concept of a smart sensor is that of a microcontroller-based sensor combining a sensing element, a signal-processing circuit and a microcontroller. The sensing element is used to sense the measurand and converts the specific measurand to a usable output following basic physical principles. The signal processor transfers the signals of the sensing element to a microcontroller-compatible output signal. The microcontroller performs the measurement of the output signal of the signal processor, takes care for the digital and algorithm signal processing, and makes a digital output signal for the outside world. Such a smart sensor probably offers the abilities of:

- calibration and compensation in real time,
- self-testing,
- computation,
- communication with its environment,
- the measurement of more than one physical or chemical quantity,
- logic decision.

The system architecture of the smart capacitive sensors is given in Chapter 3. The main elements of the smart capacitive sensor system, such as the capacitive sensing elements, the signal processor and the microcontroller are described. A concept of a systematic design combining the mechatronic and system approaches is described.

The use of a multiple-electrode structure in the capacitive sensing element can effectively reduce the electric-field-bending effect and the effect of mechanical tolerances. A typical example of such a structure is the three-layered multiple-

electrode structure of the capacitive sensing element. Combining such a multiple-electrode capacitive sensing element with a smart signal processor results in a high-performance and low-cost smart capacitive sensor.

In Chapter 4, various techniques and methods to measure small capacitances using low-cost signal processors are described. A very effective measurement technique which eliminates or significantly reduces the influence of parasitic capacitances is the two-port measurement technique. The oscillation method for capacitance measurement is very suitable to attain a microcontroller-compatible output and can be combined with the two-port measurement technique.

A signal processor, which consists of a linear capacitance-controlled oscillator and a multiplexer that can perform an accurate processing for small multiple capacitances in a low-cost way, has been designed and was realized in a 0.7 μm CMOS process. The measured resolution and nonlinearity over a measurement range of 2 pF are 12×10^{-6} and 300×10^{-6}, respectively. The high-performance input amplifier allows parasitic capacitances at the input of up to about 3 nF.

In Chapter 5, the design of a low-cost, high-performance capacitive absolute angular-position sensor is described. The design aspects of the capacitive sensing elements, the improved algorithms, the influence of the nonidealities in the capacitive sensing elements and the self-calibration technique are discussed in detail.

The use of the three-signal technique eliminates the unknown offset and unknown gain errors of the signal processor. An extension of the three-signal technique results in the *Ratio of Two Linear Combinations of the Capacitances (RTLCC)* technique in the multiple-electrode capacitive sensor. This technique eliminates many nonidealities in both the capacitive sensing element and the signal processor, such as electric-field-bending effect, nonflatness, eccentricity, obliqueness, spatial drift and spatial low-frequency noise in the sensing element, and offset voltages, input bias currents, gain error, and low-frequency drift and noise in the signal processor. For the application of this technique, the structure of the capacitive sensing element with multiple electrodes is optimized and an optimum algorithm is derived.

This advanced technique takes advantage of the use of the memory of the microcontroller. The use of this memory is also essential to enable the use of the novel self-calibration technique. This calibration technique can eliminate major errors without use of a reference sensor.

By a theoretical analysis of the physical aspects of the capacitor, the optimum geometrical parameters of the sensing element with respect to the accuracy have been derived. This optimum depends on the nonlinearity caused by many nonidealities, such as eccentricity, obliqueness, deformation of electrodes and electric-field bending effects on the one hand, and on nonflatness, mechanical stability, and sensitivity to pollution and humidity on the other hand.

A prototype of the smart capacitive absolute angular-position sensor has been built and tested. For the angular position measurement, a high degree of accuracy (±26″), was obtained over the measurement range of 360°. The resolution, repeatability and reproducibility of the prototype are better than 1.5″, 3.6″ and 2.5″ for a measurement time of 150 ms, respectively.

In Chapter 6, a novel low-cost contactless resistive-potentiometric position sensor is presented. The sensing element is a modified resistive potentiometer with a sliding contact which is not directly in contact with the resistive layer of the potentiometer. For the position measurement, an accuracy of ±0.3% is obtained over the measurement range, which is limited to 270°.

In Chapters 7 and 8, a new method for the measurement of the low speed of moving objects is presented. In this new method, by changing the algorithm but using the same signal processor, the capacitive sensing element described in Chapter 5, or the contactless resistive-potentiometric sensing element described in Chapter 6 can be used to measure low speed. For the measurement of a constant-speed (30 rpm), the accuracies amount to 0.45 rpm and 3.4 rpm in a measurement time of 50 ms when using the capacitive sensing element and the contactless resistive-potentiometric sensing element, respectively. The relatively great inaccuracy of the contactless potentiometric speed sensor is due to the large mechanical tolerance of the potentiometric element. It is concluded that a simple sensing element with relative large mechanical (dynamic) tolerance is not suitable to measure speed accurately.

In Chapter 9, a comparison of the specifications between smart capacitive sensors and the contactless resistive-potentiometric sensors is presented. Both of them use similar signal processors and measurement methods and can be used to measure position and speed. A comparison of the results shows that the capacitive sensor with a multiple-electrode structure has a better performance for many specifications. However, for some applications the simplicity and low-cost of the contactless resistive-potentiometric sensor are major advantages.

Finally, in Chapter 10, conclusions are given and recommendations are made for further research.

Samenvatting

Hoofdstuk 1 bevat een korte introductie van pientere capacitieve sensoren en beschrijft het doel van het werk dat het onderwerp is van deze thesis. Capaciteiten worden gebruikt als sensorelementen om verschillende fysische en mechanische hoeveelheden op directe of indirecte wijze te meten. Deze elementen hebben het voordeel van laag energiegebruik, hoge resolutie en eenvoudige structuur. De praktische toepassing van capacitieve sensoren in de industrie is echter beperkt vanwege een aantal moeilijk oplosbare fysische, elektrische en mechanische problemen, zoals de fysische effecten van buiging van het elektrisch veld, het zuiver meten van zeer kleine capaciteiten, niet-lineariteit, drift van parameters, kruisgevoeligheid, nauwkeurigheid, stabiliteit en dynamisch bereik. De pientere capacitieve sensor biedt een oplossing om deze tekortkomingen te verbeteren. In deze thesis definiëren wij een pientere sensor als een sensor met tenminste een van de volgende functies: een logische functie, de bi-directionele communicatie en het nemen van een beslissing.

Hoofdstuk 2 bevat een kort overzicht betreffende positie- en snelheidssensoren, en presenteert enige algemene fysische aspecten van capacitieve positie- en snelheidssensoren. Een aantrekkelijk concept voor een pientere sensor is een microcontroller-based sensor waarin een sensorelement, een signaalbewerkingscircuit en een microcontroller zijn gecombineerd. Het sensorelement wordt gebruikt om de measurand te sensen en om, in overeenstemming met fysische basisprincipes, de specifieke te meten grootheid om te zetten in een bruikbaar uitgangssignaal. De signaalprocessor zet de signalen van het sensorelement om in een microcontroller-compatible uitgangssignaal. De microcontroller verzorgt de meting van het uitgangssignaal van de signaalprocessor, zorgt voor de digitale en algorithmische bewerking van het signaal, en maakt een digitaal uitgangssignaal voor de buitenwereld. Zo'n pientere sensor biedt waarschijnlijk de mogelijkheden om:

- te calibreren en compenseren in real time,
- zichzelf te testen,
- rekenkundige bewerkingen uit te voeren,
- te communiceren met de omgeving,
- meer dan een fysische of chemische hoeveelheid te meten,
- een logische beslissing te nemen.

De systeemarchitectuur van de pientere capacitieve sensoren wordt besproken in hoofdstuk 3. De voornaamste elementen van het systeem, zoals de capacitieve sensorelementen, de signaalprocessor en de microcontroller worden beschreven. Een

concept wordt beschreven voor een systematisch ontwerp dat de mechatronische benadering en de systeem benadering combineert.

Het gebruik van een meervoudige-elektrode-structuur van het capacitieve sensorelement kan het effect van de buiging van het elektrisch veld en het effect van mechanische toleranties effectief reduceren. Een typisch voorbeeld van zo'n structuur is de drie-laagse meervoudige-elektrode-structuur van het capacitieve sensor element. Combinatie van een sensorelement met zo'n structuur met een pientere signaalprocessor resulteert in een high-performance en low-cost pientere capacitieve sensor.

In hoofdstuk 4 worden verschillende technieken en methoden beschreven om kleine capaciteiten te meten met low-cost signaalprocessors. Een bijzonder effectieve meettechniek waarmee de invloed van parasitaire capaciteiten wordt geëlimineerd of aanzienlijk gereduceerd is de tweepoort-meettechniek. De oscillatiemethode voor het meten van capaciteit is zeer geschikt om een microcontroller-compatible uitgangssignaal te verkrijgen en kan gecombineerd worden met de tweepoort-meettechniek.

Een signaalprocessor, bestaande uit een lineaire capaciteitsgestuurde oscillator en een multiplexer, die een nauwkeurige bewerking kan uitvoeren voor kleine veelvoudige capaciteiten op een goedkope wijze, is ontworpen en gerealiseerd in een 0,7 μm CMOS proces. De gemeten resolutie en niet-lineariteit over een meetbereik van 2 pF is, respectivelijk, $12x10^{-6}$ en $300x10^{-6}$. De high-performance ingangsversterker kan parasitaire capaciteiten aan de ingang accepteren tot ongeveer 3 nF.

Hoofdstuk 5 beschrijft het ontwerp van een goedkope, high-performance capacitieve hoek-encoder. De ontwerpaspecten van de capacitieve sensorelementen, de verbeterde algorithmes, de invloed van de niet-idealiteiten in de capacitieve sensorelementen en de autocalibratietechniek worden in detail beschreven.

Het gebruik van de drie-signaaltechniek elimineert de onbekende offset en de onbekende versterkingsfouten van de signaalprocesssor. Een uitbreiding van de drie-signaaltechniek resulteert in de *Ratio of Two Linear Combinations of the Capacitances (RTLCC)* techniek bij de meervoudige-elektrodesensor. Met deze techniek zijn veel niet-idealiteiten geelimineerd, in zowel het capacitieve sensorelement als in de signaalprocessor, zoals het effect van buiging van het elektrische veld, onvlakheid, excentriciteit, scheefstand, mechanische drift en ruimtelijke laag-frequente ruis in het sensor element, en offsetspanningen, ingangs-biasstromen, versterkingsfouten en laag-frequente drift en ruis in de signaalprocessor. Om deze techniek toe te kunnen passen wordt de structuur van het capacitieve sensorelement met meervoudige elektroden geoptimaliseerd en een optimum algorithme gedefinieerd.

Deze geavanceerde techniek maakt gebruik van het geheugen van de microcontroller. Het gebruik van dit geheugen is een essentiële voorwaarde om de nieuw-ontwikkelde auto-calibratietechniek te kunnen gebruiken. Met deze calibratietechniek kunnen belangrijke fouten geëlimineeerd worden zonder gebruik te maken van een referentiesensor.

Door de fysieke aspecten van de capaciteiten theoretisch te analyseren zijn de geometrische parameters van het sensorelement geoptimaliseerd. Dit optimum hangt af van de niet-lineariteit veroorzaakt door vele niet-idealiteiten, zoals excentriciteit,

scheefstand, vervorming van elektroden en effecten van elektrisch-veldbuiging enerzijds, en niet-vlakheid, mechanische stabiliteit, en gevoeligheid voor vervuiling en vochtigheid anderzijds.

Een prototype van de pientere capacitieve absolute hoek-encoder is gebouwd en getest. Bij de hoekmeting werd een hoge graad van nauwkeurigheid (±26″), verkregen over een meetbereik van 360°. De resolutie, herhaalbaarheid en reproduceerbaarheid van het prototype zijn beter dan, respectievelijk, 1,5″, 3,6″ en 2,5″ bij een meettijd van 150 ms.

In hoofdstuk 6 wordt een nieuwe low-cost contactloze resistieve potentiometrische positie sensor gepresenteerd. Het sensor element bestaat uit een gemodificeerde resistieve potentiometer met een loper die niet direct in mechanisch contact is met de weerstandslaag van de potentiometer. Voor de positiemeting wordt een nauwkeurigheid van ±0,3% verkregen over een meetbereik dat beperkt is tot 270°.

In de hoofdstukken 7 en 8 wordt een nieuwe methode voor het meten van lage snelheden van bewegende voorwerpen gepresenteerd. Met deze nieuwe methode kunnen, door het algorithme aan te passen, maar met gebruikmaking van dezelfde signaalprocessor, de capacitieve sensor elementen of de contactloze resistieve potentiometrische sensorelementen gebruikt worden om lage snelheden te meten. Bij een meting van een constante snelheid van 30 omwentelingen per minuut (omw/min) bedroeg de nauwkeurigheid 0,45 omw/min en 3,4 omw/min in een meettijd van 50 ms bij het gebruik van, respectievelijk, de capacitieve sensorelement en de contactloze potentiometrische sensorelement. De grotere onnauwkeurigheid van de contactloze potentiometrische snelheidssensor wordt veroorzaakt door de grote mechanische tolerantie van het potentiometrische element. De conclusie is dat een eenvoudig sensorelement met relatief grote mechanische (dynamische) tolerantie niet geschikt is om snelheid nauwkeurig te meten.

Hoofdstuk 9 presenteert een vergelijking van de specificaties van pientere capacitieve sensoren en contactloze potentiometrische sensoren. Beiden gebruiken gelijksoortige signaalprocessors en meetmethoden, en kunnen gebruikt worden om positie en snelheid te meten. Een vergelijking van de resultaten geeft aan dat de capacitieve sensor met een meervoudige-elektrodestructuur een beter resultaat levert voor veel specificaties. Echter, bij sommige toepassingen vormen de eenvoud en de lage kosten van de contactloze resistieve-potentiometrische sensor een belangrijk voordeel.

Hoofdstuk 10, tenslotte, bevat de conclusies en de aanbevelingen voor verder onderzoek.

Acknowledgments

The work described in this thesis was carried out at the Electronics Research Laboratory, Delft University of Technology, The Netherlands.

This thesis would not have appeared without the help and cooperation of many people, not only at the Delft University of Technology. I would like to take this opportunity to thank all of these people, including those whose names are not mentioned below.

First, I would like especially to thank to my tutor and supervisor Dr. Gerard C.M. Meijer, not only for many significant and detailed discussions, and technical writing, but also for helping me to get accustomed to working in The Netherlands.

I would also like to thank Prof. Arthur van Roermund for reading the earlier versions of this thesis and helping me to improve the clarity.

Further I would like to thank:

My colleague Gerben de Jong for his valuable and efficient discussions.

My colleagues Ferry Toth, Frank van der Goes, Paul de Jong, Stoyan Nihtianov and Guijie Wang in the smart sensor group for interesting brainstorming sessions and discussions on all kinds of subjects.

Loek van Schie, Harry Kervliet, Rob Jangs, Jan Nusteling, Wil G.M. Straver, Piet J. Bos, for repairing and upgrading PCs, for building various testing set-ups, for managing the software on PCs and workstations.

The people at the Laboratory for Micro-Engineering, Jo Spronck, Marcus Bonse for technical discussions and the realization of the mechanical parts of capacitive sensors.

The people at Enraf BV, Thijs van der Lee, Dorus Bertels for technical discussions.

Mrs. J.B. Zaat-Jones for doing a fast and splendid correction job.

The Foundation of Technical Sciences (STW) for their financial support under contract DEL 44.3532 which was of crucial important to this research.

And last, but far from least, I would like to thank Guijie Wang, my wife and colleague, for her continuous support.

List of Publications

Journal publications

X. Li and G.C.M. Meijer, "A novel smart resistive-capacitive position sensor," IEEE Trans. Instrum. Meas., vol. 44, pp. 768-770, 1995.

X. Li, G.C.M. Meijer, G.W. de Jong and J.W. Spronck, "An accurate low-cost capacitive absolute angular-position sensor with a full-circle range," IEEE Trans. Instrum. Meas., vol. 45, no. 2, April 1996, pp. 516-520.

X. Li, G.W. de Jong and G.C.M. Meijer, "The application of the capacitor's physics to optimize capacitive angular-position sensors," IEEE Trans. Instrum. Meas., vol. 46, no. 1, Feb. 1997, pp. 8-14.

X. Li and G.C.M. Meijer, "A new method for the measurement of low speed using a multiple-electrode capacitive sensor," IEEE Trans. Instrum. Meas., vol. 46, no. 2, April, 1997.

X. Li, G.C.M. Meijer and G.W. de Jong, "A microcontroller-based self-calibration technique for a smart capacitive angular-position sensor," to be published in IEEE Trans. Instrum. Meas., vol. 46, no. 3, June, 1997.

X. Li, G.W. de Jong, F.N. Toth, F.M.L. van der Goes and G.C.M. Meijer, "Low-cost CMOS interface for capacitive sensors and its application in a capacitive angular encoder," to be published in Analog Integrated Circuits and Signal Processing, Special issue on smart sensor interfaces, 1997.

X. Li and G.C.M. Meijer, "A novel low-cost non-contact resistive potentiometric sensor for the measurement of low speed," to be published in IEEE Trans. Instrum. Meas., 1997.

Conference proceedings

X. Li and G.C.M. Meijer, "A smart resistive-capacitive position sensor," in Proc. Dutch conference on Sensor Technology, Enschde, The Netherlands, Feb. 17-18, 1994, pp. 135-139.

X. Li and G.C.M. Meijer, "A novel smart resistive-capacitive angular PSD," in Proc. IEEE IMTC/94, Hamamatsu, Japan, May 10-12, 1994, pp. 308-311.

X. Li, G.C.M. Meijer and G.W. de Jong, "An accurate smart capacitive angular-position sensor with a full circle range," in Proc. IEEE IMTC/95, Waltham, USA, April 23-26, 1995, pp. 80-83.

X. Li and G.C.M. Meijer, "A self-calibration technique for a smart capacitive angular-position sensor," in Proc. IEEE IMTC/96, Brussels, Belgium, June 1996, pp. 774-777.

X. Li and G.C.M. Meijer, "A high-performance capacitive absolute angular encoder," in Proc. Dutch conference on Sensor Technology, Delft, The Netherlands, March 1996. pp. 151-154.

X. Li and G.C.M. Meijer, "A new method for the measurement of very low speeds using a multiple-electrode capacitive sensor," in Proc. IEEE CPEM/96, Braunschweig, Germany. June 1996, pp. 349-350.

X. Li, G.W. de Jong, F.N. Toth, F.M.L. van der Goes, G.C.M. Meijer and A.H.M. van Roermund, "Low-cost CMOS interface for capacitive sensors and its application in a capacitive angular encoder," in Proc. ET'96, Sofia, Bulgaria, Sept. 1996.

X. Li, G.C.M. Meijer and E.J. Schnitger, "A novel smart interface for voltage-generating sensors," in Proc. IEEE IMTC/97, Ottawa, Canada, May 19-21, 1997.

G. Wang, G.C.M. Meijer, F.M.L. van der Goes, X. Li and H.M.M. Kerkvliet, "A low-cost smart sensor system for resistive (bridge) and capacitive sensors," to be published in Proc. ICEMI/97, Beijing, China, Oct. 14-16, 1997.

X. Li and G.C.M. Meijer, "A low-cost and accurate DC current measurement system," to be submitted in Proc. ICECS/97, Cairo, Egypt, Dec. 15-18, 1997.

Internal reports

X. Li, "Design of the non-contact potentiometric position sensor," Faculty of Electrical Engineering, TU Delft, Aug. 1993.

X. Li, "A new structure of the capacitive angular-position sensor," Faculty of Electrical Engineering, TU Delft, Sept. 1993.

X. Li, "Design of smart capacitive sensor with full-circle measurement range," Faculty of Electrical Engineering, TU Delft, Aug. 1994.

Biography

Xiujun Li was born in Tianjin, China on February 19, 1963. He received his B.Sc. in physics and M.Sc. in electrical engineering from Nankai University, Tianjin, China in 1983 and 1986, respectively.

He was with the Department of Electronic Science, Nankai University from July 1986 to August 1992. He worked toward his Ph.D. at the Department of Electrical Engineering, Delft University of Technology, The Netherlands from September 1992 to August 1996, where he was involved in scientific research on smart capacitive sensors and smart signal processors. From September 1996, he has been employed as assistance researcher at the Department of Electrical Engineering, Delft University of Technology, where he is involved in research and the development of low-cost interfaces for smart sensors. His research interests are in the area of smart capacitive sensors and smart signal processing.